Opportunistic Spectrum Access using Localization Techniques

A dissertation submitted in partial fulfillment of the requirements for the degree of Doctor of Philosophy at George Mason University

By

Ahmed O. Nasif
Master of Science
Wright State University, 2005
Bachelor of Science
Bangladesh University of Engineering and Technology, 2003

Director: Dr. Brian L. Mark, Associate Professor
Department of Electrical and Computer Engineering

Spring Semester 2009
George Mason University
Fairfax, VA

Copyright © 2009 by Ahmed O. Nasif
All Rights Reserved

Dedication

I dedicate this dissertation to my parents.

Acknowledgments

From the bottom of my heart I thank my advisor Dr. Brian L. Mark, for all his encouragement, guidance and support. None of this would be possible without his active involvement and his faith in me. It is a pleasure to acknowledge the members of the dissertation committee, Dr. Bernd-Peter Paris, Dr. Jill K. Nelson and Dr. Robert Simon for their invaluable inputs and suggestions. I sincerely thank the faculty and staff of The Department of Electrical & Computer Engineering of George Mason University for their guidance and cooperation. A special thanks to the U.S. National Science Foundation for supporting this work under Grants CNS-0520151 and ECS-0426925.

I cannot thank enough my parents and all my family for their unwavering support, encouragement and love. Finally, I thank the Almighty for all the blessings in my life.

Table of Contents

Page

List of Figures ix

Abstract xi

1 Introduction 1

1.1 Overview 2

1.2 Summary of chapters 3

2 Background 5

2.1 Dynamic Spectrum Access 5

2.1.1 Dynamic exclusive use model 5

2.1.2 Open sharing model (*spectrum commons*) 5

2.1.3 Hierarchical access model 6

2.2 Software-defined radios and cognitive radios 6

2.3 Spectrum holes 8

2.4 Basic components of OSA 10

2.4.1 Spectrum opportunity identification 10

2.4.2 Spectrum opportunity exploitation 11

2.4.3 Regulatory policy 12

2.5 Spectrum sensing 12

2.6 Power control and resource allocation 15

2.7 Use of localization information in OSA 17

3 MIFTP Estimation 20

3.1 Introduction 20

3.2 Opportunistic Spectrum Sharing 23

3.2.1 Opportunistic spectrum access 23

3.2.2 Maximum interference-free transmit power 25

3.2.3 Role of localization 29

3.3 Signal Strength-based Localization 29

3.3.1 Canonical Signal Strength Model 29

3.3.2 Cramér-Rao bound 32

3.3.3 Unknown Transmit Power . . . 34
3.4 Approximation for MIFTP . . . 38
3.4.1 Known transmit power . . . 38
3.4.2 Unknown transmit power . . . 42
3.5 Numerical Results . . . 44
3.5.1 Distance $d_{p,a}$ . . . 45
3.5.2 Interference probability threshold, ε_{int} . . . 49
3.5.3 Shadowing noise, σ_W . . . 50
3.5.4 Primary transmit power, s_p . . . 50
3.5.5 Cramér-Rao bound, $J_{p,a}^{-1}$ . . . 50
3.5.6 Summary . . . 55
3.6 Multiple Co-channel Primary Transmitters . . . 55
3.7 Discussion . . . 58
4 Multiple Co-channel Transmitters . . . 60
4.1 Introduction . . . 60
4.2 Collaborative OSA Model . . . 61
4.2.1 SS-based observation model . . . 62
4.2.2 Definition of MIFTP . . . 62
4.2.3 T-map . . . 64
4.3 Collaborative Sensing Scheme . . . 65
4.3.1 With no information . . . 66
4.3.2 With true information . . . 66
4.3.3 With estimated information . . . 68
4.3.4 Measurement clustering and collaborative sensing . . . 69
4.4 Maximum Interference-Free Transmit Power . . . 70
4.4.1 True MIFTP calculation . . . 70
4.4.2 Critical distance estimate, $\hat{D}_b^*(p)$, and spectrum hole detection . . . 72
4.4.3 Interference probability and MIFTP approximation . . . 73
4.5 Numerical Results . . . 75
4.5.1 Mitigation of cochannel interference . . . 76
4.5.2 MIFTP vs. distance . . . 77
4.5.3 MIFTP vs. shadowing noise and interference probability threshold . . . 81
4.5.4 T-map and spectrum hole harvesting . . . 81
4.6 Discussion . . . 82
5 Measurement clustering . . . 84

5.1 Introduction . . . 84
5.2 Measurement clustering criteria . . . 85
5.2.1 Net MMSE Criterion . . . 86
5.2.2 MDL Criterion . . . 87
5.2.3 Measurement clustering . . . 87
5.3 Numerical results . . . 88
5.4 Discussion . . . 92
6 Spectrum Sensing with SS-AOA Measurements and Directional Transmissions . 93
6.1 Introduction . . . 93
6.2 Optimal Hybrid SS-AOA localization . . . 95
6.2.1 SS measurement model . . . 96
6.2.2 Directional primary transmissions . . . 97
6.2.3 AOA measurement model . . . 97
6.2.4 Hybrid SS-AOA localization . . . 99
6.3 Measurement Selection Scheme . . . 99
6.3.1 CRB on localization error . . . 99
6.3.2 Selection rule . . . 100
6.4 Angular thresholds for directional transmissions . . . 103
6.5 Numerical Results . . . 107
6.5.1 Optimal hybrid SS-AOA localization . . . 107
6.5.2 Measurement selection scheme . . . 110
6.5.3 Angular specification for directional transmissions . . . 111
6.6 Discussion . . . 112
7 Conclusions . . . 114
A Appendix . . . 118
A.1 Proof of Proposition 2 . . . 118
A.2 Proof of Proposition 3 . . . 118
A.3 Derivation of (3.38) . . . 119
A.4 Proof of Proposition 4 . . . 119
A.5 Proof of Proposition 5 . . . 121
A.6 Derivation of (3.46) . . . 122
A.7 Proof of Proposition 6 . . . 122
B Appendix . . . 124
B.1 CRB of $\hat{\boldsymbol{\theta}}_{1B}$ and $\hat{\boldsymbol{\theta}}_{1C}$ . . . 124
B.2 Proof of Proposition 8 . . . 125
B.3 Proof of Proposition 9 . . . 126

B.4 Proof of Lemma 1 . . . 127
B.5 Proof of Corollary 1 . . . 127
B.6 Proof of Proposition 10 . . . 128
B.7 Value of $\boldsymbol{H}_0$ . . . 129
C Appendix . . . 130
C.1 The components of the FIM, $\boldsymbol{J}_j$ . . . 130
D Appendix . . . 131
D.1 A Simulation example with directional primary transmissions . . . 131
D.2 CRB on the estimation error of θ_l and θ_u . . . 134
D.3 Derivation of thresholds θ_l^{th} and θ_u^{th} . . . 135
Bibliography . . . 137

List of Figures

Figure Page

3.1 FAR node a outside coverage area of primary transmitter p. 28
3.2 Illustration of relationship between r and β. 39
3.3 Illustration of relationship between r, r_0, and β. 43
3.4 MIFTP versus $d_{p,a}$, when $\epsilon = 4$. 47
3.5 $\hat{P}_{\text{int}}$ versus $d_{p,a}$, when $\epsilon = 4$ and s_p is known. 48
3.6 MIFTP versus $d_{p,a}$, when $\epsilon = 5$. 48
3.7 $\hat{P}_{\text{int}}$ versus $d_{p,a}$, when $\epsilon = 5$. 49
3.8 MIFTP versus ε_{int}, when $\epsilon = 4$. 51
3.9 MIFTP versus σ_W, when $\epsilon = 4$. 52
3.10 MIFTP versus s_p, when $\epsilon = 4$. 53
3.11 $\sqrt{J_{p,a}^{-1}}$ versus σ_W, when $\epsilon = 4$ and s_p is unknown. 54
3.12 Effect of cochannel interference on localization accuracy. 56
3.13 Effect of cochannel interference in worst-case scenario. 57
4.1 Mean values of σ_{Ba}. 67
4.2 Localization error $\mathcal{E}_1$ vs. number of measurements. 76
4.3 MIFTP vs. d_{bp}, for single primary transmitter p. 78
4.4 Average interference probability surface due to $\hat{s}_b^*(p)$ in the coverage region $\overline{B}_{\text{cov}}(p)$. 78
4.5 MIFTP vs. d_{bp}, for two primary transmitters, p and p'. 79
4.6 MIFTP vs. shadowing noise, σ_W. 80
4.7 MIFTP vs. maximum interference probability threshold, ε_{int}. 80
4.8 Pictorial illustration of a T-map and spectrum hole harvesting in space. . . 81
5.1 Average detection probability, $\widehat{\Pr}(\hat{M} = M)$ vs. N. 89
5.2 Average detection probability, $\hat{\Pr}(\hat{M} = M)$ vs. σ_W. 90
5.3 True locations and coverage radii of the primary transmitters. 91

5.4 Clustering due to correct identification of M. 91
5.5 Clustering due to incorrect identification of M. 92
6.1 Determining θ_l and θ_u. 104
6.2 Localization error vs. reference SNR. 108
6.3 Localization error vs. number of antenna elements. 109
6.4 Localization error vs. shadowing noise. 109
6.5 Impact of measurement selection in the case of unknown transmit power. . 110
6.6 Difference between the estimated lower threshold, $\hat{\theta}_l^{\text{th}}$ and θ_l. 111
6.7 Difference between the estimated upper threshold, $\hat{\theta}_u^{\text{th}}$ and θ_u. 112
B.1 Diagram for the proof of Proposition 9. 126
D.1 Power pattern of a directional antenna. 132
D.2 Estimation accuracy due to directional transmission. 133

Abstract

OPPORTUNISTIC SPECTRUM ACCESS USING LOCALIZATION TECHNIQUES

Ahmed O. Nasif, PhD

George Mason University, 2009

Dissertation Director: Dr. Brian L. Mark

The scarcity of radio spectrum poses a significant challenge to the sustained growth of wireless communications, since most of the useful radio spectrum is already allocated for licensed users. However, recent spectrum measurement studies have shown that there are plenty of white spaces or spectrum holes that could be utilized opportunistically by "secondary" users, provided that they do not cause harmful interference to the primary users.

In this dissertation, we develop efficient methods by which a group of secondary users equipped with cognitive radios can determine and access spectrum holes opportunistically based on signal measurements. The cognitive radios are frequency-agile in that they can dynamically tune to different frequency channels for transmission and reception. By exchanging signal strength measurements, a group of cognitive radios can calculate maximum likelihood estimates of the location and transmit powers of the primary transmitters in the system. We apply the Cramér-Rao bound (CRB) to characterize the error in the primary system parameter estimates. The parameter and error estimates are then used to derive an approximation to the Maximum Interference-Free Transmit Power (MIFTP), which is the maximum allowable power that a given cognitive radio can use on a given frequency channel subject to an interference constraint. To mitigate interference from multiple cochannel

primary transmitters, secondary nodes maintain a distributed database that records the location, power, and error estimates of cochannel nodes for each frequency channel.

The proposed MIFTP approximation takes into account errors in spectrum sensing such that the approximation becomes more conservative when measurement errors accrue, and conversely, it becomes more accurate when better measurement data is available. The property of being conservative is important, since secondary users must avoid causing harmful interference to primary users. We also propose two model identification and measurement clustering criteria to identify the number of cochannel primary transmitters and to cluster the measurements appropriately for more accurate estimation of the primary system parameters. Finally, we extend the proposed opportunistic spectrum techniques to incorporate angle-of-arrival information for improved localization accuracy and hence tighter estimates for the MIFTP.

Chapter 1: Introduction

The performance of all wireless systems fundamentally depend on the available radio spectrum, transmit power and channel impairments consisting mainly of fading, interference and noise. Clearly, the vision of ubiquitous wireless services is in direct conflict with the limited radio spectrum, making bandwidth a precious resource. To avoid the degradation of quality-of-service (QoS), traditionally spectrum has been statically allocated and regulated by government bodies, for example, the Federal Communications Commission (FCC) in the U.S.A. A wireless technology is restricted to operate within a fixed allocated spectrum with a limited transmit power, by means of expensive licensing rights. But studies involving real-time field measurements of frequency occupancy in licensed bands reveal that a significant amount of the allocated spectrum is highly underutilized [1, 2]. Hence, the problem is one of poor spectrum utilization and not of actual spectrum scarcity. On the other hand, the systems operating in the unlicensed bands (e.g., the industrial, scientific and medical (ISM)) have seen tremendous success and resulted in many technological advancements (e.g. Bluetooth). This has led government bodies to rethink their philosophy of static spectrum allocation, and focus is now being shifted towards dynamic spectrum access policies. For example, the DARPA and the NSF are investigating opportunistic use of the unused bands in the XG (neXt Generation) communication program [3] and the "NeTS-ProWiN" project [4], respectively. Ever since the early reports of scanty spectrum occupancy were published, the research interest of the communications community on this topic has spiked, as evidenced in the recent literature (e.g., see the proceedings of IEEE's DySPAN (Dynamic SPectrum Access Networks) symposiums).

Opportunistic spectrum access implemented by *cognitive radios* has been proposed as a prospective solution to inefficient spectrum usage [5]. Cognitive radios are envisioned

as intelligent agents capable of dynamically sensing and accessing a range of spectra in their environment without adversely affecting the existing systems. *Opportunistic spectrum access is still in its infancy* [6]. The IEEE 802.22 Working Group is in the process of developing the first wireless air interface (i.e., MAC and PHY) standard based on cognitive radios for the TV broadcast bands [7]. This dissertation is motivated by the potential benefits and unique challenges of opportunistic spectrum access as a technology to realize the vision of anytime anywhere wireless connectivity.

1.1 Overview

The success of opportunistic spectrum access using cognitive radios depends on the resolution of many complex technical, economical and regulatory issues. The key signal processing tasks of a cognitive radio can be broadly categorized into (a) spectrum sensing or radio-scene analysis, (b) channel-state estimation and predictive modeling, and (c) transmit-power control and spectrum management [5]. The common goal of these three tasks is to enable cognitive radios to operate in a non-disruptive manner with the incumbent/primary system. An essential requirement to accomplish this is to ensure that the interference caused by the cognitive radio does not degrade the operation of the primary beyond a prescribed level.

In this dissertation, we focus on spectrum sensing and transmit-power upper bounds of cognitive radios. In order to perform spectrum sensing, we use localization techniques to characterize the primary system. In our approach, received signal strength measurements are shared among cognitive radios to perform collaborative sensing. Once the required unknown quantities of the primary system are identified, the problem of spectrum sensing can be formulated as a parameter estimation problem. Since disruption of the primary due to interference caused by the cognitive radios is of prime concern, we are particularly interested in the error associated with our localization-based sensing scheme. Once the parameters associated with the primary is estimated, we derive the maximum allowable power a cognitive radio can use subject to an interference constraint. The derived upper

bound compensates for the sensing error, such that when larger error is expected the bound becomes more conservative. Our proposed approach to sensing and transmit power bound can be a part of a protocol to deal with spectrum sensing, power control and admission control for cognitive radios.

1.2 Summary of chapters

- In Chapter 2, we introduce the basic concepts and terminology of opportunistic spectrum access and cognitive radios. Then, we discuss the research literature relevant to the developments made in this thesis. A brief survey of the key issues, namely, spectrum sensing, power control and localization for opportunistic spectrum access is presented.

- In Chapter 3, we consider a scenario in which cognitive radios opportunistically share a fixed spectrum resource with a set of primary nodes. We develop a collaborative scheme for a group of cognitive radios to estimate the maximum power at which they can transmit on a given frequency channel, without causing harmful interference to the primary receivers. The proposed scheme relies on signal strength measurements taken by a group of cognitive radios, which are then used by a target node to characterize the spatial size of its perceived spectrum hole in terms of the maximum permissible transmit power. We derive an approximation to the maximum interference-free transmit power using the Cramér-Rao bound on localization accuracy. The presented numerical results demonstrate the effectiveness of the proposed scheme under a variety of scenarios.

- To generalize the developments of Chapter 3, in Chapter 4 we present a collaborative algorithm to enable opportunistic spectrum access for cognitive radios in the presence of multiple co-channel transmitters. A spectrum hole detection and estimation technique based on received signal strength observations is developed, which allows the coexistence of both licensed and unlicensed transmitters. We address the issue of

how to perform collaborative spectrum sensing in the presence of multiple co-channel transmitters and how to determine the maximum transmit power that can be used for a given frequency channel by a cognitive radio while avoiding harmful interference to the licensed network. Simulation results are provided to validate the feasibility of our approach and to evaluate the performance of our scheme.

- In Chapter 5, we consider the problem of localizing multiple cochannel transmitters belonging to a licensed or primary network using signal strength measurements taken by a group of unlicensed or secondary nodes. Traditional localization techniques can be applied to multiple transmitter localization, provided that: (1) the total number of cochannel transmitters in the system is known, and (2) an appropriate set of clustered measurements is available. In this chapter, we present two criteria to determine the total number of cochannel transmitters in the primary system. The first criterion is called the *net MMSE* criterion, which uses the Cramér-Rao lower bound on localization accuracy. The second criterion is the information theoretic criterion, *minimum description length*. Both of these criteria lead to measurement clustering algorithms in a natural way. Our numerical results demonstrate the effectiveness of the proposed approach to measurement clustering.

- In Chapter 6, we consider a group of nodes that collaboratively localize a noncooperative target transmitter. We propose an optimal hybrid localization scheme based on signal strength (SS) and angle-of-arrival (AOA) measurements. Such a localization scheme may play a crucial role in sensing mechanisms for cognitive radios. Numerical results show that when only a handful of SS measurements is available, a significant accuracy improvement is possible by using just one or two line-of-sight AOA measurements. We present a measurement selection rule that can further improve localization accuracy when a larger number of measurements is available.

- A conclusion for this dissertation is drawn in Chapter 7. Some topics of future research interest are mentioned.

Chapter 2: Background

In this chapter, we discuss some basic aspects of opportunistic spectrum access (OSA) using cognitive radios (CRs), including some terminology. We provide a brief survey of the research literature on the topic, focusing on spectrum sensing, power control and localization relevant to OSA.

2.1 Dynamic Spectrum Access

As opposed to static spectrum management policy, the term *dynamic spectrum access* (DSA) stands for a variety of approaches aimed at spectrum reform, (see [6] and references therein). Different DSA techniques can be broadly categorized under three models.

2.1.1 Dynamic exclusive use model

Maintaining the basic structure of the current spectrum regulation policy, this model aims to improve spectrum efficiency by introducing flexibility. Two different approaches have been proposed. To ensure the most profitable use of the limited spectrum resource, the *spectrum property rights* approach allows licensees to sell and trade spectrum and to freely choose technologies [8]. The *dynamic spectrum allocation* approach exploits the spatial and temporal traffic statistics of different services [9].

2.1.2 Open sharing model (*spectrum commons*)

Inspired by the phenomenal success of wireless services in the unlicensed ISM radio band (e.g., WiFi, Bluetooth), this approach employs open sharing among peer users as the basis of spectral management. Both centralized [10],[11] and distributed [12–14] approaches have been initially investigated.

2.1.3 Hierarchical access model

In this model, the primary and secondary users form a hierarchical access structure. The secondary users are allowed to use the licensed spectrum provided that the interference perceived by primary users (licensees) is not over a prescribed level. Two different models have been proposed.

Spectrum underlay

Instead of detection and exploitation of spectrum white space, this approach is based on the worst case assumption that primary users transmit all the time. Therefore, the secondary user's transmit power is severely constrained such that it operates below the noise floor of primary users. Typically, secondary users can potentially achieve short-range high data rate with extremely low transmission power by spreading signals over a wide frequency band (e.g., Ultra Wide Band (UWB)).

Spectrum overlay

This approach relies on the detection of spatial and temporal spectrum white space. Once such an opportunity is identified, the secondary users can use the available spectrum in a non-intrusive manner. In this dissertation, this is the specific DSA model we adopt, which is also known as *opportunistic spectrum access* (OSA). It may be possible to further improve spectrum efficiency by using underlay and overlay approaches simultaneously. For example, see [15] for a combined overlay-underlay waveform design technique suitable for CRs.

2.2 Software-defined radios and cognitive radios

Software-defined radio (SDR), promoted by Joseph Mitola in 1991, is "generally a multiband radio that supports multiple air interfaces and protocols and is reconfigurable through software run on a DSP or general-purpose microprocessor" [16]. The FCC describes the SDR as "a radio that includes a transmitter in which the operating parameters of frequency

range, modulation type or maximum output power (either radiated or conducted), or the circumstances under which the transmitter operates in accordance with Commission rules, can be altered by making a change in software without making any changes to hardware components that affect the radio frequency emissions" [17]. An example of a simple SDR (or simply software radio) is a dual-mode cell phone capable of switching between analog and digital transmissions depending on the strength of the signals it receives. More advanced SDRs are actively being developed, e.g., SourceForge's Open SDR and the GNU Radio project [18].

In 1999 Joseph Mitola coined the term "cognitive radio" and suggested its use to enhance the flexibility of personal wireless services by means of a new language called the *radio knowledge representation language* (RKRL) [16],[19]. The FCC defines a cognitive radio (CR) as "a radio that can change its transmitter parameters based on interaction with the environment in which it operates" [20]. Inspired by the computational view of cognition, Simon Haykin offers the following definition for CR [5]: "Cognitive radio is an intelligent wireless communication system that is aware of its surrounding environment (i.e., outside world), and uses the methodology of understanding-by-building to learn from the environment and adapt its internal states to statistical variations in the incoming RF stimuli by making corresponding changes in certain operating parameters (e.g., transmit-power, carrier-frequency, and modulation strategy) in real-time, with two primary objectives in mind:

- highly reliable communications whenever and wherever needed;
- efficient utilization of the radio spectrum."

CRs represent a new paradigm of communication systems where principles of cognition are used to improve performance. DSA is an important application of CR, but by no means the only one. CRs implemented under the SDR platform are seen as a promising technology to realize the vision of OSA system. We use the terms *frequency agile radio* (FAR), CR and secondary radio interchangeably.

2.3 Spectrum holes

"A spectrum hole is a band of frequencies assigned to a primary user, but, at a particular time and specific geographic location, the band is not being utilized by that user" [21]. In this definition, the band of frequencies may stand for *white spaces* (frequencies which are free of RF interferers except for ambient noise made up of natural and man-made sources) or *grey spaces* (frequencies which are partially occupied by low-powered interferers). In other words, it is the region of space-time-frequency in which a particular secondary use is possible.

Assuming that the primary transmitter is always active/ON, we focus on exploiting spatial spectrum holes, which is the region of space and frequency where secondary transmission can be allowed. An example is the region outside a TV transmitter's coverage area. One approach to characterize this kind of spectrum hole is to identify the primary receivers and permit secondary transmissions such that the primary receptions are not disrupted. Primary receivers are much harder to identify than primary transmitters if we assume that the primary and secondary systems do not cooperate, which is a reasonable assumption. For secondary users to use the TV bands, [22] proposed to exploit the local oscillator leakage power emitted by the RF front end of TV receivers to detect the presence of primary receivers. The drawbacks of this approach are the short detection range and long detection time.

In the probe spectrum access method [23], secondary transmissions are coordinated through a central controller (base station (BS)) via a control channel. The FAR nodes in the vicinity of a transmitter do not transmit, but they receive a probe signal to measure the interference caused by far away FAR's transmission. Probe signals are designed to cause minimal interference. The probe transmission power level is adjusted so that interference is below a threshold. When an acceptable probe transmission power is found, the far away FAR node can transmit at that power level. Since only one probe signal is allowed at a time, a TDMA-type MAC must be used to incorporate multiple FAR transmission. Knowledge

of the primary's spectrum is needed to design a minimal-interfering probe signal and this makes the application of this approach rather limited. As an alternative approach, instead of identifying primary receivers, we can characterize the primary system by estimating the primary transmitter's location and coverage radius. We adopt this particular approach.

In temporal spectrum holes, secondary transmissions are allowed during the idle times of the primary users. An example of this is the satellite links that transmit intermittently. The exploitation of temporal spectrum opportunities have been studied in [24–27] and the references therein. The success of this kind of scheme depends crucially on the accurate prediction of the silent periods of the primary [24–26]. Typically, secondary opportunities in time are studied in terms of probability of missed detection, probability of false alarm and sensing time to evaluate a scheme's performance, reliability and complexity. These approaches are vulnerable to deviations from the assumed model details about the primary's transmissions due to real-world uncertainties. In [27], by modeling the primary user's spectrum occupancy as a Markov chain, a decision-theoretic framework for optimal PHY-MAC joint design of OSA based on the theory of partially observable Markov decision processes (POMDPs) is presented. The design objective is to maximize the secondary's throughput under the constraint that the probability of collision perceived by any primary user is below a predetermined threshold.

Besides temporal and spatial aspects, the primary's signal waveform can be viewed as another dimension of spectrum holes [28]. For example, a direct sequence spread spectrum (DSSS) signal with a spreading code of four chips can accommodate four different users using conventional signal processing techniques. If at any given time and space only one such signal is identified in the primary network, then a spectrum hole consisting of another three signals exists which can be used by the secondary network. In [28], the time and frequency domain behaviors of existing signals are characterized by signal detection followed by feature extraction, clustering, signal classification, machine learning and prediction. Then some decision metrics or policies are used to transmit new signals so that the new signals do not interfere with the existing ones.

2.4 Basic components of OSA

A single-link *spectrum opportunity* is defined as an opportunity between two secondary users to communicate without disturbing the primary receivers and without being disturbed by the primary transmitters [6]. Interference constraints can be specified in terms of at least two parameters: (i) maximum interference power level tolerated by an active primary receiver, (ii) maximum probability that the interference level at an active primary receiver may exceed a predefined threshold. Basic components of an OSA model are:

- spectrum opportunity identification (identifying and tracking idle channels that are dynamic both in time and in space),
- spectrum opportunity exploitation (whether and how a secondary transmission should take place),
- regulatory policy (defining basic etiquettes for secondary users to ensure compatibility with legacy systems).

2.4.1 Spectrum opportunity identification

Spectrum opportunity identification can be performed using traditional signal detection techniques, such as matched filtering, energy detection and cyclostationary feature detection [29]. The particular choice of a detector depends on the a priori knowledge about the primary's transmissions and complexity. Optimal detection can be performed using a matched filter, since it maximizes the SNR, but it requires information about the primary signal's modulation type, order, pulse shaping, packet format, timing and carrier synchronization to achieve coherency. The energy detector performs suboptimal noncoherent detection and is attractive owing to its simple implementation. Some drawbacks are threshold determination, inability to detect spread spectrum signals, lack of robustness against frequency selective fading and interference. The cyclostationary feature detector can be used to get better results compared to energy detectors. Due to hardware and energy limitations, a CR needs a strategy to intelligently select channels to perform spectrum

sensing. Spectrum sensing has two (often conflicting) objectives: (a) find a free channel for immediate use, (b) use and gather statistical information on channel occupancy for future access. The optimal sensing strategy can be viewed as a sequence of decisions giving the best tradeoff between these two objectives. The results of [27], show that for jointly optimal spectrum detector and access strategy, the detector must be designed under the Neyman-Pearson criterion and operate with probability of missed detection equal to the maximum tolerable probability of interference to the primary system.

2.4.2 Spectrum opportunity exploitation

Since the outcome of the spectrum detector is not error-free, intelligent spectrum access strategies are necessary. An optimal access strategy should take into account the operating characteristics of the spectrum detector. For example, if the probability of missed detection is high, the access strategy should be conservative. On the other hand, if the probability of false alarm is high the approach should be aggressive. Once a decision is made to access a particular channel, an appropriate modulation and power control scheme must be utilized.

OFDM is seen as an attractive modulation scheme because of its reconfigurable subcarrier structure, which can be used over noncontiguous frequency bands. But careful design is needed to make sure that the subcarrier spacing and symbol interval match the spectral and temporal characteristics of spectrum hole opportunities. Also, cross-channel spectrum leakage and nonlinearities of the transmitter's power amplifier need to be prevented.

Power control is a challenging issue for OSA networks. As an example, even for a single secondary user, ignoring shadowing and fading, the transmit power is constrained by the detection range of the secondary node and the transmit power of the primary. Development of power control schemes that consider shadowing, fading, co-channel interference aggregation and other sensing limitations are actively being pursued by researchers. For spatial spectrum holes, as found in TV broadcast bands, where the spectrum holes vary very slowly in time, the power allocation problem is equivalent to a graph coloring problem [30],[31], which is unfortunately NP-hard. Therefore, suboptimal approaches have been proposed.

2.4.3 Regulatory policy

Regulatory policy establishes rules of cooperation and joint usage between primary and secondary users, which is a critical aspect of OSA. Policy compliance can be executed using specific parameters available in a node, e.g., power spectral estimate, location, traffic type, priorities, delay constraints and other observable of the environment. The range of policies may vary from non-aggressive (do-no-harm policy, e.g., maintain complete orthogonality at all times) to aggressive (e.g., operate without restrictions in times of national emergency). Some major challenges include software implementation of policy, device testing and verification for policy compliance, and resolution of multiple conflicting policies. To determine policy compliance, it may be highly desirable to consider a *policy reasoner* (PR) that is capable of interacting with the sensor/radio and respond to requests by providing constraints (e.g., transmit power limit, transmission duration, etc.) [32].

2.5 Spectrum sensing

Spectrum hole detection has been extensively studied by researchers. Most approaches involve a detector that provides a binary decision on the primary's occupancy based on some observation statistics. Fundamental limits of sensing, threshold determination of the detector using side information and effects of collaboration have been investigated. Performance optimization in terms of the detector's ROC characteristics has also received considerable attention. Here, we provide a brief survey of these developments.

A CR can use its received signal to determine whether the primary signal is present or not by conducting a hypothesis test. Some fundamental limits of such a detection scheme is studied in [33]. If the primary's signal is known, the optimal detector is just a matched filter (coherent detector), requiring $\mathcal{O}(\frac{1}{SNR})$ samples to meet a predetermined probability of error constraint. But in CR settings, the primary's transmitted signal is more likely to be unknown. In that case, the optimal detector is just an energy detector (radiometer), requiring $\mathcal{O}(\frac{1}{SNR^2})$ samples. The difference between these two detectors becomes significant

at low SNR. In this regime, the optimal detector for an undecodable BPSK signal (a BPSK signal in AWGN with unknown bit sequence) and in fact, any zero-mean constellation performs similarly to an energy detector. Interestingly, a significant decrease in the number of samples can be achieved by simply looking at the pilot signal portion of a transmission. The effects of noise uncertainty and quantization can make matters much worse. While noise uncertainty can induce SNR_{walls} (a lower bound on SNR below which detection becomes impossible), for radiometers, these walls become absolute for quantized detectors with noise uncertainty. However, a pilot signal under noise uncertainty can still be detected since it is highly unlikely for the noise to pick an exact pilot signal to confuse the matched filter. These results show that the commonsense rule of "don't transmit if you can decode" is inadequate and it is important for CRs to detect the presence of undecodable signals.

In [34], the authors analyze the performance of spectrum sensing using energy detectors under a lognormal shadowing and Rayleigh fading environment. The detector's performance is studied in terms of probability of missed detection (P_m) and probability of false alarm (P_f), which are averaged over the fading statistics. For lognormal shadowing, the probability of detection is not known in closed-form and is calculated numerically. For shadowing, the performance worsens as the shadowing variance increases, whereas for Rayleigh fading the performance degrades significantly. Particularly, achieving $P_m < 10^{-2}$ results in $P_f > 0.9$. A significant improvement in sensing is observed by adopting the *OR-rule* or *1-out-of-N-rule* for fusing the decisions of N collaborating nodes. This is because for large N, there is a high probability that at least one node will see a better channel, even compared to a non-fading AWGN case. However, spatial correlation among collaborating users is seen to degrade performance.

A model for optimizing the parameters involved in channel sensing based on energy detector is proposed in [35]. The primary traffic is modeled as an ON-OFF process with exponentially distributed ON-OFF times. The channel is periodically sensed, where the sensing periodicity (T_p) depends on the QoS of the primary system. This is because T_p characterizes the maximum duration the primary may tolerate the interference caused by

the secondary. A fraction of T_p, say T_m, is spent on monitoring the channel (for an energy detector this is the integration time). If at the end of T_m, the channel is sensed idle, then data transmission is performed in $(T_p - T_m)$. If the channel is sensed busy at the end of T_m, then a sequential search for idle channels begin for a period of $\bar{T}_{\text{search}}$. The authors present a way to optimize (minimize) $\bar{T}_{\text{search}}$ and T_m such that the secondary's throughput is maximized while protecting the primary system. At the optimal $\bar{T}_{\text{search}}$, sensing time is long enough to decrease false alarms, but not too long to incur unnecessary delay.

In [36], a relay-based cooperative spectrum sensing approach with known channel state information (CSI) under Rayleigh fading is proposed. Considering a two-user cognitive network, improvement in detection probability and detection time (agility) is shown when a suitable relay node is available. In a TDMA-based relay protocol, in the first slot the cognitive user (U_1) sends a message to its intended receiver and relay node (U_2) listens. Then in slot two, U_1 receives the relay transmission of its own message by U_2 and derives the observation statistic by canceling out its message part. Such a scheme is shown to yield improved detection and agility if the received power from the primary user at the relay node U_2 is greater than that of U_1. This is because under this condition there is a gain in the SNR of the observed statistic of U_1. In [37], this insight is used to develop a practical algorithm to allow cooperation between cognitive users in random networks.

In [38], the threshold for an optimal Bayesian energy detector is determined. The network configuration consists of two links, one primary and one secondary. The detection threshold is obtained by minimizing a cost function that depends on the interference caused to the primary receiver due to missed detection, transmission opportunity loss due to false alarm and side information. The side information may include received signal power, noise variance, spatial location of the cognitive and the primary receivers and a priori transmission probability of the primary user. Numerical results show that side information plays an important role in making cognitive sensing roust for a wide range of primary activity factors.

The channel capacity of different AWGN channels under received-power constraints is

considered in [39]. Such a constraint is relevant for spatial spectrum sharing where the average received power at the primary receiver due to secondary transmission needs to be upper bounded. It was shown that for the point-to-point AWGN channels the proposed received-power constraint results in a very similar capacity formula to the canonical transmit-power constraint case. This is because in the absence of fading, the received power constraint is simply a deterministically scaled version of the transmit-power constraint. In [40], capacity is calculated using average received-power constraint under different fading distributions (namely lognormal, Rayleigh, Nakagami), when only one primary and one secondary user is present. This work assumes perfect CSI and is inspired by the scenario when high powered secondary transmission is made possible by a deep fade in the channel between the secondary transmitter and the primary receiver. Extension of the analysis to peak-received-power constraint, correlated fading and multiple secondary users, all result in decreased channel capacities.

2.6 Power control and resource allocation

Traditionally, the power control and allocation problem is posed as an optimization problem with restrictions on resources and QoS given as constraints. For CR applications one has to maximize a chosen utility function, provided that the secondary's transmissions do not cause harmful interference to the primary network. Issues of noncooperation, competition, fairness and robustness become important in this regard. Below we discuss a few recent works on power control and resource allocation for CR networks. A brief discussion on more closely related work is given at the beginning of Chapter 3.

Typically the spectrum detector provides binary decisions (*hard decisions*). Optimal power control for such a detector in a single secondary link scenario consists of two modes: (i) use maximum power if the primary is not detected, (ii) do not transmit otherwise. In [41], the authors pose the power control question for a *soft sensing* spectrum detector, where the power depends on and continuously varies with the observation statistic. The motivation of this work is to identify the consequence of information loss caused by the

binary mapping of the observation statistic that is continuous. Surprisingly, for the SNR maximization objective, under peak power and average interference constraints, the optimal power control takes the typical binary form. But for the ergodic capacity maximization objective, the optimal power varies continuously as a function of the observation statistic.

In [42], a centralized near optimal joint power and channel allocation is considered. The cognitive network consists of K users, N free channels and a central controller that has knowledge of each CR's channel gain and power budget. The allocation of channel n to user k is treated as a binary variable $\alpha_{nk} \in \{0, 1\}$ and the objective is to maximize the total sum capacity of all the links. Instead of solving this mixed integer programming problem, in a suboptimal approach the problem is forced to be convex by allowing α_{nk} to vary continuously, i.e., $0 \leq \alpha_{nk} \leq 1$. At the end of the proposed algorithm, allocation is performed by quantizing the value of α_{nk} to 0 or 1. For the OSA scenario an additional SINR constraint for the nearest primary user (*critical victim*) with respect to each link is introduced. The resulting algorithm has linear complexity $\mathcal{O}(NK)$, as opposed to the exponential complexity of the optimal solution and is claimed to be near-optimal based on numerical results.

A distributed power control algorithm with heterogeneous QoS constraints is proposed in [43]. Each link is characterized by its utility function, which is a function of the SINR. Upper and lower bounds on SINR are imposed to manifest the hierarchy between primary and secondary users. The objective is to maximize the sum of all the utilities subject to the link-wise SINR constraints. The original non-convex problem is relaxed into an equivalent convex optimization problem by upper-bounding the true interference-plus-noise term for each link and applying a variable transformation. The iterative and distributed power control algorithm results from applying a Lagrangian gradient-based algorithm to solve the Karush-Kuhn-Tucker (KKT) conditions, which cannot be solved in closed form.

The application of genetic algorithms to determine intelligent power allocation strategies is studied in [44]. The following toy model is considered: given two unlicensed channels and two noncooperating users, how should each user allocate the total power between the two

channels such that the collective capacity is maximized. For this particular scenario, the optimal solution is seen to occur when the two users' allocation is in complete overlap or complete segregation depending on the value of the cross channel gains. Since the users do not cooperate, a good policy is needed to reach the *socially optimal* operating point, which is not always the Nash Equilibrium. This problem is posed as a 2-player repeated game with a memory of the immediate past two games. The concept of a genome and genetic algorithm is used to identify intelligent schemas that yield robust and optimal *payoff* (i.e., capacity). Initial simulation results look very encouraging, but issues of complexity, overhead and practical implementation need to be carefully considered.

In [45], the notion of a *secure transmission power* for CRs is introduced as a protection against malicious use of CRs. The derivation of this quantity is done assuming worst-case position of the primary user. The resulting expression is given in terms of the primary's transmit power and the corresponding received power at the secondary, noise power, primary's coverage radius and acceptable SNR thresholds. Although in some cases these quantities may be available to the CR a priori, this is unlikely to be the case in general. In our approach, in Chapter 3, we provide a localization-based method to estimate these quantities and also account for the estimation error involved.

2.7 Use of localization information in OSA

Location awareness is an essential feature of CRs. Localization for conventional wireless networks has been studied extensively. The major approaches involve location estimation by range-based, range-free or pattern matching schemes. Localization for cognitive radio networks pose unique challenges like noncooperation and robustness against a wide range of operating conditions. Below we discuss some recent works on this topic.

Localization of a primary transmitter with unknown transmit power is considered in [46]. Signal strength (SS) measurements corrupted by lognormal shadowing received by location-aware CRs are used. Raw SS measurements are averaged to mitigate the effect of shadowing. Using algebraic manipulation, the problem is posed in a matrix form with four unknowns,

where the fourth unknown is determined uniquely by the location. This fact is used to construct an equality constraint. Since the canonical least square (LS) solution is not accurate enough, a constrained and weighted LS version of the problem is constructed, where the weighting matrix reflects the reliability of the measurements. The final solution is found by solving the Lagrange multiplier and checking the KKT optimality conditions. Although the end solution is suboptimal in the mean-squared-error (MSE) sense, it can be used as the initial "guess" in an optimal localization scheme. It is worth noting that in the dB scale, the shadowing noise is additive Gaussian and hence a LS formulation in that scale would make the solution optimal. Unfortunately, in the dB scale a linear formulation is not obvious without introducing error due to linearization.

In [47], a global optimization method to localize multiple co-channel transmitters is proposed. A simple noiseless free-space path loss model is assumed and localization of M transmitters with known transmit power is performed using N SS measurements taken by sensor nodes. The cost function to be minimized is defined as the sum of the squared differences between the true observed power at each sensor and the predicted received power based on the estimated transmitter location. This non-convex optimization problem is solved using a global optimization algorithm called particle swarm optimization (PSO). The *k-means* clustering algorithm is used to generate smart initial staring points. The performance of the algorithm for a particular scenario depends on the underlying structure of the objective function and the initial locations of the *particles* with respect to the global minimum. The localization error is observed to decrease with increasing N (more information), decreasing M (decreased dimensionality) and smart initial choices (as opposed to random starting points). In a subsequent paper [48], an Expectation Maximization (EM) technique is proposed to solve the same problem, with the inclusion of additive measurement noise. The maximum likelihood (ML) solution is not straightforward since there are $2M$ unknown parameters and multiple local maxima. The set of $M \times N$ unknown received powers from each transmitter to each receiver is proposed as the *hidden* variables in the EM algorithm. As a consequence, the problem of maximization over $2M$ coupled variables

is decoupled into M 2-dimensional maximizations. The performance of the EM algorithm together with smart initial condition is observed to outperform the PSO approach.

To ensure the operation of CRs under different environment (e.g., indoor and outdoor), a cognitive positioning system (CPS) based on time-of-arrival (TOA) is proposed in [49]. CPS has the capability to adaptively control its location accuracy depending on the environment (for example, indoor operation typically requires higher accuracy). In TOA-based localization, as seen from the Cramér-Rao bound (CRB), accuracy is inversely related to the signal bandwidth (BW). Hence, once a target CR specifies its desired location accuracy, it can request a pulse transmission of the corresponding required BW from a reference CR. Such a BW determination rule for single path and multipath scenario is presented using CRB analysis. For enabling such a localization scheme, two dynamic spectrum management algorithms based on overlay and underlay-overlay hybrid approach are discussed. In [50], a location awareness engine for CRs is proposed. The objective is to enhance its cognitive capabilities using location information, which can be utilized to perform dynamic spectrum management, network planning and handover.

In [51], location information is used to identify opportunities for concurrent secondary transmissions overlayed with an infrastructure-based primary user. Using signal-to-interference ratio (SIR) analysis in a carrier sense multiple access with collision avoidance (CSMA-CA) MAC protocol, the *concurrent transmission region* is characterized, which denotes the area where secondary links can operate without interfering with the primary links. This approach can be seen as an alternative to the time- and energy-consuming wide-band spectrum sensing that is typically proposed. In [52], the network topology of primary and secondary users is treated as random and is studied using spatial statistical techniques (namely, in terms of *point processes*). Characterizing location distributions in such a way can be used to model primary users' locations and service areas. A range free geometric localization algorithm for CRs, including an approximation of the corresponding MSE, is proposed in [53].

Chapter 3: MIFTP Estimation

3.1 Introduction

In this chapter[1], we focus on the problem of estimating the size of a spectrum hole in terms of the maximum power that a FAR node can transmit on a given frequency channel without causing harmful interference to primary users. In [56], the impact of secondary transmissions on a primary receiver is studied in terms of interference probability. Because of the integral forms involved it is difficult to use the given probability expressions to solve for the allowable secondary transmit power. In [57], an additional *no-talk radius* is defined within which the secondary users must be quiet to guarantee service to primary users within some a *protected radius*. Once these distances are specified (in terms of SNR margins), the aggregate interference at the edge of the protected region is computed, which can then be used to obtain the total permissible secondary transmit power. However, this approach assumes that the primary transmit power and the local SNR at the secondary receivers are already accurately known, so that SNR can be used as a proxy for distance. In [58] a power control algorithm to be employed by secondary users sharing spectrum with a single primary transmitter is proposed. The secondary links are constrained to be low-powered so that the interference caused to the primary system can be modeled by considering a single worst-case primary receiver. The primary system's location and transmit power, are assumed to be known without error. The present chapter is complementary to [58] in the sense that we propose an approach to calculate the maximum transmit power (i.e., the MIFTP) for secondary users to avoid harmful interference to the primary receiver. The MIFTP determines the upper limit of the power control algorithm given in [58]. Furthermore, our approach does not assume knowledge of the primary system's location or transmit

[1]The contents of this chapter appeared in [54] and [55].

power. In [59], the authors consider the coexistence of a single secondary user with a primary system and quantifies the secondary's maximum allowable power. The approach is to infer the distance between the primary and secondary transmitters using the spectrum sensing decisions. In each time slot, the channel occupancy is determined by performing a hypothesis test using the energy detector operating under Raleigh fading. Successive decisions are used to estimate the probability of missed detection, which is then used to infer the distance between the primary and secondary transmitters. Once this distance is determined, the results of [57] are used to find the maximum transmit power for the secondary user. While this approach avoids explicit localization of the primary transmitter and information sharing among secondary nodes, it still requires the knowledge of the path loss function and the primary's transmit power. To avoid the limitations mentioned above, our approach exploits collaboration among secondary nodes for explicit sensing of the primary transmitter's power and location. We focus on the case of a single transmitter, but briefly discuss how the proposed approach can extend to more general situations.

A basic mechanism for opportunistic spectrum access is the Listen-Before-Talk (LBT) scheme [60]. In the LBT scheme, a FAR node "listens" on a given frequency channel. When the channel is sensed idle, the FAR node has the opportunity to "talk," i.e., to transmit on the channel for up to a certain maximum duration at a power level not exceeding a fixed threshold. To avoid causing harmful interference to the primary users, the maximum power level and the maximum talk duration in LBT must be chosen relatively conservatively in practice. This can severely limit the potential capacity gains that could be achievable with opportunistic spectrum sharing.

Higher capacity gains could be achieved if the FAR nodes were capable of collaborating and exchanging local information concerning the primary user's transmission characteristics. In [60], a simple collaborative version of LBT was shown to improve the spectrum sharing capacity gain by an order of magnitude. To further improve effectiveness of opportunistic spectrum sharing, signal strength (SS) measurements of the primary user could be shared by FAR nodes and used by a given FAR node to determine the maximum power level at

which it can transmit without causing harmful interference to the primary user. We refer to this power level as the maximum interference-free transmit power (MIFTP).

We develop a method to estimate the MIFTP for a given FAR node on a given frequency channel, based on SS measurements collected by one or more FAR nodes in the vicinity of a primary transmitter. The MIFTP characterizes the size of the spectrum hole in the spatial domain with respect to a given FAR node and frequency channel. The SS measurements may be obtained by a single FAR node at different locations at different points in time, or by collaborative sharing of measurement information among spatially separated FAR nodes. We make the conservative assumption that the primary transmitter transmits at constant power during an observation period. Thus, we do not address the separate issue of opportunistic spectrum access in the time-domain, i.e., exploiting periods for which the primary transmitter may be idle [61, 62].

Our proposed approximation for MIFTP is derived from the maximum likelihood estimate of the location of the primary transmitter based on SS measurements and the associated Cramér-Rao bound (CRB) on the error of the estimator. The estimator assumes a lognormal shadowing model of signal propagation. Using the CRB for the location estimator, an estimate for the MIFTP is derived. The canonical localization problem assumes that the transmit power is known. However, in a wireless system with opportunistic spectrum sharing, the secondary users may not have access to this information. Moreover, in some scenarios, the primary transmitter may adjust its transmit power over time. Therefore, we extend the canonical localization problem to incorporate estimation of the transmit power in addition to the position of the primary transmitter. The resulting location estimate is then used to calculate an estimate of the MIFTP, which in general is more conservative than the MIFTP derived from the canonical localization problem.

The remainder of the chapter is organized as follows. Section 3.2 describes the model and key concepts of opportunistic spectrum sharing used in this work. Section 3.3 describes the canonical SS localization model and extends the canonical model to the case where the transmit power is unknown. Section 3.4 derives an approximation for the MIFTP.

Section 3.5 presents numerical results, which demonstrate the effectiveness of the proposed approach to spectrum sharing. Section 3.6 briefly discusses how the localization accuracy is affected when multiple primary transmitters are present. Finally, the chapter is concluded in Section 3.7.

3.2 Opportunistic Spectrum Sharing

We assume a model of spectrum sharing, whereby a set of FAR nodes attempt to opportunistically make use of unused spectrum, without causing harmful interference to the primary users. The FAR nodes identify and make use of such "spectrum holes" by an opportunistic spectrum access mechanism. In this section, we discuss the concept of opportunistic spectrum access and define a critical parameter called the maximum interference-free transmit power (MIFTP). The MIFTP for a FAR node on a given frequency channel is essentially equivalent to the radius of a spectrum hole in the spatial domain. We then discuss the role of localization in computing the MIFTP.

3.2.1 Opportunistic spectrum access

In a noncooperative spectrum sharing environment, a set of users called *cooperative* or *secondary* users, seeks to make use of the spectrum resource, originally allocated to another set of users called *noncooperative* or *primary* users. The *primary* users are called *noncooperative*, since no communication between primary and secondary users are allowed. On the other hand, the *secondary* users are called *cooperative*, because they can exchange information among each other in order to perform collaborative spectrum sensing.Without loss of generality, we shall assume the existence of a common control channel that can be used by the secondary users to exchange control information.[2] The objective of a noncooperative spectrum access scheme is to maximize the utilization of the spectrum resource by providing

[2]In practice, any available channel can be used to exchange control information between two secondary users. For example, signal measurements with respect to a frequency channel γ could be exchanged on a different frequency channel ζ.

a means for the secondary users to utilize available spectrum, without causing harmful interference to noncooperative users. By contrast, cooperative spectrum access schemes, such as the family of CSMA protocols, seek to provide fair and efficient spectrum usage among the cooperative users by means of collision sensing or collision avoidance mechanisms.

Listen-Before-Talk (LBT) is a basic scheme for opportunistic spectrum access in a non-cooperative environment [60]. A FAR node implementing LBT *listens* to a given frequency channel. When the received power on the channel falls below a threshold η, the FAR node may then use the channel for its own transmission during the *talk* state. We shall assume that channel contention among the cooperative FAR nodes is resolved using an appropriate medium access control (MAC) protocol. The FAR node that accesses the channel transmits at a signal level not exceeding a certain maximum transmit power s^*. This power level, which we call the maximum interference-free transmit power (MIFTP), may be estimated on the basis of signal measurements obtained during the *listen* state. Under the LBT scheme, the maximum duration of the *talk* phase is limited to a certain value $\tau_{\max}$. The value of $\tau_{\max}$ may be fixed or also estimated based on measurements taken during the *listen* state. The interdependencies of the parameters η, $\tau_{\max}$, and s^* are studied in [60].

In [60], a variation of the basic LBT scheme, called *cooperative LBT*, is considered. In collaborative LBT, a group of FAR nodes share information obtained during their respective listen states. Each FAR node in the group executes the individual LBT scheme. If at least one FAR node in the group detects the presence of a signal from a primary user, then all of the FAR nodes are alerted and revert to the listen state. By collaborative sharing of information, cooperative LBT can achieve significantly higher capacity gains.

In this work, we take the idea of collaborative spectrum access a step further, by allowing the FAR nodes to share more detailed information obtained from SS measurements. Using such information, the FAR nodes can more accurately estimate the MIFTP values that limit their respective transmit powers during the talk state. In particular, the FAR nodes share SS measurements, as well as their own locations, with each other. It is assumed that the FAR nodes know their own locations via GPS (Global Positioning System) or some type of

self-localization scheme (cf. [63–66]).

3.2.2 Maximum interference-free transmit power

Next, we provide a formal definition for the MIFTP. Consider a FAR node a and a primary transmitter p, which transmits on a given frequency channel γ. We define a spectrum hole with respect to γ for the FAR node a in terms of the maximum power at which the node a can transmit without causing harmful interference to any potential primary receiver or victim node v, within the range of the primary transmitter p. This maximum power level, called the MIFTP, is defined more precisely as the maximum transmit power of node a on a *target frequency channel* γ, such that the probability of interference to any victim node v is less than a prescribed threshold (cf. [60]).

We shall assume that all transmissions are omnidirectional and the signal propagation is governed by a lognormal shadowing model (cf. [67]). All quantities denoting power are expressed in dBm. Hence, the propagation loss between two nodes i and j can be expressed in dB as

$$L_{i,j} = g(d_{i,j}, \epsilon_{i,j}) + W, \tag{3.1}$$

where the function $g(d, \epsilon)$, represents the path loss component, with ϵ denoting the path loss factor. Although in practice, $\epsilon_{i,j}$ depends on the specific propagation condition between nodes i and j (for example, line-of-sight versus non-line-of-sight, indoor versus outdoor, urban versus rural, etc.), throughout this work we shall assume that $\epsilon_{i,j}$ is a fixed known constant, i.e., $\epsilon_{i,j} = \epsilon$. For simplicity, we assume that $g(d, \epsilon) = 10\epsilon \log_{10} d$ and denote it by $g(d)$. More complicated path loss models could be incorporated into our analysis, such as the empirical propagation model (EPM-73) [68], Longley-Rice model [69], or the TIREM (Terrain Integrated Rough Earth Model) [70]. In fact, this would be necessary for practical systems, since the different links involved (primary-primary, primary-secondary, secondary-secondary) are not homogeneous. But here, without loss of generality, we adopt the generic

path loss model to focus on the issue of MIFTP estimation, and our results can be applied to real systems as long as a valid propagation model is used.

We assume that the shadowing noise is a zero mean, Gaussian random variable $W \sim \mathcal{N}(0, \sigma_W^2)$. The received power at node v due to node p is given by

$$R_v = s_p - L_{p,v} = s_p - g(d_{p,v}) + W, \tag{3.2}$$

where s_p is the transmit power of node p. The received power at node v from node a is given by

$$I_v = s_a - L_{a,v} = s_a - g(d_{a,v}) + W, \tag{3.3}$$

where s_a is the transmit power of a.

The *outage probability* of a victim node v with respect to the transmitter p, is the probability that the received power R_v from node p is below a predefined detection threshold $r_{\min}$:

$$P_{\text{out}}(p, v) \triangleq P\left\{R_v < r_{\min}\right\}, \tag{3.4}$$

when p is transmitting. In general, $r_{\min}$ is determined by the primary receiver's structure, noise statistics and QoS.

The *coverage distance* is the maximum distance between the node p and any potential victim node v such that the outage probability does not exceed a predefined threshold $\varepsilon_{\text{cov}} > 0$:

$$d_{\text{cov}}(p) \triangleq \max\left\{d_{p,v} : P_{\text{out}}(p, v) \leq \varepsilon_{\text{cov}}\right\} = g^{-1}\left(s_p - r_{\min} + \sigma_W Q^{-1}(1 - \varepsilon_{\text{cov}})\right), \tag{3.5}$$

where $g^{-1}(\cdot)$ denotes the inverse of $g(\cdot)$ and $Q(x) \triangleq \frac{1}{\sqrt{2\pi}} \int_x^\infty e^{-\frac{t^2}{2}} dt$ denotes the standard Q-function. Note that $d_{\text{cov}}(p)$ depends on s_p, $r_{\min}$, ε_{cov}, σ_W^2 and the path loss function $g(\cdot)$.

We assume that the FAR node knows or can estimate s_p and therefore can evaluate $d_{\text{cov}}(p)$. The circle centered at node p with radius $d_{\text{cov}}(p)$ is the *coverage area* of the transmitter p. Any potential victim node v, which lies outside of coverage area of node p would be oblivious to the interference caused by the FAR node a. The *interference probability* with respect to a given victim node v is the probability that I_v exceeds a predefined interference tolerance threshold $i_{\max}$:

$$P_{\text{int}}(a, v) \triangleq \Pr\{I_v \geq i_{\max}\}, \tag{3.6}$$

when node a is transmitting. This threshold can be set to meet the primary system's interference tolerance policy. Under the lognormal shadowing model (3.1), the interference probability is given by

$$P_{\text{int}}(a, v) = Q\left(\frac{i_{\max} - s_a + g(d_{a,v})}{\sigma_W}\right). \tag{3.7}$$

For a fixed primary transmitter p and FAR node a, the *MIFTP* is the maximum transmit power of the FAR node such that the interference probability with respect to any potential victim node within the coverage distance from node p does not exceed a threshold $\varepsilon_{\text{int}} > 0$:

$$s_a^* \triangleq \max\{s_a : P_{\text{int}}(a, v) \leq \varepsilon_{\text{int}}, \forall v : d_{p,v} \leq d_{\text{cov}}(p)\}. \tag{3.8}$$

Alternatively, the MIFTP can be defined in terms of the worst-case interference probability:

$$P_{\text{int}}(a) = \sup_v P_{\text{int}}(a, v) = Q\left(\frac{i_{\max} - s_a + g(d_a^*)}{\sigma_W}\right), \tag{3.9}$$

where $d_a^* \triangleq d_{p,a} - d_{\text{cov}}(p)$ is called the *critical distance* for the FAR node a with respect to the primary transmitter p and the supremum is taken over all potential victim nodes v

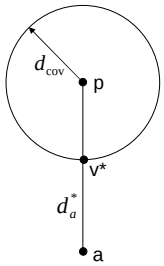

Figure 3.1: FAR node a outside coverage area of primary transmitter p.

such that $d_{p,v} \leq d_{\text{cov}}(p)$. Then

$$s_a^* = \max\{s_a : P_{\text{int}}(a) \leq \varepsilon_{\text{int}}\}.$$

Proposition 1. *The MIFTP is given by*[3]

$$s_a^* = \begin{cases} i_{max} + g(d_a^*) - \sigma_W Q^{-1}(\varepsilon_{int}), & \textit{if } d_{p,a} > d_{\text{cov}}(p), \\ -\infty, & \textit{otherwise.} \end{cases} \tag{3.10}$$

Proof. If the FAR node a lies within the coverage area of node p, i.e., if $d_{p,a} \leq d_{\text{cov}}$, a victim node v can be placed arbitrarily close to node a within the coverage area. Hence, there is no positive value of s_a at which the FAR node could transmit without causing harmful interference to potential victim nodes lying within the coverage area. This implies that the MIFTP, s_a^*, is zero in this case.

If the FAR node lies outside the coverage area of node p (see Fig. 3.1), then $d_{p,a} > d_{\text{cov}}(p)$. In this case, the minimum distance to a potential victim node lying within the coverage area is given by

$$d_a^* = d_{p,a} - d_{\text{cov}}(p).$$

To avoid causing harmful interference to victim nodes lying within the coverage area of

[3]When $s_a^* = -\infty$, the FAR node should not attempt to transmit on the target frequency channel.

node p, the transmit power, s_a, of the FAR node a must be such that the condition in (3.8) is satisfied. Using (3.3), we find that this is equivalent to requiring that

$$s_a \leq i_{\max} + g(d_a^*) - \sigma_W Q^{-1}(\varepsilon_{\text{int}}). \tag{3.11}$$

□

3.2.3 Role of localization

Our proposed scheme for discovering spectrum holes is based on localizing the primary transmitters and using the location estimates to approximate the MIFTP. Localization in this context differs from more conventional scenarios (cf. [71]) in two respects: (1) The FAR nodes collaboratively localize the primary transmitter. (2) No cooperation is assumed between the FAR node and the primary transmitter. For the purpose of spectrum hole estimation, localization techniques based on the SS and angle-of-arrival (AOA) information are more appropriate than time-of-arrival (TOA) or time-difference-of-arrival (TDOA) methods. This is because in the noncooperative scenario, knowledge of the transmit waveform, which is required to extract the TOA information, is typically not available or difficult to obtain. For TDOA estimation, the conventional generalized cross-correlation method can be very demanding. This is because even for a single TDOA estimate, the received (digitized) signals at two nodes need to be transmitted to a common site for processing, [72] p. 54. Since antenna arrays needed to collect AOA measurements, are expensive and can be difficult to deploy, we only consider location estimation using SS in this chapter.

3.3 Signal Strength-based Localization

3.3.1 Canonical Signal Strength Model

Let P_T denote the total signal power received at a FAR node located at position (x, y). Let (x_p, y_p) denote the location of the primary transmitter. The total received signal power

consists of two components:

$$P_T = P_r + P_n, \tag{3.12}$$

where P_r is the received signal power from the primary transmitter and P_n denotes the noise power. The noise power P_n is primarily due to thermal noise power at the receiver, which generally does not depend on the location of the receiver. Even if other sources of noise are present, it is reasonable to assume that the total noise power P_n is constant for short periods of time and hence can be estimated in advance. Therefore, we shall assume that the signal power P_r in (3.12) can be obtained directly from measurements.

The signal power P_r can be modeled as follows:

$$P_r = k10^{\frac{s_p}{10}} \frac{G^2\Gamma}{d^\epsilon}, \tag{3.13}$$

where s_p is the transmitted power from the primary transmitter (measured in dBW or dBm), $d = \sqrt{(x-x_p)^2 + (y-y_p)^2}$ is the distance between the transmitter and the FAR node, ϵ is the path loss factor, G is a random variable that captures the effect of multipath or fast fading, Γ is a random variable that captures the effect of shadowing or slow fading, and k is given by $k = \frac{g_t g_r}{4\pi}$, where g_t and g_r are the antenna gains of the transmitter and receiver, respectively. The fast fading parameter G is modeled either as a Rayleigh or as a Rician random variable, while the slow fading parameter Γ is modeled by a lognormal distribution. In units of dBW, (3.13) can be written as:

$$P_r = z + \kappa + 10\log_{10}\Gamma + 10\log_{10} k, \tag{3.14}$$

where $z = s_p - 10\epsilon\log_{10} d$ and $\kappa = 20\log_{10} G$. The fast fading term κ varies in time on

a short time-scale. By averaging the received power over a given time interval, the time-averaged version of (3.14) can be written as

$$\overline{P}_r = z + \bar{\kappa} + 10\log_{10}\Gamma + 10\log_{10} k, \tag{3.15}$$

where $\bar{\kappa}$ is the time-average of the fast fading component κ.

Let us assume that the transmitter power s_p, the time-averaged fast fading component $\bar{\kappa}$, the term $E[10\log_{10}\Gamma] + 10\log_{10} k$, and the path loss factor ϵ are known. The basic observation equation for SS-based localization can then be written as follows:

$$S = z + W, \tag{3.16}$$

where the "observed" signal strength S is defined by

$$S \triangleq \overline{P}_r - \bar{\kappa} - E[10\log_{10}\Gamma] - 10\log_{10} k, \tag{3.17}$$

and W is a zero-mean Gaussian random variable with variance $\sigma_W^2 = \mathrm{Var}[10\log_{10}\Gamma]$.

We assume that the location and transmit power of the primary transmitter is constant during an observation period. Now suppose that a set of uncorrelated observed SS measurements, $\{S_1, \cdots, S_N\}$, is available, together with a corresponding set of position coordinates $\{\boldsymbol{L}_1, \cdots, \boldsymbol{L}_N\}$, where $\boldsymbol{L}_i = [x_i, y_i]^T$, $i = 1, \cdots, N$. The set of observables,

$$\mathcal{O} \triangleq \{(S_i, \boldsymbol{L}_i) : i = 1, \cdots, N\},$$

may be obtained in several ways. For example, consider a scenario in which N FAR nodes, located at positions $\boldsymbol{L}_1, \cdots, \boldsymbol{L}_N$, collect the SS observables $S_1, \cdots, S_N$ at a given observation window. The FAR nodes exchange their observables among each other, such that at least one of the FAR nodes receives the entire set $\mathcal{O}$. Such a FAR node can then compute an estimate $\hat{\boldsymbol{L}} = [\hat{X}_p, \hat{Y}_p]^T$ of the location of the primary transmitter. Alternatively, the

observable set $\mathcal{O}$ may be obtained by measurements from a single FAR node at N different points in time along a trajectory as the node moves in the coverage area. In general, a given observable $(S_i, \boldsymbol{L}_i)$ may be obtained either from a measurement taken by the FAR node itself in the past, or from a measurement by another FAR node, which shares this information with the given FAR node.

Given a set of observations, $\mathcal{O}$, the observation equations can be written in vector form as follows:

$$\boldsymbol{S} = \boldsymbol{z} + \boldsymbol{W}, \tag{3.18}$$

where

$$\boldsymbol{S} = [S_1, \cdots, S_N]^T, \ \boldsymbol{z} = [z_1, \cdots, z_N]^T, \ \boldsymbol{W} = [W_1, \cdots, W_N]^T, \tag{3.19}$$

with

$$z_i = s_p - 10\epsilon \log_{10} d_i \text{ and } d_i = \sqrt{(x_i - x_p)^2 + (y_i - y_p)^2}. \tag{3.20}$$

It will be convenient to define $\boldsymbol{d} = [d_1, \cdots, d_N]^T$, such that $\boldsymbol{z} = s_p\mathbf{1} - 10\epsilon \log_{10} \boldsymbol{d}$, where $\mathbf{1}$ is a $N \times 1$ vector of all ones. An estimate $\hat{\boldsymbol{L}}$ of the location of the primary transmitter can be obtained from the SS observation equation (3.18).

3.3.2 Cramér-Rao bound

The CRB provides a lower bound on the variance (or covariance matrix) of any unbiased estimate of an unknown parameter. For the SS localization model of (3.18) , the CRB of any unbiased estimate $\hat{\boldsymbol{L}}$ of $\boldsymbol{L}$ is given by

$$E_{\boldsymbol{L}}[(\hat{\boldsymbol{L}} - \boldsymbol{L})(\hat{\boldsymbol{L}} - \boldsymbol{L})^T] \geq \boldsymbol{J}_{\boldsymbol{L}}^{-1}, \tag{3.21}$$

where $E_{\boldsymbol{L}}[\cdot]$ denotes conditional expectation with respect to $\boldsymbol{L}$ and $\boldsymbol{J_L}$ is the Fisher information matrix (FIM) given by

$$\boldsymbol{J_L} = E_{\boldsymbol{L}}\left[\frac{\partial}{\partial \boldsymbol{L}} \ln f_{\boldsymbol{S}|\boldsymbol{L}}(\boldsymbol{S}) \left(\frac{\partial}{\partial \boldsymbol{L}} \ln f_{\boldsymbol{S}|\boldsymbol{L}}(\boldsymbol{S})\right)^T\right], \tag{3.22}$$

where $f_{\boldsymbol{S}|\boldsymbol{L}}(\boldsymbol{S})$ is the likelihood function. In (3.21), the matrix inequality $\boldsymbol{A} \geq \boldsymbol{B}$ should be interpreted as the assertion that the matrix $\boldsymbol{A} - \boldsymbol{B}$ is non-negative definite. The CRB provides a lower bound on the mean-squared errors for the components of $\boldsymbol{L}$.

The FIM can be expressed as follows:

$$\boldsymbol{J_L} = \left(\frac{10\epsilon}{\sigma_W \ln 10}\right)^2 \boldsymbol{H}\boldsymbol{D}^2\boldsymbol{H}^T, \tag{3.23}$$

where

$$\boldsymbol{H} \triangleq \begin{bmatrix} \cos\phi_1 & \cos\phi_2 & \cdots & \cos\phi_N \\ \sin\phi_1 & \sin\phi_2 & \cdots & \sin\phi_N \end{bmatrix}, \tag{3.24}$$

$$\boldsymbol{D} \triangleq \text{diag}\left[d_1^{-1}, \cdots, d_N^{-1}\right], \tag{3.25}$$

and

$$\phi_i = \tan^{-1}\left(\frac{y_p - y_i}{x_p - x_i}\right), \quad i = 1, \cdots, N, \tag{3.26}$$

is the angle between x-axis and the line connecting (x_i, y_i) and (x_p, y_p), measured counter-clockwise. Here diag[$\cdot$] denotes a diagonal matrix. The expression (3.23) can be derived by essentially following the derivation of FIM given in [71] for TOA-based localization.

The CRB $\boldsymbol{J_L}^{-1}$ provides a lower bound on the mean squared error (MSE) of the unbiased estimate $\hat{\boldsymbol{L}} = [\hat{X}_p, \hat{Y}_p]^T$. We denote this quantity as $\mathcal{E}_{\hat{\boldsymbol{L}}}(\boldsymbol{L})$, which can be expressed in

closed-form:

$$\mathcal{E}_{\hat{\boldsymbol{L}}}(\boldsymbol{L}) = \frac{2\left(\frac{\sigma_W \ln 10}{10\epsilon}\right)^2 \sum_{i=1}^{N} d_i^{-2}}{\sum_{i=1}^{N}\sum_{j=1}^{N} d_i^{-2} d_j^{-2} \sin^2(\phi_i - \phi_j)}. \tag{3.27}$$

We write $\mathcal{E}_{\hat{\boldsymbol{L}}}(\boldsymbol{L})$ to denote the lower bound on the MSE of $\hat{\boldsymbol{L}}$ as a function of $\boldsymbol{L}$. It can be shown (cf. [71, 73]) that the CRB is achieved by the maximum likelihood estimator (MLE) asymptotically as $\sigma_W^2 \to 0$. We denote the MLE by $\hat{\boldsymbol{L}}_{\mathrm{ML}}$.

3.3.3 Unknown Transmit Power

Up to this point, we have assumed that the transmit power s_p of the primary transmitter is known. In reality, s_p is more likely to be unknown, since no cooperation between the FAR node and the primary transmitter is assumed. In the *noncooperative* localization scenario, in addition to s_p, the antenna parameters of the transmitter are treated as unknowns. We lump all of these unknown parameters into s_p, such that s_p represents the model uncertainty due to the transmitter characteristics, instead of representing just the transmit power [74]. The key parameters of the propagation environment, namely, ϵ and σ_W, may also be treated as unknowns and can be estimated separately [75, 76]. For the ease of exposition and in order to focus on the localization issue, we treat the transmit power as the only unknown quantity of the model besides the transmitter location. In this section, we assume that s_p is a deterministic unknown quantity which is to be estimated by the FAR node along with the primary transmitter's location $\boldsymbol{L} = [x_p, y_p]^T$. The parameter vector of interest and its estimator are denoted by

$$\boldsymbol{\Theta} = [x_p, y_p, s_p]^T \text{ and } \hat{\boldsymbol{\Theta}} = [\hat{X}_p, \hat{Y}_p, \hat{S}_p]^T,$$

respectively.

Next, we show that for the SS model of (3.18), the MLE of $\boldsymbol{\Theta}$ can be approximated as

an unbiased estimate that achieves the CRB under certain conditions. The CRB for $\boldsymbol{\Theta}$ is given by

$$E_{\boldsymbol{\Theta}}[(\boldsymbol{\Theta}-\hat{\boldsymbol{\Theta}})(\boldsymbol{\Theta}-\hat{\boldsymbol{\Theta}})^T] \geq \boldsymbol{J}_{\boldsymbol{\Theta}}^{-1},$$

where the FIM $\boldsymbol{J}_{\boldsymbol{\Theta}}$ is defined as

$$\boldsymbol{J}_{\boldsymbol{\Theta}} = E_{\boldsymbol{\Theta}}\left[\frac{\partial}{\partial \boldsymbol{\Theta}} \ln f_{\boldsymbol{S}|\boldsymbol{\Theta}}(\boldsymbol{S}) \left(\frac{\partial}{\partial \boldsymbol{\Theta}} \ln f_{\boldsymbol{S}|\boldsymbol{\Theta}}(\boldsymbol{S})\right)^T\right], \tag{3.28}$$

and $f_{\boldsymbol{S}|\boldsymbol{\Theta}}(\boldsymbol{S})$ denotes the likelihood function.

The next proposition gives a closed-form expression for the FIM, analogous to (3.23).

Proposition 2. *The FIM is given by*

$$\boldsymbol{J}_{\boldsymbol{\Theta}} = \frac{1}{\sigma_W^2}\boldsymbol{B}\boldsymbol{G}\boldsymbol{D}^2\boldsymbol{G}^T\boldsymbol{B}, \tag{3.29}$$

where $\boldsymbol{D}$ is given by (3.25),

$$\boldsymbol{B} \triangleq diag\left[\frac{-10\epsilon}{\ln 10}, \frac{-10\epsilon}{\ln 10}, 1\right], \tag{3.30}$$

$$\boldsymbol{G} \triangleq \begin{bmatrix} \cos\phi_1 & \cdots & \cos\phi_N \\ \sin\phi_1 & \cdots & \sin\phi_N \\ d_1 & \cdots & d_N \end{bmatrix}. \tag{3.31}$$

A proof of (3.29) is given in Appendix A.1.

By multiplying out the matrices in (3.29) we can rewrite the FIM as

$$\boldsymbol{J}_{\boldsymbol{\Theta}} = \begin{bmatrix} \boldsymbol{J}_{\boldsymbol{L}} & \boldsymbol{a} \\ \boldsymbol{a}^T & \frac{N}{\sigma_W^2} \end{bmatrix}, \tag{3.32}$$

where $\boldsymbol{J_L}$ denotes the FIM as defined in (3.23) and

$$\boldsymbol{a} \triangleq -\frac{10\epsilon}{\sigma_W^2 \ln 10}\left[\sum_{i=1}^{N}\frac{\cos\phi_i}{d_i}, \sum_{i=1}^{N}\frac{\sin\phi_i}{d_i}\right]^T.$$

Using the matrix inversion formula (see [77], p. 33), we have

$$\boldsymbol{J}_{\boldsymbol{\Theta}}^{-1} = \begin{bmatrix} \boldsymbol{J}_{\boldsymbol{L}}^{-1} + b^{-1}\boldsymbol{c}\boldsymbol{c}^T & -b^{-1}\boldsymbol{c} \\ -b^{-1}\boldsymbol{c}^T & b^{-1} \end{bmatrix}, \tag{3.33}$$

where

$$b \triangleq \frac{N}{\sigma_W^2} - \boldsymbol{a}^T\boldsymbol{J}_{\boldsymbol{L}}^{-1}\boldsymbol{a} \tag{3.34}$$

and $\boldsymbol{c} \triangleq \boldsymbol{J}_{\boldsymbol{L}}^{-1}\boldsymbol{a}$, assuming that $\boldsymbol{J}_{\boldsymbol{L}}^{-1}$ exists. From $\boldsymbol{J}_{\boldsymbol{\Theta}}^{-1}$ we can get lower bounds on the MSE of the primary transmitter's transmit power and position. We denote these two quantities as $\mathcal{E}_{\hat{S}_p}(\boldsymbol{\Theta})$ and $\mathcal{E}_{\hat{\boldsymbol{L}}}(\boldsymbol{\Theta})$, respectively, where

$$\mathcal{E}_{\hat{S}_p}(\boldsymbol{\Theta}) = \left[\boldsymbol{J}_{\boldsymbol{\Theta}}^{-1}\right]_{(3,3)} = b^{-1}, \tag{3.35}$$

and

$$\mathcal{E}_{\hat{\boldsymbol{L}}}(\boldsymbol{\Theta}) = \left[\boldsymbol{J}_{\boldsymbol{\Theta}}^{-1}\right]_{(1,1)} + \left[\boldsymbol{J}_{\boldsymbol{\Theta}}^{-1}\right]_{(2,2)} = \mathrm{Tr}(\boldsymbol{J}_{\boldsymbol{L}}^{-1} + b^{-1}\boldsymbol{c}\boldsymbol{c}^T) = \mathcal{E}_{\hat{\boldsymbol{L}}}(\boldsymbol{L}) + \mathcal{E}_{\hat{S}_p}(\boldsymbol{\Theta})\mathrm{Tr}(\boldsymbol{c}\boldsymbol{c}^T), \tag{3.36}$$

where $\mathcal{E}_{\hat{\boldsymbol{L}}}(\boldsymbol{L})$ denotes the lower bound on the MSE of the primary transmitter's position estimate given in (3.27).

We note that for any non-zero $\boldsymbol{a}$, $\mathrm{Tr}(\boldsymbol{c}\boldsymbol{c}^T) > 0$. Therefore, $\mathcal{E}_{\hat{\boldsymbol{L}}}(\boldsymbol{\Theta}) > \mathcal{E}_{\hat{\boldsymbol{L}}}(\boldsymbol{L})$ and the position estimation accuracy degrades by $\mathcal{E}_{\hat{S}_p}(\boldsymbol{\Theta})\mathrm{Tr}(\boldsymbol{c}\boldsymbol{c}^T)$. Since estimating more parameters can only increase the bound on the variance (cf. [78], p. 232), this is the price we pay for

estimating the extra parameter s_p. We write $\mathcal{E}_{\hat{S}_p}(\boldsymbol{\Theta})$ and $\mathcal{E}_{\hat{\boldsymbol{L}}}(\boldsymbol{\Theta})$ to denote the lower bound on the MSE of $\hat{S}_p$ and $\hat{\boldsymbol{L}}$, respectively, given as a function of $\boldsymbol{\Theta}$.

Proposition 3. *For sufficiently small σ_W,*

$$f_{\hat{\boldsymbol{\Theta}}|\boldsymbol{\Theta}}(\hat{\boldsymbol{\Theta}}) \propto \exp\left\{-\frac{1}{2}(\hat{\boldsymbol{\Theta}}-\boldsymbol{\Theta})^T \boldsymbol{J}_{\boldsymbol{\Theta}}(\hat{\boldsymbol{\Theta}}-\boldsymbol{\Theta})\right\}, \tag{3.37}$$

which shows that $\hat{\boldsymbol{\Theta}}$ is a multivariate Gaussian random variable with mean $E_{\boldsymbol{\Theta}}[\hat{\boldsymbol{\Theta}}] = \boldsymbol{\Theta}$.

A proof is given in Appendix A.2.

In Appendix A.3, we show that

$$\frac{\partial}{\partial \boldsymbol{\Theta}} \ln f_{\boldsymbol{S}|\boldsymbol{\Theta}}(\boldsymbol{S}) = \boldsymbol{J}_{\boldsymbol{\Theta}}(\hat{\boldsymbol{\Theta}}-\boldsymbol{\Theta}), \tag{3.38}$$

i.e., the estimation error vector is a linear function of the score function $\frac{\partial}{\partial \boldsymbol{\Theta}} \ln f_{\boldsymbol{S}|\boldsymbol{\Theta}}(\boldsymbol{S})$. Assuming that an unbiased estimate exists, a well-known result in estimation theory [79] allows us to conclude that the CRB is achieved by the MLE, which we denote by $\hat{\boldsymbol{\Theta}}_{\mathrm{ML}}$. Since an unbiased estimate exists for sufficiently small shadowing noise variance, we can conclude that the CRB is achieved by $\hat{\boldsymbol{\Theta}}_{\mathrm{ML}}$ asymptotically, as $\sigma_W^2 \to 0$.

3.4 Approximation for MIFTP

The true MIFTP, as given in Proposition 1, cannot be calculated directly, since the true location, $\boldsymbol{L} = [x_p, y_p]^T$, of the primary transmitter p is unknown. In this section, we derive an approximation for the MIFTP for the case when the transmit power is known as well as the case in which it is unknown.

3.4.1 Known transmit power

Assume first that the transmit power s_p of the primary transmitter is a known constant. Let $\hat{\boldsymbol{L}}_{\mathrm{ML}} = [\hat{X}_p, \hat{Y}_p]^T$ denote the MLE of $\boldsymbol{L}$. Given a set of $N \geq 3$ independent SS measurements from the primary transmitter, obtained by the FAR nodes, $\hat{\boldsymbol{L}}_{\mathrm{ML}}$ provides an unbiased estimate of $\boldsymbol{L}$ as the shadowing noise tends to zero; i.e., $\hat{\boldsymbol{L}}_{\mathrm{ML}}$ is asymptotically *efficient* as $\sigma_W^2 \to 0$. As discussed in Section 3.3.2, in this asymptotic regime, the mean squared error of $\hat{\boldsymbol{L}}_{\mathrm{ML}}$ achieves the CRB, which we denote by $\boldsymbol{J}_{\boldsymbol{L}}^{-1}$.

Suppose that the FAR node a is located at $\boldsymbol{L}_a = [x_a, y_a]^T$. Given $\hat{\boldsymbol{L}}_{\mathrm{ML}}$, the MLE for the distance $d_{p,a}$, denoted by $\hat{D}_{p,a}$, can be obtained by applying the invariance principle (cf. [78], p. 217), which states that the MLE of a function $h(\cdot)$ of $\boldsymbol{L}$ is given by $h(\hat{\boldsymbol{L}})$, where $\hat{\boldsymbol{L}}$ denotes the MLE of $\boldsymbol{L}$. Hence, we obtain

$$\hat{D}_{p,a} = \sqrt{\left(\hat{X}_p - x_a\right)^2 + \left(\hat{Y}_p - y_a\right)^2}. \tag{3.39}$$

Proposition 4. *In the asymptotic regime $\sigma_W^2 \to 0$, the MLE $\hat{D}_{p,a}$ achieves the associated CRB, given by*

$$J_{p,a}^{-1} \triangleq \boldsymbol{H}_{p,a}^T \boldsymbol{J}_{\boldsymbol{L}}^{-1} \boldsymbol{H}_{p,a}, \tag{3.40}$$

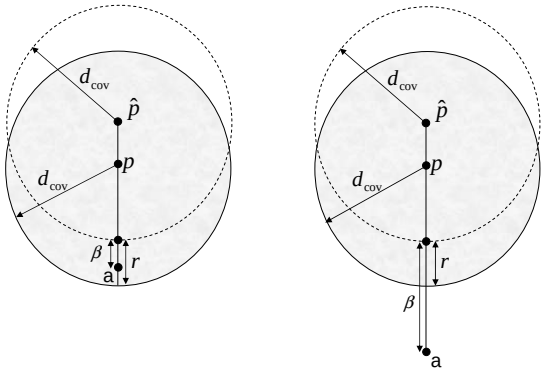

(a) $|r| > \beta$ (b) $|r| < \beta$

Figure 3.2: Illustration of relationship between r and β. If $0 < |r| < \beta$, $s_a^* \neq -\infty$. Otherwise, $s_a^* = -\infty$.

where

$$\boldsymbol{H}_{p,a} \triangleq [\cos\phi_{p,a},\ \ \sin\phi_{p,a}]^T,\ \ \phi_{p,a} = \tan^{-1}\left(\frac{y_p - y_a}{x_p - x_a}\right).$$

A proof is given in Appendix A.4.

Let $E_{p,a} \triangleq \hat{D}_{p,a} - d_{p,a}$ denote the estimation error of $\hat{D}_{p,a}$. Proposition 4 implies that in the asymptotic regime $\sigma_W^2 \to 0$, $E_{p,a}$ is Gaussian with zero mean and variance $J_{p,a}^{-1}$, i.e.,

$$E_{p,a} \sim \mathcal{N}\left(0, J_{p,a}^{-1}\right). \tag{3.41}$$

Define $\beta \triangleq \hat{D}_{p,a} - d_{\text{cov}}(p)$. Suppose $E_{p,a} = r$. If $|r| \geq \beta > 0$, then in the worst case, the FAR node lies within $d_{\text{cov}}(p)$ of the true primary transmitter p (see Fig. 3.2(a)). In this scenario, the FAR node must not transmit, i.e., $s_a^* = -\infty$, to avoid potentially harmful interference to the victim nodes. If $0 < |r| < \beta$, then the FAR can transmit with positive power, i.e., $s_a^* \neq -\infty$ (see Fig. 3.2(b)).

Proposition 5. *Under the assumption (3.41) and for* $|r| \leq 0.993\beta$*, the interference probability conditioned on* $E_{p,a}$ *is upper bounded as follows:*

$$P_{int}(a, v|E_{p,a} = r) \leq Q(b_1 + b_2|r|), \tag{3.42}$$

where

$$b_1 \triangleq \frac{i_{max} + 10\epsilon \log_{10} \beta - s_a}{\sigma_W},\ b_2 \triangleq -\frac{50\epsilon}{\beta\sigma_W \ln 10}. \tag{3.43}$$

A proof is given in Appendix A.5.

Requiring that $s_a \neq -\infty$, we obtain

$$P_{\text{int}}(a, v) = \int_{-\beta}^{\beta} P_{\text{int}}(a, v|E_{p,a} = r) f_{E_{p,a}}(r) dr,$$

where $f_{E_{p,a}}(r)$ denotes the probability density function (pdf) of $E_{p,a}$. We can then show that

$$P_{\text{int}}(a, v) \leq \int_{-\infty}^{\infty} Q(b_1 + b_2 r) \frac{1}{\sqrt{2\pi J_{p,a}^{-1}}} \exp\left\{-\frac{r^2}{2J_{p,a}^{-1}}\right\} dr = Q\left(\frac{b_1}{\sqrt{1 + b_2^2 J_{p,a}^{-1}}}\right),$$

where the last equality can be found in [80], p. 102.

To obtain an expression for the MIFTP, we require the FAR node transmitter power, s_a, to satisfy

$$Q\left(\frac{b_1}{\sqrt{1 + b_2^2 J_{p,a}^{-1}}}\right) \leq \varepsilon_{\text{int}},$$

which implies

$$s_a \leq i_{\max} + 10\epsilon \log_{10} \beta - \sigma_W \sqrt{1 + \left(\frac{50\epsilon}{\beta \sigma_W \ln 10}\right)^2 J_{p,a}^{-1}} \cdot Q^{-1}(\varepsilon_{\text{int}}). \tag{3.44}$$

The right-hand side of (3.44) provides an approximation for the MIFTP, but since the true CRB of $\hat{D}_{p,a}$, i.e., $J_{p,a}^{-1}$ is unknown, we replace it with the MLE of $J_{p,a}^{-1}$, which is denoted by $\hat{J}_{p,a}^{-1}$. This is justified by the invariance principle mentioned earlier and also illustrated in Section 3.5 in our numerical studies.

Recall that for $s_a^* \neq -\infty$, we require that a particular realization of the random variable $E_{p,a} = r$, satisfy the worst case scenario $0 < |r| < \beta$. Since we do not know r, we can only ensure that for $\beta > 0$, the event $(|E_{p,a}| < \beta)$ is satisfied with high probability. Particularly, for $s_a^* \neq -\infty$ and $\varepsilon > 0$ (close to 1), we require $\beta > \beta^* > 0$, where

$$\beta^* \triangleq \min\left\{\tilde{\beta} : \Pr(|E_{p,a}| < \tilde{\beta}) \geq \varepsilon\right\} \tag{3.45}$$

$$= \sqrt{J_{p,a}^{-1}} \cdot Q^{-1}\left(\frac{1-\varepsilon}{2}\right). \tag{3.46}$$

For example, for $\varepsilon = 0.9973$, $\beta^* \approx 3\sqrt{J_{p,a}^{-1}}$. Again as before, we replace $J_{p,a}^{-1}$ by $\hat{J}_{p,a}^{-1}$, i.e., we have $\hat{\beta}^* = \sqrt{\hat{J}_{p,a}^{-1}} \cdot Q^{-1}\left(\frac{1-\varepsilon}{2}\right)$. A derivation of (3.46) is given in Appendix A.6.

Hence, we obtain the following approximation for the MIFTP:

$$\hat{s}_a = \begin{cases} i_{\max} + 10\epsilon \log_{10} \beta - \sigma_W \sqrt{1 + \left(\frac{50\epsilon}{\beta \sigma_W \ln 10}\right)^2 \hat{J}_{p,a}^{-1}} \cdot Q^{-1}(\varepsilon_{\text{int}}), & \text{if } \beta > \hat{\beta}^* > 0 \\ -\infty, & \text{otherwise.} \end{cases} \tag{3.47}$$

We point out that as the accuracy of the estimate $\hat{D}_{p,a}$ improves, the CRB estimate $\hat{J}_{p,a}^{-1}$

tends to zero and the right-hand side of (3.47) converges to the true MIFTP as given in (3.10). The approximate formula (3.47) for MIFTP requires at least three independent SS measurements, i.e., $N \geq 3$, which should be obtained from FAR nodes in the vicinity of the primary transmitter.

3.4.2 Unknown transmit power

If the primary transmitter power s_p is unknown, it can be estimated together with the location $\boldsymbol{L}$ as a parameter vector $\boldsymbol{\Theta} = [\boldsymbol{L}, s_p]$, as discussed in Section 3.3.3. From that section, we know that the MLE, $\hat{\boldsymbol{\Theta}}_{\mathrm{ML}}$, achieves the CRB asymptotically as $\sigma_W^2 \to 0$. Note that, since $d_{\mathrm{cov}}(p)$ depends on s_p (cf. (3.5)), in this case we need to estimate $d_{\mathrm{cov}}(p)$ as well. Hence it is convenient to work in terms of $\widetilde{\boldsymbol{\Theta}} \triangleq [d_{p,a} \quad d_{\mathrm{cov}}(p)]^T$ and its associated CRB $\boldsymbol{J}_{\widetilde{\boldsymbol{\Theta}}}^{-1}$, instead of $\boldsymbol{\Theta}$ and its associated CRB $\boldsymbol{J}_{\boldsymbol{\Theta}}^{-1}$. Invoking the invariance principle again, we have $\hat{\widetilde{\boldsymbol{\Theta}}}_{\mathrm{ML}} = [\hat{D}_{p,a} \quad \hat{D}_{\mathrm{cov}}(p)]^T$, where $\hat{D}_{p,a} = \sqrt{\left(\hat{X}_p - x_a\right)^2 + \left(\hat{Y}_p - y_a\right)^2}$ and $\hat{D}_{\mathrm{cov}}(p) = g^{-1}(\hat{S}_p - r_{\min} + \sigma_W Q^{-1}(1 - \varepsilon_{\mathrm{cov}}))$.

Define $E_1 \triangleq E_{p,a} - E_{\mathrm{cov}}$, where $E_{p,a} \triangleq \hat{D}_{p,a} - d_{p,a}$ and $E_{\mathrm{cov}} \triangleq \hat{D}_{\mathrm{cov}}(p) - d_{\mathrm{cov}}(p)$.

Proposition 6. *In the asymptotic regime $\sigma_W \to 0$, E_1 can be modeled as $E_1 \sim \mathcal{N}\left(0, J_1^{-1}\right)$, where $J_1^{-1} \triangleq Tr\left(\boldsymbol{J}_{\widetilde{\boldsymbol{\Theta}}}^{-1}\right) - 2\left[\boldsymbol{J}_{\widetilde{\boldsymbol{\Theta}}}^{-1}\right]_{(1,2)}$.*

A proof is given in Appendix A.7.

Define $\beta_1 \triangleq \hat{D}_{p,a} - \hat{D}_{\mathrm{cov}}(p)$. Let $E_{p,a} = r$ and $E_{\mathrm{cov}} = r_0$. The FAR node can transmit with positive power, i.e., $s_a^* \neq -\infty$, if $0 < |r - r_0| < \beta_1$, otherwise $s_a^* = -\infty$ (see Fig. 3.3). Here, the critical distance from the FAR node is given by

$$d_a^* = d_{p,a} - d_{\mathrm{cov}}(p) = \hat{D}_{p,a} - r - (\hat{D}_{\mathrm{cov}}(p) - r_0) = \beta_1 - r_1,$$

where $r_1 \triangleq r - r_0$. We note that here r_1 plays the same role as r of Section 3.4.1. Similarly

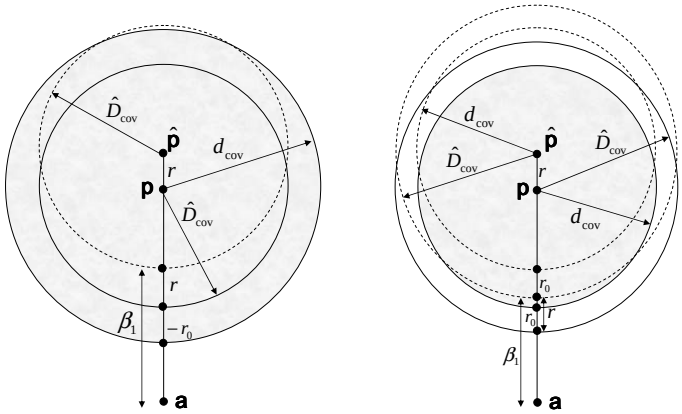

(a) $r_0 = \hat{D}_{cov} - d_{cov} < 0$ (b) $r_0 = \hat{D}_{cov} - d_{cov} > 0$

Figure 3.3: Illustration of relationship between r, r_0, and β. In both cases, $0 < |r - r_0| < \beta_1$, which implies that $s_a^* \neq -\infty$.

as before, for $s_a^* \neq -\infty$ we require $\beta_1 > \beta_1^* > 0$, where $\beta_1^* \triangleq \min\left\{\tilde{\beta}_1 : \Pr(|E_1| < \tilde{\beta}_1) \geq \varepsilon\right\} = \sqrt{J_1^{-1}} \cdot Q^{-1}\left(\frac{1-\varepsilon}{2}\right)$.

Analogous to Proposition 5, we obtain the following result for the case of unknown transmit power.

Proposition 7. *For $|r_1| \leq 0.993\beta_1$, the interference probability conditioned on E_1 is upper bounded as follows:*

$$P_{int}(a, v|E_1 = r_1) \leq Q(b_1 + b_2|r_1|), \tag{3.48}$$

where b_1 and b_2 are given in (3.43).

The proof of Proposition 7 is similar to that of Proposition 5, which is given in Appendix A.5.

Integrating out r_1 in (3.48), we get

$$P_{\text{int}}(a, v) \quad \leq \quad Q\left(\frac{b_1}{\sqrt{1 + b_2^2 J_1^{-1}}}\right), \tag{3.49}$$

which leads to an upper bound on the transmit power s_a by requiring the right-hand side of (3.49) to be less than ε_{int}.

Similarly as before, for $s_a^* \neq -\infty$ we require $\beta_1 > \beta_1^* > 0$, where $\beta_1^* \triangleq \min\left\{\tilde{\beta}_1 : \Pr(|E_1| < \tilde{\beta}_1) \geq \varepsilon\right\} = \sqrt{J_1^{-1}} \cdot Q^{-1}\left(\frac{1-\varepsilon}{2}\right)$. Finally, using the invariance principle we obtain the following approximation for the MIFTP:

$$\hat{s}_a = \begin{cases} i_{\max} + 10\epsilon \log_{10} \beta_1 - \sigma_W \sqrt{1 + \left(\frac{50\epsilon}{\beta_1 \sigma_W \ln 10}\right)^2 \hat{J}_1^{-1}} \cdot Q^{-1}(\varepsilon_{\text{int}}), & \text{if } \beta_1 > \hat{\beta}_1^* > 0, \\ -\infty, & \text{otherwise,} \end{cases} \tag{3.50}$$

where $\hat{\beta}_1^* = \sqrt{\hat{J}_1^{-1}} \cdot Q^{-1}\left(\frac{1-\varepsilon}{2}\right)$.

3.5 Numerical Results

In this section, we present plots of the MIFTP and the approximate MIFTP estimated from SS measurements under a range of parameter settings. We choose our simulation parameters keeping in mind the application to unused digital television broadcast bands operating at the UHF band [81]. We consider two cases: i) the transmit power, s_p, of the primary node, p, is known and the FAR nodes only estimate the location $\boldsymbol{L}$, and ii) s_p is unknown and the FAR nodes estimate s_p along with $\boldsymbol{L}$. The crucial parameters affecting the MIFTP estimation are $d_{p,a}$, s_p, ε_{int}, σ_W, ϵ, N and the CRB $J_{p,a}^{-1}$. We shall assume that the remaining parameters are known constants. Each of the MIFTP values is calculated as an average over 1000 simulation trials and is shown with the associated 95% confidence interval. We set the parameters as follows:

- Detection thresholds for the victim and FAR nodes are $r_{\min} = -83$ and $r_a = -121$ dBm, respectively.
- $\varepsilon_{\text{cov}} = 0.05$, $i_{\max} = -100$ dBm, $\varepsilon_{\text{int}} = 0.01$.

- Standard deviation of shadowing noise, $\sigma_W = 8$ dB.
- Primary node location $\boldsymbol{L} = (50, 50)$ [km].

Five different scenarios are considered below.

3.5.1 Distance $d_{p,a}$

We vary $d_{p,a}$ from 20 to 100 km and position the target FAR node at $\boldsymbol{L}_a = (x_a, y_a)$, where

$$\boldsymbol{L}_a = \boldsymbol{L} + \frac{d_{p,a}}{\sqrt{2}}(1, 1). \tag{3.51}$$

For a given transmit power of the primary transmitter, $s_p = 80$ dBm, we find $d_{\text{det}}(a)$, the *detection distance* of the FAR nodes (cf. [60]). It denotes the radius beyond which the FAR nodes cannot detect the primary signal and is given by $d_{\text{det}}(a) = g^{-1}(s_p - r_a + \sigma_W Q^{-1}(1 - \varepsilon_{\text{cov}}))$, where r_a denotes the FAR node's detection threshold. The *detection region* of a FAR node a is the circular region centered at a with radius d_{det}.

For each simulation trial, we randomly place N FAR nodes, with uniform distribution, inside the circle with radius equal to $d_{\text{det}}(a)$ and centered at $\boldsymbol{L}$. The set of SS measurements to compute the MLE of $\boldsymbol{L}$ or $\boldsymbol{\Theta}$ is collected by these FAR nodes, which can be used by other FAR nodes further away to estimate their MIFTP values. The FAR nodes estimate the MLE of $\boldsymbol{L}$ assuming a fixed path loss factor $\epsilon = 4$, which is a typical value for the shadowed urban cellular radio. Nodes lying outside $d_{\text{sense}}(a)$ use $\hat{\boldsymbol{L}}_{\text{ML}}$ or $\hat{\boldsymbol{\Theta}}_{\text{ML}}$ to estimate MIFTP based on (3.47) or (3.50). To find the ML location and transmit power estimates, we need to solve the following nonlinear optimization problem:

$$\hat{\boldsymbol{L}}_{\text{ML}} = \arg\max_{\boldsymbol{L}} f_{\boldsymbol{S}|\boldsymbol{L}} \qquad \text{or} \qquad \hat{\boldsymbol{\Theta}}_{\text{ML}} = \arg\max_{\boldsymbol{\Theta}} f_{\boldsymbol{S}|\boldsymbol{\Theta}}, \tag{3.52}$$

where $f_{\boldsymbol{S}|\boldsymbol{L}}$ and $f_{\boldsymbol{S}|\boldsymbol{\Theta}}$ denote the likelihood functions conditioned on $\boldsymbol{L}$ and $\boldsymbol{\Theta}$, respectively. To solve this we use the *fmincon* routine of Matlab®, which employs a sequential quadratic

programming method. As the initial location estimate, we choose the midpoint of the rectangle that circumscribes the union of the detection regions of the FAR nodes making the SS measurements. The initial power estimate is set to 60 dBm. Alternatively, one could use the suboptimal estimates given in [46] as the initial starting point of the optimization problem.

Figs. 3.4(a) and 3.4(b) plot the true and estimated MIFTP values vs. $d_{p,a}$ for both known and unknown s_p when $N = 5, 10, 15, 20$. The confidence intervals shown in the plots arise due to randomness in the localizing FAR node positions, as well as the shadowing noise. We see that the accuracy of the approximate MIFTP formula improves with increasing $d_{p,a}$ and increasing N. When $\epsilon = 4$, roughly for $N \geq 10$, the performance degradation due to the estimation of s_p becomes negligible.

We can also calculate the probability of interference, $\hat{P}_{\text{int}}$, which results when the FAR node transmits with power level equal to the MIFTP estimate. Let $\hat{s}_a^i$ denote the MIFTP estimate for the ith simulation trial, $i = 1, \cdots, M$. Then the probability of interference under the MIFTP approximation is given by

$$\hat{P}_{\text{int}} = \frac{1}{M} \sum_{i=1}^{M} P_{\text{int}}(a|\hat{s}_a^i), \tag{3.53}$$

where $P_{\text{int}}(a|\hat{s}_a)$ denotes the interference probability given the FAR node transmit power $\hat{s}_a$ (cf. (3.9)).

Fig. 3.5 shows the plot of $\hat{P}_{\text{int}}$ versus $d_{p,a}$ for $\epsilon = 4$ when s_p is known. We observe that $\hat{P}_{\text{int}}$ increases with increasing $d_{p,a}$, but it is always less than ε_{int}. When s_p is unknown, $\hat{P}_{\text{int}}$ decreases further, since the MIFTP estimate becomes more conservative. In our simulations plotted in Figs. 3.6 and 3.7, we found that the MIFTP values depend strongly on the path loss factor ϵ. For larger values of ϵ, the accuracy of the MIFTP approximation improves significantly and the effect of N decreases. This is because, although the received signal becomes weaker as ϵ increases, the sensitivity of the MIFTP approximation on the location

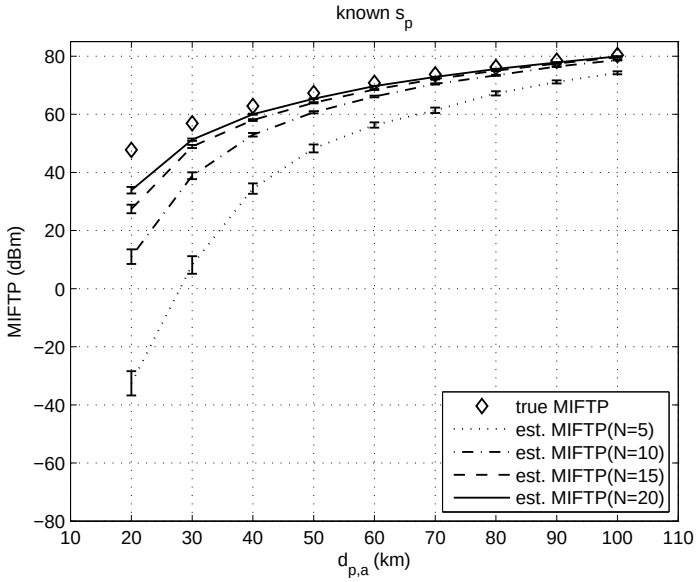

(a) s_p is known.

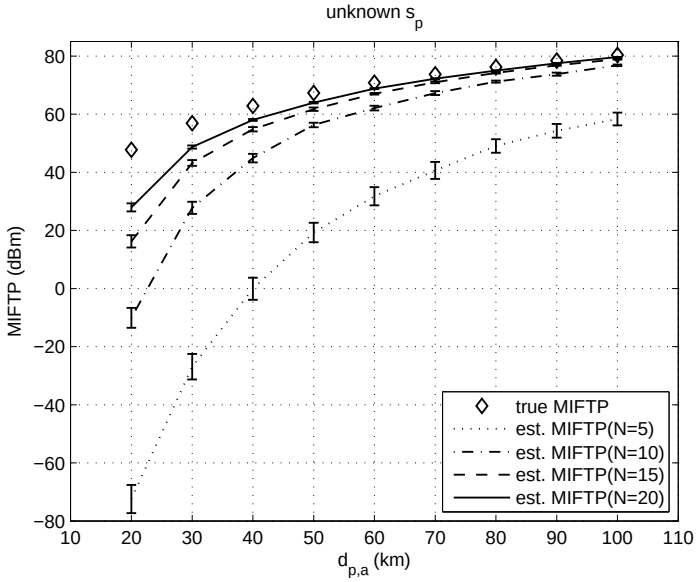

(b) s_p is unknown.

Figure 3.4: MIFTP versus $d_{p,a}$, when $\epsilon = 4$.

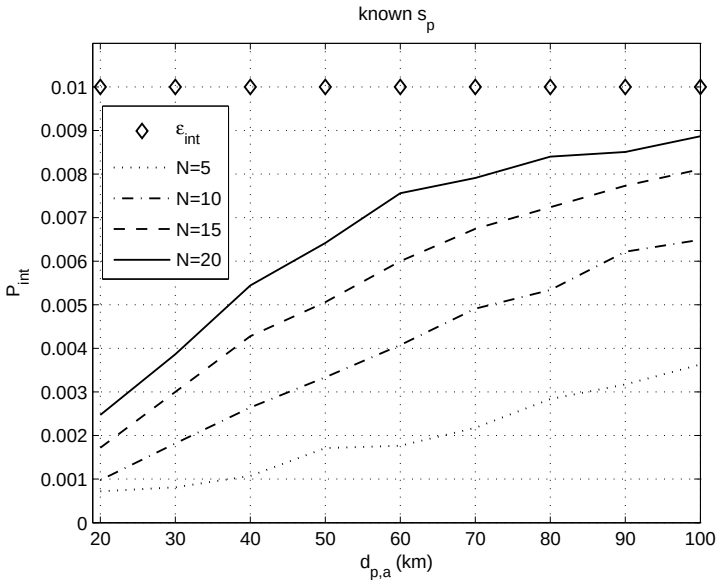

Figure 3.5: $\hat{P}_{\text{int}}$ versus $d_{p,a}$, when $\epsilon = 4$ and s_p is known.

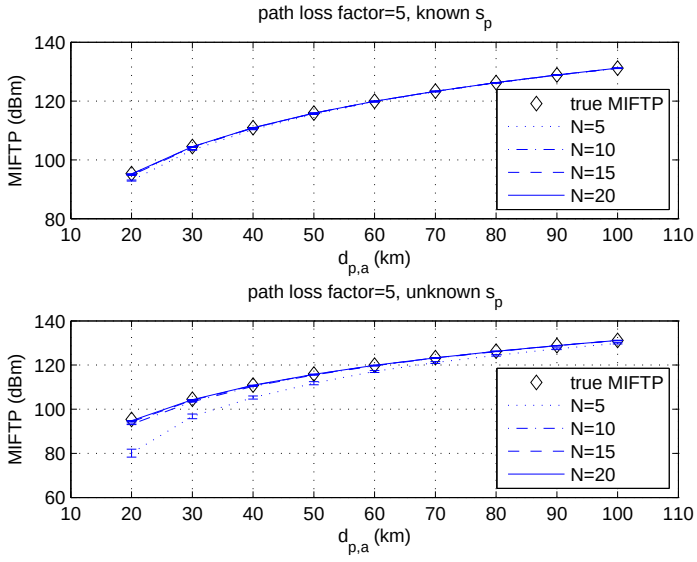

Figure 3.6: MIFTP versus $d_{p,a}$, when $\epsilon = 5$.

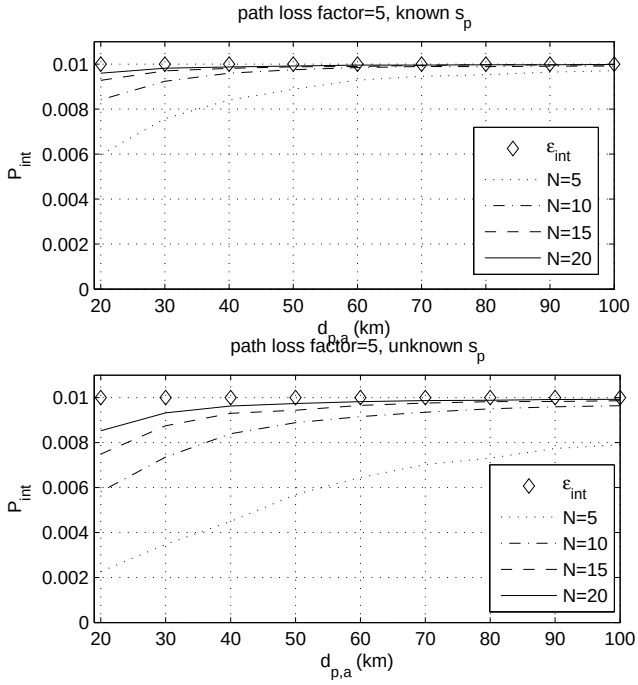

Figure 3.7: $\hat{P}_{\text{int}}$ versus $d_{p,a}$, when $\epsilon = 5$.

estimation error reduces. For $\epsilon = 5$, $\hat{P}_{\text{int}}$ increases as the MIFTP approximation becomes tighter, but always remains smaller than ε_{int}. Therefore, the approximate MIFTP can safely be used by the FAR node as an upper bound on the allowable transmit power.

3.5.2 Interference probability threshold, ε_{int}

In this scenario, we set $\epsilon = 4$, and $d_{p,a} = 50$ km. The location of the FAR node is set according to (3.51) and the values of the other parameters are set as in the previous scenario. For known s_p, Fig. 3.8(a) shows a plot of MIFTP vs. the interference probability threshold, ε_{int}, which is varied from 0.001 to 0.1. The same is repeated in Fig. 3.8(b) for the case of unknown s_p. We have also observed that the MIFTP increases relatively slowly with increasing ε_{int}. Also, the gap between the true and approximate MIFTP values decreases slowly with increasing ε_{int}. For $N \geq 10$, the performance degradation due to estimating the unknown s_p is negligible. We have observed that $\hat{P}_{\text{int}}$ increases almost linearly with

increasing ε_{int}, but is always less than the specified threshold. From Figs. 3.8(a) and 3.8(b), we see that for $N \geq 10$, the MIFTP increases relatively slowly as ε_{int} increases. In particular, the difference between the MIFTP value when $\varepsilon_{\text{int}} = 0.001$ and when $\varepsilon_{\text{int}} = 0.1$ is about 15 dB.

3.5.3 Shadowing noise, σ_W

Here, we set $\varepsilon_{\text{int}} = 0.01$, keep all other parameters as before, and vary σ_W from 4 to 10 dB. From Figs. 3.9(a) and 3.9(b), we see that the MIFTP decreases almost linearly with increasing shadowing noise variance. The gap between the true and approximate MIFTP values does not depend strongly on the shadowing noise. Again, for $N \geq 10$, the performance degradation due to estimating the unknown s_p is negligible. We have also observed that $\hat{P}_{\text{int}}$ does not change appreciably with σ_W and is always less than ε_{int}.

3.5.4 Primary transmit power, s_p

Now, we set $\sigma_W = 8$ dB, and keep all other parameter values as before. Figs. 3.10(a) and 3.10(b) plot the true and approximate MIFTP values as s_p is varied from 20 to 80 dBm, for known and unknown s_p, respectively. We observe that the true MIFTP decreases by only a small amount. The accuracy of the approximate MIFTP formula falls off quickly with increasing s_p when $N \leq 5$. However, increasing N results in a significant improvement in MIFTP accuracy for high values of s_p. We have observed that $\hat{P}_{\text{int}}$ decreases with increasing s_p as the MIFTP approximation becomes looser and is always less than ε_{int}.

3.5.5 Cramér-Rao bound, $J_{p,a}^{-1}$

One of the crucial aspects of the MIFTP approximation is the use of the MLE of the CRB on position, $\hat{J}_{p,a}^{-1}$, instead of the true one, $J_{p,a}^{-1}$. Here, we look at the effect of this substitution by plotting in Fig. 3.11, the square root of $J_{p,a}^{-1}$ and the square root of its associated MLE $\hat{J}_{p,a}^{-1}$ as a function of σ_W for $N = 10, 15, 20$. As before, we fix $d_{p,a} = 50$ km and randomly place

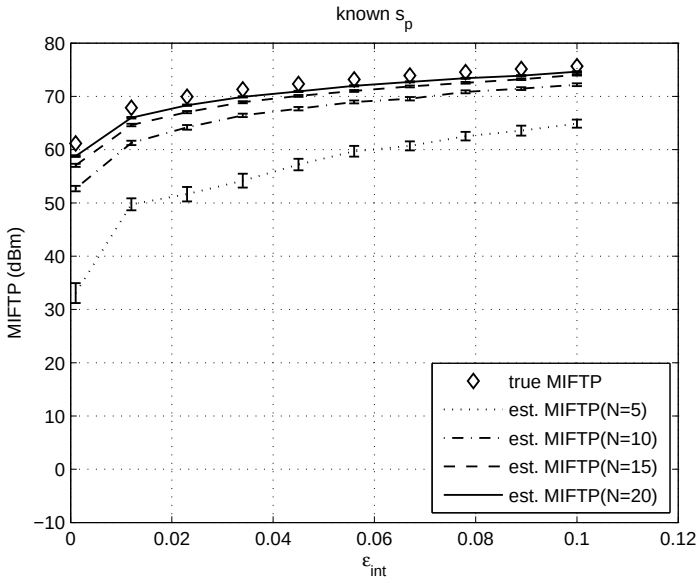

(a) s_p is known.

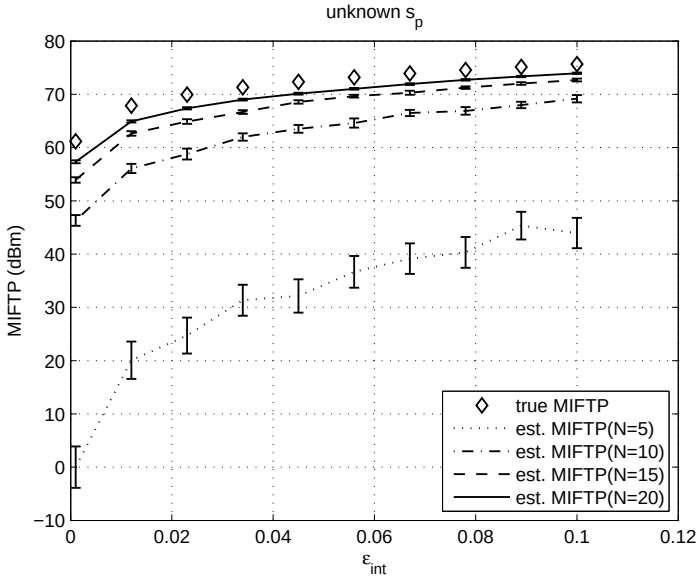

(b) s_p is unknown.

Figure 3.8: MIFTP versus ε_{int}, when $\epsilon = 4$.

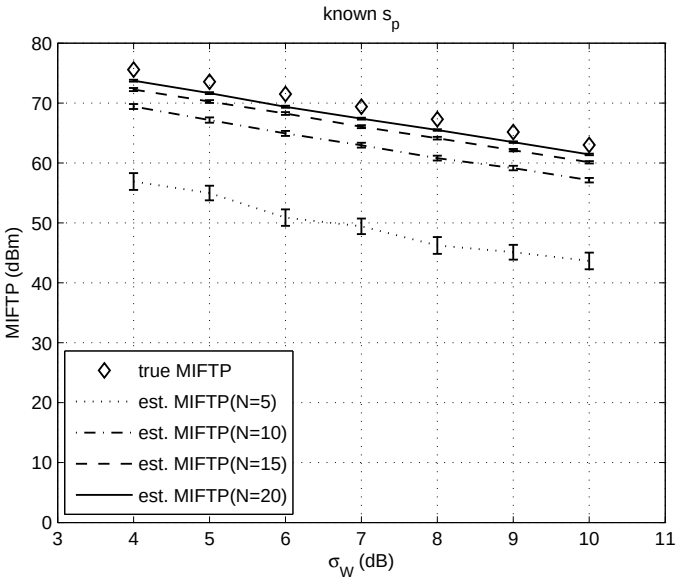

(a) s_p is known.

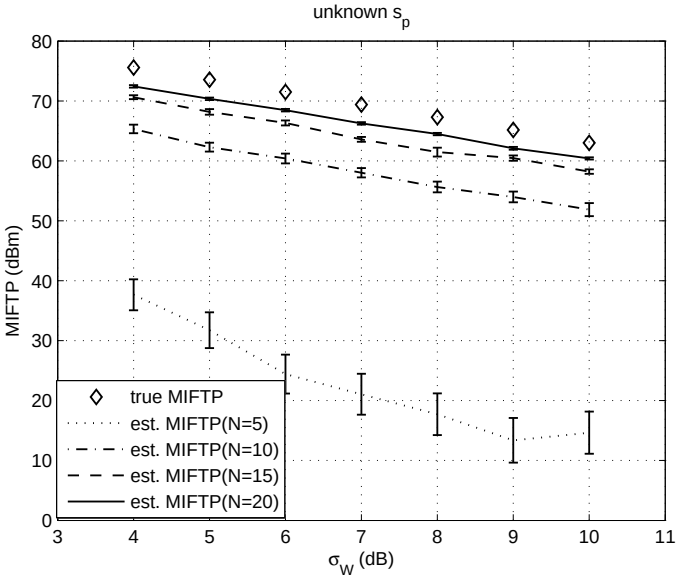

(b) s_p is unknown.

Figure 3.9: MIFTP versus σ_W, when $\epsilon = 4$.

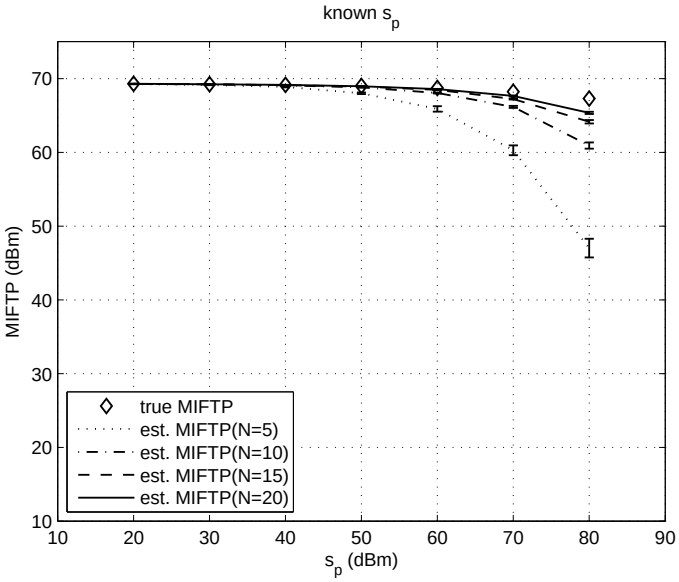

(a) s_p is known.

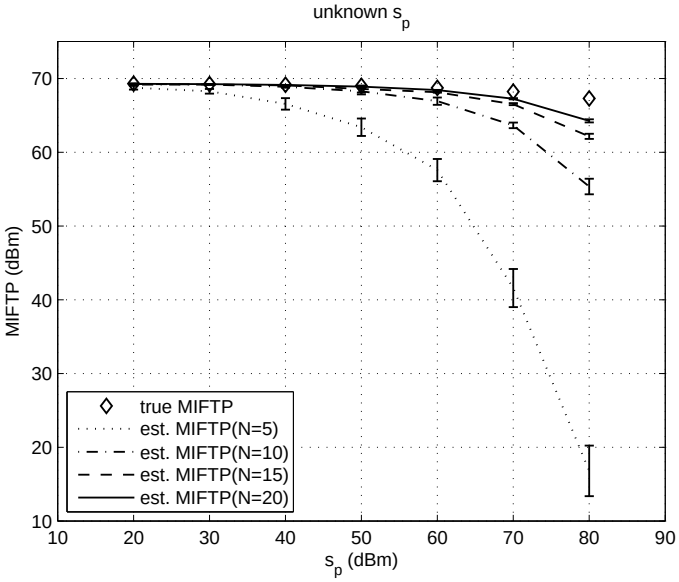

(b) s_p is unknown.

Figure 3.10: MIFTP versus s_p, when $\epsilon = 4$.

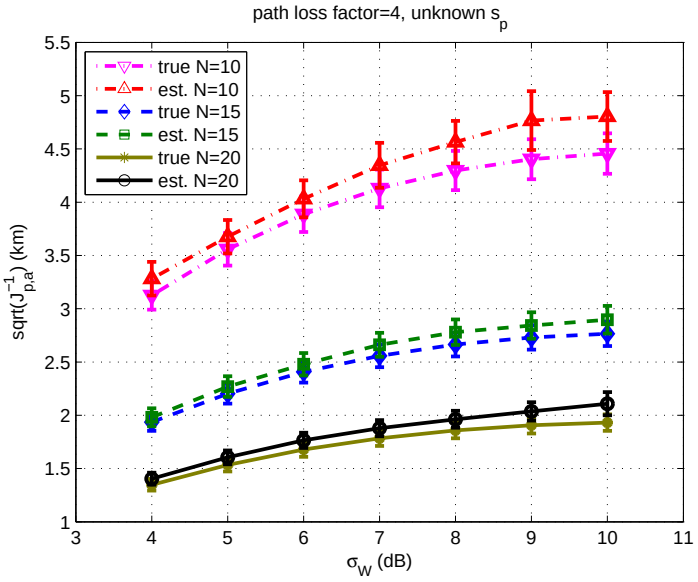

Figure 3.11: $\sqrt{J_{p,a}^{-1}}$ versus σ_W, when $\epsilon = 4$ and s_p is unknown.

N localizing FAR nodes, with uniform distribution, inside the coverage circle of the primary transmitter and average over 1000 trials to obtain the performance metrics of interest. As expected, with increasing N the CRB on location, $J_{p,a}^{-1}$, decreases, although the decrease is not significant for $N > 10$. This plot shows that the CRB does not depend strongly on σ_W in the chosen range. From the confidence intervals, we observe that the geometrical arrangement (i.e., the relative positions with respect to the primary transmitter) of the localizing nodes have only a small effect on the CRB estimation with known s_p for all N and with unknown s_p, when $N \geq 10$.

Another key observation is that in almost all cases, the MLE of the CRB is greater than its true value. This justifies the use of the estimated CRB in the MIFTP approximation formulas, since such overestimation of the true CRB ensures that the approximate MIFTP underestimates the true MIFTP. We have also plotted the CRB on the primary transmit power s_p, i.e., $\mathcal{E}_{\hat{S}_p}(\mathbf{\Theta})$, versus σ_W for $N = 10, 15, 20$. We observed that $\mathcal{E}_{\hat{S}_p}(\mathbf{\Theta})$ depends only weakly on σ_W and can be estimated quite accurately when $N \geq 10$.

3.5.6 Summary

The proposed MIFTP approximation performs well when a sufficient number of measurements is available. The accuracy of the approximation appears to be quite sensitive the value of the path loss factor. Increasing the number of measurements N significantly improves the accuracy and robustness of the MIFTP estimator. When $N = 10$ and s_p is known, we found that the MIFTP estimator is quite accurate over the entire range of parameter values that were used in the above scenarios. For $N \geq 10$, the estimation performance degradation due to unknown s_p and the effect of the localizing nodes' position with respect to the primary node is small. The plot of the CRB shows that the use of the invariance principle to estimate the true CRB is well justified. Finally, in all cases of our simulation studies, we found that the interference probability, $\hat{P}_{\text{int}}$, calculated using the MIFTP approximation is always less than the specified threshold ε_{int}.

3.6 Multiple Co-channel Primary Transmitters

In the previous sections we discussed in detail the proposed collaborative sensing and MIFTP estimation for successful opportunistic spectrum access. Our approach is to explicitly account for the error involved in the estimation process in order to avoid harmful interference to the primary system. We focused on the simple scenario where a single primary transmitter is being sensed by a cooperative FAR network, to determine the upper limit of interference-free transmit power of a single secondary transmitter. But for practical systems, one must consider the existence of multiple co-channel and potentially overlapping primary systems. In such a scenario, a FAR node must guarantee interference-free transmission with respect to all the victim nodes located inside the coverage area of all the co-channel transmitters in the primary network.

As far as SS-based sensing is concerned, there is another important aspect. The co-channel interference of primary transmitters will introduce error in the SS measurements used to perform the sensing. Specifically, the total received SS S, due to M co-channel

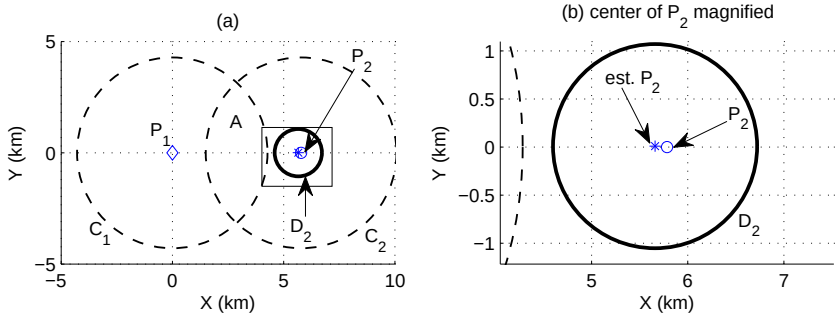

Figure 3.12: In (a), circles C_1 and C_2 (dashed line) denote the *sensing distance* for primary transmitters P_1 and P_2, respectively. Region A is the overlap region of C_1 and C_2, and it denotes the area where FAR nodes are most likely to receive misleading SS measurements due to interfering transmitters. Circle D_2 (solid line) denotes the *error circle* which quantifies the localization error of P_2 when $N = 10$ and FAR nodes are uniformly distributed in C_2. The mean of D_2 is the mean estimate computed from 1000 trial runs and its radius is given by the corresponding CRB estimate. A magnified version of the center of P_2 in (a) is shown in (b). Nodes uniformly distributed around P_2 can successfully estimate $\hat{P}_2$ and the effect of interference from P_1 on localization accuracy is negligible.

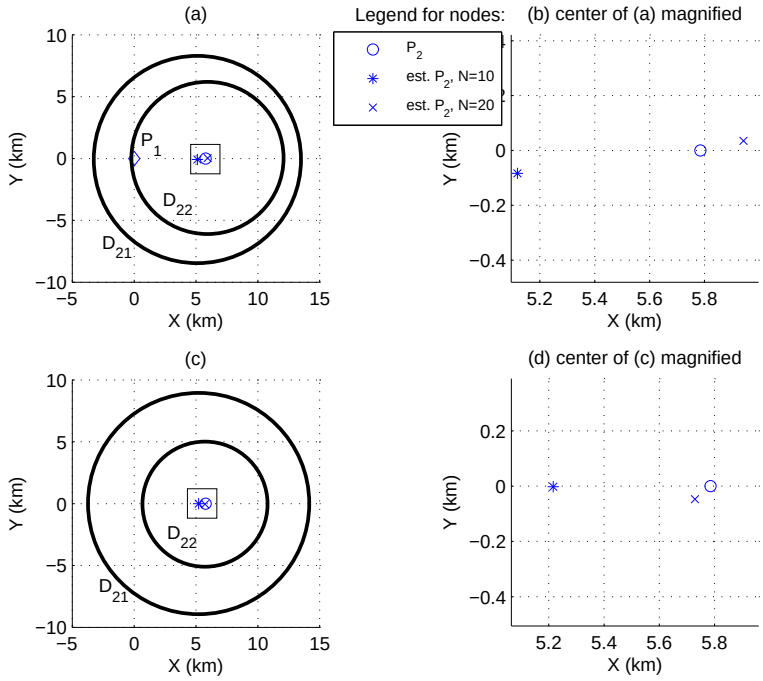

Figure 3.13: All localizing nodes are placed inside region A (not shown). In (a), the two *error circles* D_{21} and D_{22} (solid line) correspond to localization error of P_2 when P_1 is present for $N = 10$ and $N = 20$, respectively. For comparison, (c) is included, where P_1 is absent. A magnified version of the center of P_2 in (a) and (c) are shown in (b) and (d), respectively.

primary transmitters is given by

$$S \;=\; 10\log_{10}\left(\sum_{i=1}^{M} 10^{\frac{S_i}{10}}\right), \tag{3.54}$$

where S_i is the received SS due to the i^{th} primary transmitter, (cf. (3.16)). The fact that FAR nodes are likely to be more sensitive than typical primary receivers, can potentially make matters worse. Roughly speaking this is because, higher receiver sensitivity means larger *detection distance*, which means there will be a larger overlap region where FAR nodes can receive signal from multiple primary transmitters. The worst case scenario occurs when all the localizing FAR nodes are inside such an overlap region.

To provide some intuition on how the sensing accuracy is affected by multiple co-channel

transmitters, we choose $M = 2$ with equal transmit power of 80 dBm for primary transmitters P_1 and P_2 and assume homogeneous propagation conditions. We consider two scenarios. In Fig. 3.12, the FAR nodes are uniformly distributed in the coverage area, and in Fig. 3.13, all the FAR nodes are located inside the overlap region A, which is the intersection area of the two *sensing circles* corresponding to primary transmitters P_1 and P_2. Region A represents the region most susceptible to error due to interference from the two transmitters. As a measure of error in localization, we use *error circles*, the mean of which is the mean estimate computed from 1000 trial runs and its radius is given by the corresponding CRB estimate. From Fig. 3.12 we see that the FAR nodes uniformly distributed around P_2 can successfully estimate $\hat{P}_2$ and the effect of interference from P_1 on localization accuracy is negligible. In Fig. 3.13, significant degradation is seen when FAR nodes are limited to region A. For $N = 10$ the effect of whether P_1 is present or not is small. But when $N = 20$, the gain in accuracy is limited by the presence of P_1. We note that for both Figs. 3.12 and 3.13, the true location of P_2 is always contained inside the *error circles*. To improve accuracy, especially in worst-case scenarios mentioned above, the error induced due to interference can be mitigated with additional information exchange and signal processing performed by the FAR nodes. A detailed treatment of this issue is the topic of the next chapter.

3.7 Discussion

The main result of this chapter is an approximate formula for the maximum interference-free transmit power (MIFTP), which a FAR can use in a given frequency channel without causing harmful interference to victim nodes. The approximate MIFTP formula relies on location and transmit power estimates derived from signal strength measurements obtained by one or more FAR nodes in the vicinity of a given primary transmitter. In effect, the MIFTP provides a concrete characterization of the size of the spectrum hole in the spatial domain and can be applied directly to opportunistic spectrum access mechanisms. Our numerical results validate the accuracy of the proposed MIFTP estimation formula for several different scenarios and over a range of parameter settings.

The proposed scheme for spectrum hole estimation can be used to significantly enhance the performance of spectrum access methods, such as the Listen-Before-Talk (LBT) scheme [60], by exploiting collaboration among the FAR nodes. Although we have focused on the case of a single primary transmitter, the approach proposed in this paper can be generalized to the case of multiple primary transmitters and FAR nodes simultaneously transmitting over the same frequency channel. In the case of two primary transmitters, it is reasonable to assume that they are spatially separated such that they do not cause mutual interference. Under this assumption, it turns out that the effect of one transmitter on the measurements taken by a FAR node in the vicinity of the second transmitter, typically has a very small impact on MIFTP calculation with respect to the second transmitter. Moreover, given parameters estimates with respect to co-channel interferers (primary or secondary) of a local primary transmitter, a set of FAR nodes can incorporate the co-channel interference into the MIFTP calculation. These issues will be addressed more fully in the next chapter.

Chapter 4: Multiple Co-channel Transmitters

4.1 Introduction

In an uncoordinated OSA scheme, the secondary system may have only very limited prior information about the primary system, yet the operation of the secondary system must appear transparent to the primary. In particular, the number of transmitters, their transmit powers and locations, are generally not known a priori. In such a scenario, the secondary nodes can rely on collaboration among each other to sense the primary system. When multiple primary transmitters are present, measurements used to sense the primary system become more "noisy" due to cochannel interference, which may lead to secondary transmissions that cause harmful interference to the primary users. In such a model, the challenge is to characterize the primary transmitters using a collection of measurements taken by secondary nodes, and in the process also take into account the sensing error. In an infrastructureless network environment, for secondary nodes it is highly desirable to sense the primary transmitters in a distributed and iterative fashion. Once the primary transmitters have been identified, the allowable transmit power or the MIFTP of the secondary nodes needs to be determined. Again, it is possible to pose this problem in a centralized formulation, akin to the traditional power control and power allocation schemes. But for decentralized applications, it is useful to find the MIFTP in a distributed manner for the same reason mentioned above. In other words, a particular secondary node, given knowledge of the cochannel transmitters, should be able to estimate its own MIFTP.

In Chapter 3, we proposed an approach to collaborative spectrum hole detection and estimation based on signal strength (SS) observations obtained by a group of secondary nodes with respect to a single primary transmitter. In particular, an approximate expression for the maximum interference-free transmit power (MIFTP) for a single secondary node was

obtained. In various wireless systems, for example, cellular systems, one must consider the existence of multiple co-channel primary and secondary transmitters.

In this chapter[1], we propose a scheme for SS-based sensing and collaboration strategy in the presence of multiple co-channel primary and secondary transmitters. Knowledge of co-channel transmitters can be used along with the raw SS measurements to achieve robustness with respect to co-channel interference. We show that spectrum holes can be identified accurately provided that locally sensed information about co-channel transmitters is shared among the secondary nodes. In particular, we propose the maintenance of a distributed database, called the *T-map*, containing co-channel transmitter information including location, power, error estimates, and other information. Using the T-map, a method is proposed to determined the MIFTP that can be allocated to a particular secondary node without causing harmful interference to the existing co-channel primary and secondary nodes.

The remainder of the chapter is organized as follows. Section 4.2, describes the OSA model in detail. Section 4.3 presents a collaborative spectrum sensing scheme to mitigate co-channel interference. An expression for MIFTP in the presence of multiple transmitters is obtained in Section 4.4. Section 4.5, presents some numerical results to validate the feasibility of our proposed approach. Finally, the chapter is concluded in Section 4.6.

4.2 Collaborative OSA Model

Consider a group of CRs deployed in the coverage area of a licensed network consisting of multiple primary transmitters operating on a given channel $\nu \in \mathcal{C}$, where $\mathcal{C}$ denotes the set of channels under consideration. We propose a collaborative OSA scheme that identifies the spatial regions where the CRs can reuse the channel ν, without causing harmful interference to the primary receivers and to each other. In the literature, this is referred to as *spectrum hole discovery*. No direct communication between the primary and CR nodes is possible, but CRs can communicate with each other for robust spectrum sensing. Without loss of generality, we assume the existence of a common control channel that can be used by the

[1]A preliminary version of this chapter appeared in [82].

CRs to exchange control information.

4.2.1 SS-based observation model

We assume that all transmissions are omnidirectional and the propagation model is homogeneous, with lognormal shadowing. The received signal strength (SS) at node i due to node j is denoted by

$$R_{ij} = s_j - g(d_{ij}) + W_{ij} \text{ [dBm]}, \tag{4.1}$$

where s_j is the transmit power of node j, $g(d_{ij})$ is the path loss between two nodes separated by d_{ij}, and $W_{ij} \sim \mathcal{N}(0, \sigma_W^2)$. Assume that $g(d)$ is continuous, monotonically increasing and invertible. In general, $g(\cdot)$ is also a function of the path loss factor, antenna heights, antenna polarization, carrier frequency, terrain details etc., but for simplicity we assume that these other parameters can be estimated separately. Since multipath fast fading occurs on a much smaller time scale than shadowing, it is fair to assume that the fast fading can be practically eliminated by employing averaging (see [27,83]). The net SS received at node i due to a set of cochannel transmitters $\mathcal{J}$ in dBm is given by

$$R_i = 10 \log_{10} \left(\sum_{j \in \mathcal{J}} 10^{\frac{R_{ij}}{10}} \right), \tag{4.2}$$

4.2.2 Definition of MIFTP

Denote the set of the cochannel primary transmitters and the secondary nodes by $\mathcal{P}$ and $\mathcal{A}$, respectively. Each node $a \in \mathcal{P} \cup \mathcal{A}$ has an associated location (x_a, y_a) and transmit power s_a. The primary receivers are referred to as *victim* nodes, since they can potentially be disrupted by secondary transmissions. The *coverage distance* of primary transmitter $p \in \mathcal{P}$

is given by

$$d_{\text{cov}}(p) = g^{-1}\left(s_p - r_{\min} + \sigma_W Q^{-1}(1-\varepsilon_{\text{cov}})\right), \tag{4.3}$$

where s_p is the transmit power of p, ε_{cov} is a predefined upper limit on the outage probability of an intended receiver located inside the coverage area of p, $r_{\min}$ is the detection threshold of primary receivers (i.e., victims), $g^{-1}(\cdot)$ denotes the inverse of $g(\cdot)$ and $Q(x) \triangleq \frac{1}{\sqrt{2\pi}}\int_x^\infty e^{-\frac{t^2}{2}}dt$ denotes the standard Q-function (cf. (3.5)).

We define the *coverage region* of $p \in \mathcal{P}$ as the closed ball or disk centered at p with radius $d_{\text{cov}}(p)$, denoted by $\overline{B}_{\text{cov}}(p)$. The coverage region corresponds to the geographical area in which the received signal from p is sufficiently strong to satisfy a certain quality-of-service requirement. Nodes residing within the coverage region are potential *victim* nodes, since they may be receiving transmissions from node p and may experience interference from cochannel secondary transmitters. Nodes outside the coverage region will be oblivious to interference caused by secondary transmissions. Similarly, all secondary nodes detecting the signal of a particular primary transmitter p, must be located within the *detection radius* $d_{\text{det}}(p)$, defined as

$$d_{\text{det}}(p) = g^{-1}(s_p - r_a + \sigma_W Q^{-1}(1-\varepsilon_{\text{cov}})), \tag{4.4}$$

where r_a is the detection threshold of the secondary nodes.

Consider a set of existing cochannel secondary transmitters $\mathcal{A}_T \subset \mathcal{A}$ and a secondary node $b \in \mathcal{A} \setminus \mathcal{A}_T$ that is considering to reuse the same channel. Define $\mathcal{A}_0 \triangleq \mathcal{A}_T \cup \{b\}$. Denote by I_v, the aggregate interference power received at a victim node v due to the transmissions of nodes in $\mathcal{A}_0$. We ignore the effect of interference caused by cochannel primary transmitters. Typically, this would be taken into account in the design of the primary network. If this is not the case, we can simply treat the primary cochannel transmitters as secondary transmitters for the purpose of interference analysis. The *interference probability*

with respect to v is defined as the probability that I_v exceeds a predefined threshold $i_{\max}$:

$$P_{\text{int}}\left(\mathcal{A}_0, v\right) \triangleq \Pr\left\{I_v \geq i_{\max}\right\}, \tag{4.5}$$

when each node $a \in \mathcal{A}_0$ is transmitting with power s_a. This threshold can be set to satisfy the interference tolerance policy of the primary system.

The objective of the proposed OSA scheme is to quantify the MIFTP that can be allocated to secondary node b. The MIFTP for node b is defined as the maximum power that can be allocated to b such that the interference probability with respect to any potential victim node within the coverage distance of a transmitter $p \in \mathcal{P}$ does not exceed a threshold $\varepsilon_{\text{int}} > 0$, $\forall p \in \mathcal{P}$. More formally, the MIFTP for node b with respect to a single transmitter p can be defined as follows (cf. (3.8)):

$$s_b^*(p) = \max\{s_b : P_{\text{int}}(\mathcal{A}_0; s_b, x, y) \leq \varepsilon_{\text{int}}; \forall (x,y) \in \overline{B}_{\text{cov}}(p)\}, \tag{4.6}$$

where the notation $P_{\text{int}}(\mathcal{A}_0; s_b, x, y)$ is meant to emphasize that the interference probability is a function of node b's transmit power s_b and the location (x, y) of a potential victim node v. The MIFTP of node b in the presence of the set of cochannel primary transmitters $\mathcal{P}$ is then given by $s_b^* \triangleq \min_{p \in \mathcal{P}} s_b^*(p)$.

4.2.3 T-map

In a network consisting of multiple cochannel transmitters, the parameter of interest is $\boldsymbol{\Theta} \triangleq \{\boldsymbol{\theta}_p, \forall p \in \mathcal{P} \cup \mathcal{A}_T\}$, with $\boldsymbol{\theta}_p \triangleq (x_p, y_p, s_p)$, where s_p is the transmit power of node p, located at (x_p, y_p). It is clear from (4.6) that in order to compute the MIFTP, it is necessary to estimate $\boldsymbol{\Theta}$. The presence of cochannel interference increases the error in estimating $\boldsymbol{\Theta}$, which can be mitigated if the secondary nodes share their estimates with other more distant secondary nodes (see Section 4.3). Therefore, we propose the maintenance of a distributed database, called the *T-map* (Transmitter-map), containing relevant information about all

cochannel transmitters.

In Chapter 3, it was shown that given a set of SS measurements, the maximum likelihood (ML) estimator is optimal in the mean square error (MSE) sense and optimality is achieved as the observation noise becomes vanishingly small. The ML estimate (MLE) of the Cramér-Rao Bound (CRB) was found to provide an accurate approximation for the estimation error. Hence, we propose that the T-map store the MLEs of each transmitter's parameters and the associated CRBs:

$$\boldsymbol{T} \triangleq \left\{ \left(\hat{\boldsymbol{\theta}}_p, \hat{\boldsymbol{J}}_{\boldsymbol{\theta}_p}^{-1} \right), \forall p \in \mathcal{P} \right\} \cup \left\{ \boldsymbol{\theta}_a, \forall a \in \mathcal{A}_T \right\}, \tag{4.7}$$

where $\hat{\boldsymbol{\theta}}_p$ is the MLE[2] of $\boldsymbol{\theta}_p$ and $\hat{\boldsymbol{J}}_{\boldsymbol{\theta}_p}^{-1}$ is the MLE of the associated CRB.

In general, the true parameters of some nodes in $\mathcal{A}_T$ may not be known. In this case, we treat these particular secondary transmitters as primary transmitters and estimate their corresponding unknown parameters. For a given frequency channel ν and time t, the T-map $\boldsymbol{T}(\nu, t)$ characterizes the spatial region where secondary transmissions can be allowed. For a static set of primary transmitters, the T-map maintained by a secondary node should converge after a certain time period. In a dynamic scenario, the T-map should track changes that take place in the spectrum occupancy profile over time.

4.3 Collaborative Sensing Scheme

To estimate the MIFTP, the secondary nodes must first update the T-map from their received SS measurements. This SS observation set is denoted by $\mathcal{O} \triangleq \{(R_a, \boldsymbol{L}_a) : a \in \mathcal{A}\}$, where R_a is the net SS received due to all cochannel transmitters at the secondary node a, located at $\boldsymbol{L}_a \triangleq (x_a \ y_a)$. In the proposed scheme, SS measurements are shared *locally* among neighboring nodes and localization estimates are shared *globally* via the T-map construct. Through collaborative information sharing, the T-map is maintained in a

[2]Throughout this chapter, all estimates indicated by ˆ represent MLEs.

distributed fashion by means of networking protocols. Cochannel interference due to the primary transmitters introduces error in the SS measurements. For example, to localize $p \in \mathcal{P}$, instead of $\{R_{ap} : a \in \mathcal{A}\}$ only $\{R_a : a \in \mathcal{A}\}$ can be observed, resulting in higher estimation error. This effect can be mitigated by sharing the estimates of the interfering primary transmitters among the secondary nodes via the T-map and by accounting for the associated cochannel interference. In the remainder of this section, we consider the case $M = 2$. Generalization of the approach to arbitrary M is straightforward.

4.3.1 With no information

Given a set of independent local observations $\mathcal{O}_1 \triangleq \{(R_a, \boldsymbol{L}_a) : a \in \mathcal{A}_1 \subset \mathcal{A}\}$ in the vicinity of a primary transmitter, say $p_1 \in \mathcal{P}$, the MLE of the parameter $\boldsymbol{\theta}_1 \triangleq [x_{p_1} \;\; y_{p_1} \;\; s_{p_1}]^T$ can be found. In the absence of any information about other cochannel transmitters, the log-likelihood function has the following form:

$$F_{1A}(\boldsymbol{\theta}_1) \triangleq \sum_{a \in \mathcal{A}_1} \ln f_{R_a|\boldsymbol{\theta}_1}, \tag{4.8}$$

where $R_a|\boldsymbol{\theta}_1 \sim \mathcal{N}(s_{p_1} - g(d_{ap_1}), \sigma_W^2)$. The MLE is found by solving the optimization problem $\hat{\boldsymbol{\theta}}_{1A} = \arg\max_{\boldsymbol{\theta}_1} \quad F_{1A}(\boldsymbol{\theta}_1)$.

4.3.2 With true information

If the *true* parameter $\boldsymbol{\theta}_2 \triangleq [x_{p_2} \;\; y_{p_2} \;\; s_{p_2}]^T$, of another cochannel transmitter p_2, is known, the observations in $\mathcal{O}_1$ can be modeled as

$$R_a = 10 \log_{10} \left(10^{\frac{R_{ap_1}}{10}} + 10^{\frac{R_{ap_2}}{10}} \right) = \kappa^{-1} \ln \left(e^{\kappa R_{ap_1}} + e^{\kappa R_{ap_2}} \right),$$

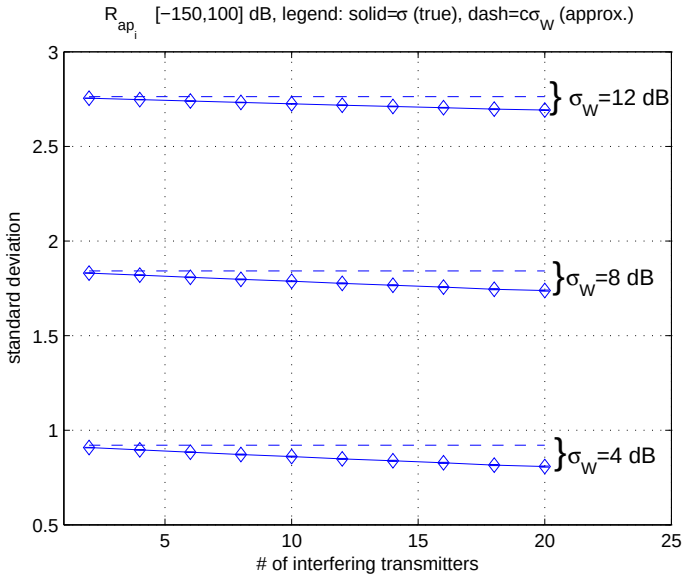

Figure 4.1: Plot shows the mean values of σ_{Ba}, calculated according to (4.9)-(4.10), with the associated 99.7% confidence intervals generated from 10^4 random realizations of $u_{ap_i} \in [-150, 100]$ dB, $\forall p_i \in \mathcal{P}$, where $|\mathcal{P}| \in [2, 20]$.

where $\kappa \triangleq \frac{\ln 10}{10}$. Approximating the sum of independent lognormal random variables by another lognormal [84], yields $R_a|\boldsymbol{\theta}_1, \boldsymbol{\theta}_2 \sim \mathcal{N}(\frac{\mu_{Ba}}{\kappa}, \frac{\sigma^2_{Ba}}{\kappa^2})$, where

$$\mu_{Ba} \triangleq \ln(k_1) - \frac{\sigma^2_{Ba}}{2}, \quad \sigma^2_{Ba} \triangleq \ln\left(1 + \frac{k_2^2}{k_1^2}\right), \tag{4.9}$$

$$k_1 \triangleq e^{\frac{\kappa^2\sigma_W^2}{2}}\left(e^{\kappa u_{ap_1}} + e^{\kappa u_{ap_2}}\right), \quad k_2^2 \triangleq e^{\kappa^2\sigma_W^2}\left(e^{\kappa^2\sigma_W^2} - 1\right)\left(e^{2\kappa u_{ap_1}} + e^{2\kappa u_{ap_2}}\right), \tag{4.10}$$

and $u_{ij} \triangleq s_j - g(d_{ij})$. Note that u_{ap_2} is known and $\boldsymbol{\theta}_1$ is the only unknown. The log-likelihood function is $F_{1B}(\boldsymbol{\theta}_1) \triangleq \sum_{a\in\mathcal{A}_1} \ln f_{R_a|\boldsymbol{\theta}_1,\boldsymbol{\theta}_2}$, with ML solution

$\hat{\boldsymbol{\theta}}_{1B}(\boldsymbol{\theta}_1) = \arg\max_{\boldsymbol{\theta}_1} \; F_{1B}(\boldsymbol{\theta}_1)$.

We have observed (see Fig. 4.1) that in the region of practical interest, $u_{ap_i} \in [-150, 100]$ dBm, $\sigma_{Ba} \lesssim \kappa\sigma_W, \forall a$, where $x_1 \lesssim x_2$ means that x_1 is upper bounded by x_2 which is not too far from x_1. If the observations R_a are scaled as $\widetilde{R}_a = \kappa R_a$, this approximation can be used to obtain an equivalent but simpler objective function compared to $F_{1B}(\boldsymbol{\theta}_1)$. In this

case, we have $\hat{\boldsymbol{\theta}}_{1B} = \arg\max_{\boldsymbol{\theta}_1} \quad \widetilde{F}_{1B}(\boldsymbol{\theta}_1)$, where

$$\widetilde{F}_{1B}(\boldsymbol{\theta}_1) \triangleq \sum_{a \in \mathcal{A}_1} \ln f_{\widetilde{R}_a|\boldsymbol{\theta}_1,\boldsymbol{\theta}_2}, \tag{4.11}$$

and $\widetilde{R}_a|\boldsymbol{\theta}_1, \boldsymbol{\theta}_2 \sim \mathcal{N}\left(\ln\left(\sum_{i=1,2} e^{\kappa u_{ap_i}}\right), \kappa^2\sigma_W^2\right)$.

4.3.3 With estimated information

In many cases, only the *estimated* information about other cochannel transmitters is available, via the distributed maintenance of the T-map. Assume that the ML estimated parameters $(\hat{\boldsymbol{\theta}}_2, \hat{\boldsymbol{J}}_{\boldsymbol{\theta}_2}^{-1})$ of transmitter p_2 are known. Note that here $\hat{\boldsymbol{\theta}}_2$ is found by solving the likelihood function F_{2A} corresponding to p_2 (similar to F_{1A}), i.e., $\hat{\boldsymbol{\theta}}_2 \equiv \hat{\boldsymbol{\theta}}_{2A}$ and $\hat{\boldsymbol{J}}_{\boldsymbol{\theta}_2}^{-1} \equiv \hat{\boldsymbol{J}}_{\boldsymbol{\theta}_{2A}}^{-1}$. Instead of u_{ap_2}, we can obtain $\hat{u}_{ap_2}$, where $\hat{u}_{ap_2} \triangleq \hat{S}_{p_2} - g(\hat{D}_{ap_2})$ denotes the MLE of u_{ap_2} and $\hat{\boldsymbol{\theta}}_2 = [\hat{X}_{p_2}\ \hat{Y}_{p_2}\ \hat{S}_{p_2}]^T$ denotes the MLE of $\boldsymbol{\theta}_2$, via the invariance principle (cf. [78, p. 217]), which states that the MLE of a function $q(\cdot)$ of $\boldsymbol{\Phi}$ is given by $q(\hat{\boldsymbol{\Phi}})$, where $\hat{\boldsymbol{\Phi}}$ denotes the MLE of $\boldsymbol{\Phi}$. Since the MLE of the CRB approaches the estimation error as $\sigma_W \to 0$ (cf. Chapter 3), R_{ap_2} can be modeled as follows:

$$R_{ap_2} = u_{ap_2} + W_{ap_2} = \hat{u}_{ap_2} + W_{2a} + W_{ap_2},$$

where $W_{2a} \sim \mathcal{N}(0, \hat{\sigma}_{2a}^2)$ with $\hat{\sigma}_{2a}^2 \triangleq \hat{\boldsymbol{H}}_a^T \hat{\boldsymbol{J}}_{\boldsymbol{\theta}_2}^{-1} \hat{\boldsymbol{H}}_a$. Again, $\hat{\boldsymbol{H}}_a$ is the MLE of $\boldsymbol{H}_a$ where

$$\boldsymbol{H}_a \triangleq \left[\frac{\partial u_{ap_2}}{\partial x_{p_2}}, \frac{\partial u_{ap_2}}{\partial y_{p_2}}, \frac{\partial u_{ap_2}}{\partial s_{p_2}}\right]^T = \left[-\dot{g}(d_{ap_2})\cos\phi_{ap_2}, -\dot{g}(d_{ap_2})\sin\phi_{ap_2}, 1\right]^T, \tag{4.12}$$

and $\dot{g}(d) \triangleq \frac{\partial g(d)}{\partial d}$. Hence, $R_{ap_2}|\hat{\boldsymbol{\theta}}_2 \sim \mathcal{N}(\hat{u}_{ap_2}, \hat{\sigma}_{2a}^2 + \sigma_W^2)$ and $R_a|\boldsymbol{\theta}_1, \hat{\boldsymbol{\theta}}_2 \sim \mathcal{N}(\frac{\mu_{Ca}}{\kappa}, \frac{\sigma_{Ca}^2}{\kappa^2})$, where

$$\mu_{Ca} \triangleq \ln(k_3) - \frac{\sigma_{Ca}^2}{2}, \quad \sigma_{Ca}^2 \triangleq \ln\left(1 + \frac{k_4^2}{k_3^2}\right), \quad k_3 \triangleq e^{\frac{\kappa^2\sigma_W^2}{2}}\left(e^{\kappa u_{ap_1}} + e^{\kappa\hat{u}_{ap_2} + \frac{\kappa^2\hat{\sigma}_{2a}^2}{2}}\right),$$

$$k_4^2 \triangleq \left(e^{\kappa^2\sigma_W^2} - 1\right)e^{2\kappa u_{ap_1} + \kappa^2\sigma_W^2} + \left(e^{\kappa^2\hat{\sigma}_{2a}^2 + \kappa^2\sigma_W^2} - 1\right)e^{2\kappa\hat{u}_{ap_2} + \kappa^2\hat{\sigma}_{2a}^2 + \kappa^2\sigma_W^2}.$$

The corresponding log-likelihood function is $F_{1C}(\boldsymbol{\theta}_1) \triangleq \sum_{a\in\mathcal{A}_1} \ln f_{R_a|\boldsymbol{\theta}_1,\hat{\boldsymbol{\theta}}_2}$, and the ML solution is given by $\hat{\boldsymbol{\theta}}_{1C} = \arg\max_{\boldsymbol{\theta}_1} \quad F_{1C}(\boldsymbol{\theta}_1)$. Similar to Section 4.3.2, to simplify the objective function we can use the scaled observations to solve $\hat{\boldsymbol{\theta}}_{1C} = \arg\max_{\boldsymbol{\theta}_1} \quad \widetilde{F}_{1C}(\boldsymbol{\theta}_1)$, where

$$\widetilde{F}_{1C}(\boldsymbol{\theta}_1) \triangleq \sum_{a\in\mathcal{A}_1} \ln f_{\widetilde{R}_a|\boldsymbol{\theta}_1,\hat{\boldsymbol{\theta}}_2}, \tag{4.13}$$

and $\widetilde{R}_a|\boldsymbol{\theta}_1, \hat{\boldsymbol{\theta}}_2 \sim \mathcal{N}\left(\ln\left(e^{\kappa u_{ap_1}} + e^{\kappa\hat{u}_{ap_2} + \frac{\kappa^2\hat{\sigma}_{2a}^2}{2}}\right), \kappa^2\sigma_W^2\right)$. Note that $\hat{\boldsymbol{\theta}}_{1C} \to \hat{\boldsymbol{\theta}}_{1B}$, as $\sigma_{2a} \to 0, \forall a$. Our hypothesis is that $\hat{\boldsymbol{\theta}}_{1B}$ and $\hat{\boldsymbol{\theta}}_{1C}$ are better estimators than $\hat{\boldsymbol{\theta}}_{1A}$ in terms of mitigating the error induced by cochannel interference. The effectiveness of this proposed collaborative sensing strategy is studied numerically in Section 4.5. The CRBs corresponding to $\hat{\boldsymbol{\theta}}_{1B}$ and $\hat{\boldsymbol{\theta}}_{1C}$ for arbitrary M are derived in Appendix B.1.

4.3.4 Measurement clustering and collaborative sensing

When multiple cochannel transmitters are present, accurate localization depends on: (1) knowing the number of cochannel transmitters, M, in the primary system, and (2) using an appropriate set of SS measurements. In other words, we need to divide the available signal strength measurements into clusters, such that each clustered measurement set can be used to localize a particular primary transmitter. In Chapter 5, this issue is addressed,

and two schemes for measurement clustering, one based on minimum description length (cf. [85]) and the other based on minimum MSE, are proposed. Both schemes produce an estimate, $\hat{M}$, of the number of cochannel transmitters, together with an associated set of *initial* parameter estimates, $\{\hat{\boldsymbol{\theta}}_i\}_{i=1}^{\hat{M}}$, which is most likely to have generated the given set of measurements. The measurements are then assigned to the nearest estimated transmitter from $\{\hat{\boldsymbol{\theta}}_i\}_{i=1}^{\hat{M}}$.

Once the initial estimates are found via measurement clustering, the effect of cochannel interference can be mitigated using the approach discussed in Section 4.3.3. In particular, note that $\hat{\boldsymbol{\theta}}_{1C}$ is a better estimator than $\hat{\boldsymbol{\theta}}_{1A}$ (in terms of MSE), since it uses the information of $\hat{\boldsymbol{\theta}}_2$. Symbolically, we denote this by $\hat{\boldsymbol{\theta}}_{1A} \overset{\hat{\boldsymbol{\theta}}_2}{\rightarrow} \hat{\boldsymbol{\theta}}_{1C}$. The corresponding *compensation* for $\hat{\boldsymbol{\theta}}_2$ is given by $\hat{\boldsymbol{\theta}}_2 \overset{\hat{\boldsymbol{\theta}}_{1C}}{\rightarrow} \hat{\boldsymbol{\theta}}_{2C}$, where $\hat{\boldsymbol{\theta}}_{2C}$ denotes the modified estimator of $\hat{\boldsymbol{\theta}}_2$ incorporating the knowledge of $\hat{\boldsymbol{\theta}}_{1C}$. We can continue the procedure as $\hat{\boldsymbol{\theta}}_{1C} \overset{\hat{\boldsymbol{\theta}}_{2C}}{\rightarrow} \hat{\boldsymbol{\theta}}'_{1C}$, then $\hat{\boldsymbol{\theta}}_{2C} \overset{\hat{\boldsymbol{\theta}}'_{1C}}{\rightarrow} \hat{\boldsymbol{\theta}}'_{2C}$, and so on. A simple convergence criterion should be used to halt the recursive procedure, providing a suitable tradeoff between accuracy and computational load. For example, the rule may simply be to stop when the difference between successive iterations is sufficiently small.

4.4 Maximum Interference-Free Transmit Power

In this section, we first formulate an approach to compute the true MIFTP for a secondary node $b \in \mathcal{A} \setminus \mathcal{A}_T$ (see (4.6)) and then develop a practical approximation for the MIFTP.

4.4.1 True MIFTP calculation

The interference probability can be expressed as follows (see Appendix B.2 for a proof).

Proposition 8. *The interference probability at victim node v due to nodes in $\mathcal{A}_0$ is given*

by

$$P_{int}(\mathcal{A}_0; s_b, v) = Q\left(\frac{\kappa i_{max} - \mu}{\sigma}\right), \tag{4.14}$$

where

$$\mu \triangleq \frac{\kappa^2\sigma_W^2}{2} - \frac{\sigma^2}{2} + h, \quad \sigma^2 \triangleq \ln\left(1 + \frac{k_6^2}{k_5^2}\right), \quad h \triangleq \ln\left(L_b(v) + \sum_{a\in\mathcal{A}_T} L_a(v)\right), \tag{4.15}$$

$$k_5 \triangleq e^{\frac{\kappa^2\sigma_W^2}{2}+h}, \; k_6^2 \triangleq e^{\kappa^2\sigma_W^2}\left(e^{\kappa^2\sigma_W^2} - 1\right)\left(L_b^2(v) + \sum_{a\in\mathcal{A}_T} L_a^2(v)\right). \tag{4.16}$$

and $L_a(v) \triangleq e^{\kappa(s_a - g(d_{va}))}$ *for any secondary node* $a \in \mathcal{A}_0$.

The interference probability at victim v depends on three quantities: (i) the interference tolerance threshold, $i_{\max}$, (ii) the variance of the shadowing noise, σ_W^2, and (iii) the aggregate interference power, h, received at v. The following lemma provides a method for computing the MIFTP (see Appendix B.4 for a proof).

Lemma 1. *For a secondary node* b *such that* $(x_b, y_b) \notin \overline{B}_{\rm cov}(p)$ *the MIFTP with respect to primary transmitter* $p \in \mathcal{P}$ *is given by*

$$s_b^*(p) = \min_{(x,y)\in\overline{B}_{\rm cov}(p)} s_b^*(p; x, y), \tag{4.17}$$

where

$$s_b^*(p; x, y) \triangleq \max\{s_b : P_{\rm int}(\mathcal{A}_0; s_b, x, y) \le \varepsilon_{\rm int}\}. \tag{4.18}$$

The complexity of the optimization problem suggested by Lemma 1 can be reduced by restricting the minimization problem to the boundary of the coverage region $\overline{B}_{\rm cov}(p)$ as stated in the next proposition (see Appendix B.3 for a proof).

Proposition 9. *Given a set of secondary cochannel transmitters with parameters* $\{\boldsymbol{\theta}_a\} = \{(x_a, y_a, s_a)\}$*, all located outside the coverage region* $\overline{B}_{\mathrm{cov}}(p)$*, the maximum interference due to path loss alone is achieved on the boundary* $\partial B_{\mathrm{cov}}(p)$*, i.e., the circle centered at* p *with radius* $d_{\mathrm{cov}}(p)$*.*

Combining Lemma 1 and Proposition 9 simplifies the computation of MIFTP (see Appendix B.5 for details).

Corollary 1.

$$s_b^*(p) = \min_{(x,y)\in\partial B_{\mathrm{cov}}(p)} s_b^*(p; x, y) = \min_{\psi\in[0,2\pi)} s_b^*(p; x_p(\psi), y_p(\psi)) \tag{4.19}$$

with $s_b^*(p; x, y)$ *defined in* (4.18)*, and*

$$x_p(\psi) \triangleq x_p + d_{\mathrm{cov}}(p)\cos\psi, \quad y_p(\psi) \triangleq y_p + d_{\mathrm{cov}}(p)\sin\psi. \tag{4.20}$$

The true MIFTP as defined in Lemma 1 or Corollary 1 cannot be calculated directly, since the T-map provides only $\{\hat{\boldsymbol{\theta}}_p, \hat{\boldsymbol{J}}_{\boldsymbol{\theta}_p}^{-1} : p \in \mathcal{P}\}$ and $\{\boldsymbol{\theta}_a : a \in \mathcal{A}_T\}$. Therefore, we develop an approximation to the MIFTP of b with respect to $p \in \mathcal{P}$ by first estimating the *critical distance*, $\hat{D}_b^*(p)$ to detect the presence of a spectrum hole. Then, an estimate, $\hat{s}_b^*(p)$, for the MIFTP is obtained by considering potential victim nodes lying on the circle $\partial B_{\mathrm{cov}}(p)$.

4.4.2 Critical distance estimate, $\hat{D}_b^*(p)$, and spectrum hole detection

For a particular $p \in \mathcal{P}$, the *critical distance estimate* with respect to node b is given by

$$\begin{aligned}\hat{D}_b(p) &\triangleq \hat{D}_{pb} - \hat{D}_{\mathrm{cov}}(p) \\ &\overset{(4.3)}{=} \sqrt{(\hat{X}_p - x_b)^2 + (\hat{Y}_p - y_b)^2} - g^{-1}(\hat{S}_p - r_{\min} + \sigma_W Q^{-1}(1 - \varepsilon_{\mathrm{cov}})),\end{aligned}$$

where $\hat{D}_{pb}$ and $\hat{D}_{\text{cov}}(p)$ denote the MLEs of d_{pb} and $d_{\text{cov}}(p)$, respectively. In the asymptotic regime $\sigma_W \to 0$,

$$E_p \triangleq \hat{D}_b(p) - d_b(p) = \hat{D}_{pb} - d_{pb} - (\hat{D}_{\text{cov}}(p) - d_{\text{cov}}(p))$$

can be modeled as $E_p \sim \mathcal{N}(0, \hat{J}_{pb}^{-1})$, where $\hat{J}_{pb}^{-1}$ denotes the MLE of the CRB corresponding to the error in estimating $\hat{D}_b(p)$, (see Proposition 6).

Suppose $E_p = r$ and $\hat{D}_b(p) = r_0$. If $|r| \geq r_0 > 0$, then in the worst case, node b lies within $d_{\text{cov}}(p)$ of primary transmitter p. In this scenario, node b must not transmit, i.e., $s_b^* = -\infty$, to avoid potentially harmful interference to the victim nodes. If $0 < |r| < r_0$, then b can transmit, i.e., $s_b^* \neq -\infty$. Since we do not know r, we can only ensure that for the given realization $\hat{D}_b(p) = r_0 > 0$, the event $\{|E_p| < r_0\}$ occurs with high probability. In particular, for $s_b^* \neq -\infty$ and $\varepsilon \in (0, 1)$, we require $r_0 > \hat{R}^* > 0$, where

$$R^* \triangleq \min\{R : \Pr(|E_p| < R) \geq \varepsilon\} = \sqrt{\hat{J}_{pb}^{-1}} \cdot Q^{-1}\left(\frac{1-\varepsilon}{2}\right).$$

For example, for $\varepsilon = 0.9973$, $\hat{R}^* \approx 3\sqrt{\hat{J}_{pb}^{-1}}$. Define the set $\mathcal{D} \triangleq \left\{p \in \mathcal{P} : \hat{D}_b(p) \leq \hat{R}^*\right\}$. Whenever, $\mathcal{D} = \emptyset$, a spectrum hole with respect to b is detected, and the approximate MIFTP, $\hat{s}_b^*$ should be computed.

4.4.3 Interference probability and MIFTP approximation

An upper bound on $P_{\text{int}}(\mathcal{A}_0; s_b, v)$ is given by the following proposition, see Appendix B.6.

Proposition 10. *The interference probability $P_{int}(\mathcal{A}_0; s_b, v)$ at a particular victim v located at (x_v, y_v) can be upper bounded by $Q(\gamma)$, where $\gamma \triangleq \frac{\kappa i_{max} - \frac{\kappa^2\sigma_W^2}{2} + \frac{\sigma^2}{2} - h}{\kappa\sigma_W}$ (cf. (4.15) and (4.16)).*

Define $F(\gamma) \triangleq \hat{\Gamma} - \gamma$, where $\hat{\Gamma}$ denotes the MLE of γ. Note that γ is a function of $\boldsymbol{\theta}_p$. Under some regularity conditions [78, p. 229], the CRBs of $\boldsymbol{\theta}_p$ and γ are related as $J_\gamma^{-1} = \boldsymbol{H}_0^T \boldsymbol{J}_{\boldsymbol{\theta}_p}^{-1} \boldsymbol{H}_0$, where $\boldsymbol{H}_0 \triangleq \left[\frac{\partial \gamma}{\partial x_p} \ \frac{\partial \gamma}{\partial y_p} \ \frac{\partial \gamma}{\partial s_p}\right]^T$ and is evaluated in Appendix B.7. In Chapter 3, we provide a closed-form expression of $\boldsymbol{J}_{\boldsymbol{\theta}_p}^{-1}$ and show that it is achievable as $\sigma_W \to 0$. It can be shown that if $\boldsymbol{J}_{\boldsymbol{\theta}_p}^{-1}$ is achievable asymptotically as $\sigma_W \to 0$, then so is J_γ^{-1}, (cf. Proposition 4). This means that in the asymptotic regime $F(\gamma) \sim \mathcal{N}(0, J_\gamma^{-1})$. Suppose for a particular realization $F(\gamma) = x$ and $\hat{\Gamma} = \hat{\gamma}$. Then, the upper bound on the interference probability conditioned on $F(\gamma) = x$ is given by $Q(\hat{\gamma} - x)$. Using the total probability theorem

$$\int_{-\infty}^{\infty} Q(\hat{\gamma} - x)\, \mathcal{N}(0, J_\gamma^{-1}) dx = Q\left(\frac{\hat{\gamma}}{\sqrt{1 + J_\gamma^{-1}}}\right) \leq \frac{1}{2} e^{-\frac{\hat{\gamma}^2}{2\left(1 + J_\gamma^{-1}\right)}} \triangleq w(s_b, x, y), \tag{4.21}$$

where the first equality is obtained using a result in [80, p. 102] and the upper bound is valid for $\hat{\gamma} \geq 0$. We propose to approximate the MIFTP in terms of this upper bound w on the interference probability averaged over all possible estimation errors. If, for any realization $\hat{\gamma} < 0$, we can use $Q\left(\frac{\hat{\gamma}}{\sqrt{1+J_\gamma^{-1}}}\right)$ to compute the MIFTP. Since J_γ^{-1} is unknown, using the invariance principle we replace it by its MLE, $\hat{J}_\gamma^{-1}$, and denote the expression corresponding to (4.21) by $\hat{w}(s_b, x, y)$. In a manner analogous to Corollary 1, an approximation to the MIFTP can be computed as follows:

$$\hat{s}_b^*(p) \triangleq \min_{\psi \in [0, 2\pi)} \hat{s}_b^*(p; \hat{X}_p(\psi), \hat{Y}_p(\psi)), \tag{4.22}$$

where

$$\hat{X}_p(\psi) \triangleq \hat{X}_p + \hat{D}_{\text{cov}}(p)\cos\psi, \quad \hat{Y}_p(\psi) \triangleq \hat{Y}_p + \hat{D}_{\text{cov}}(p)\sin\psi, \tag{4.23}$$

$$\hat{s}_b^*(p;x,y) \triangleq \max\{s_b : \hat{w}(s_b,x,y) \leq \varepsilon_{\text{int}}\}. \tag{4.24}$$

A computationally simpler approximation to MIFTP can be obtained by assuming that the worst-case victim, say v^*, lies at the intersection of the circle $\partial B_{\text{cov}}(p)$ and the straight line connecting (x_b, y_b) and $(\hat{X}_p, \hat{Y}_p)$.

$$\hat{s}_b^*(p) = \max\{s_b : \hat{w}(s_b, x_{v^*}, y_{v^*}) \leq \varepsilon_{\text{int}}\}. \tag{4.25}$$

This is an one-dimensional search problem which is computationally less demanding than the two-step optimization problem given by (4.22) and (4.24). Numerical results presented in Section 4.5 suggest that this approximation is sufficiently accurate for practical scenarios. We remark that localization accuracy is incorporated into above MIFTP approximations via the CRB term, J_γ^{-1}. In particular, as the estimation error increases, the MIFTP becomes more conservative, ensuring that the interference tolerance threshold, $i_{\max}$ is met, but also making the OSA scheme less efficient. This property of being conservative is important since secondary transmissions should do no harm to the primary system.

4.5 Numerical Results

For the numerical results presented in this section, we choose system parameter values that reflect the application of OSA to digital TV broadcast bands. The SS measurements are generated using the generic path loss function $g(d) = 10\epsilon\log_{10}(d)$, where d is distance and ϵ is the path loss exponent. Unless otherwise specified, all simulations are performed with the following parameter values: detection threshold for victims $r_{\min} = -85$ dBm, detection threshold for secondary nodes $r_a = -90$ dBm, interference tolerance threshold $i_{\max} = -100$ dBm, outage probability upper limit $\varepsilon_{\text{cov}} = 0.01$, allowable interference probability

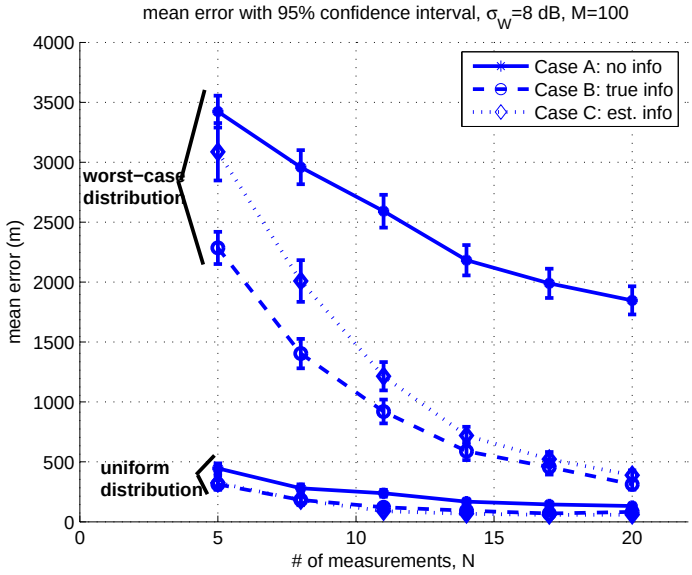

Figure 4.2: Localization error $\mathcal{E}_1$ vs. number of measurements.

upper limit to victims $\varepsilon_{\text{int}} = 0.01$, shadowing standard deviation $\sigma_W = 8$ dB and path loss exponent $\epsilon = 4$. For a particular primary transmitter p and for each simulation trial, we randomly place N secondary nodes, with uniform distribution inside the coverage region $\overline{B}_{\text{cov}}(p)$. These nodes perform localization of p by evaluating the MLEs $(\hat{\boldsymbol{\theta}}_p, \hat{\boldsymbol{J}}_{\boldsymbol{\theta}_p}^{-1})$. Each result is averaged over K trials and shown with the associated 95% confidence interval, which arises due to randomness in the localizing node positions, as well as the shadowing noise.

4.5.1 Mitigation of cochannel interference

Consider two cochannel primary transmitters p_1 and p_2 parameterized by $(8, 0, 80)$ and $(0, 0, 80)$, respectively, where the 3-tuple indicate the location and transmit power, with units of $[\text{km}, \text{km}, \text{dBm}]$. For these parameter values, $d_{\text{cov}}(p_1) = d_{\text{cov}}(p_2) = 4.6$ km and $d_{\text{det}}(p_1) = d_{\text{det}}(p_2) = 6.1$ km, (cf. (4.3) and (4.4)). Each measurement is generated by averaging over 100 raw measurements to reduce the effect of shadowing noise. We are interested in estimating $\boldsymbol{\theta}_1 = [x_{p_1} \;\; y_{p_1} \;\; s_{p_1}]^T$. To evaluate the performance of our proposed scheme, we find the ML solutions of the likelihood functions F_{1A}, $\widetilde{F}_{1B}$ and $\widetilde{F}_{1C}$ corresponding to

(4.8), (4.11) and (4.13), respectively. As a performance measure, we calculate the mean *missed distance* (m), $\mathcal{E}_1 \triangleq \frac{1}{K}\sum_{i=1}^{K}\sqrt{(\hat{X}_{p_1}(i)-x_{p_1})^2+(\hat{Y}_{p_1}(i)-y_{p_1})^2}$, over $K = 1000$ independent trials. In Fig. 4.2, we plot $\mathcal{E}_1$ as a function of the number of measurements. The bottom three curves correspond to measurements taken by secondary nodes located uniformly inside the circle with radius $d_{\text{det}}(p_1)$ centered at p_1. We observe that although the difference between Cases B and C is negligible, both cases show some improvement (≥ 50 m) over Case A. The top three curves correspond to the worst-case scenario where the measurements are taken by secondary nodes located only at the intersection of the detection regions $d_{\text{det}}(p_1)$ and $d_{\text{det}}(p_2)$. A significant accuracy improvement is seen in Cases B and C (≥ 335 m), more so in B than in C, over Case A. The improvement for the worst-case scenario is much greater because the proposed *compensation* becomes more prominent when both transmitters contribute approximately equally to the measurements.

4.5.2 MIFTP vs. distance

Now consider the following configuration of cochannel transmitters: $\boldsymbol{\theta}_p = (0, 0, 80)$, $\boldsymbol{\theta}_{a_1} = (20, 20, 40)$ and $\boldsymbol{\theta}_{a_2} = (-20, 20, 40)$. We vary the position, $(0, y_b)$ [km,km], of the test node b, where y_b ranges from 20 to 100 in increments of 10. The MIFTP of node b is computed according to the approach presented in Section 4.4. The angle ψ in (4.22) and (4.19) is discretized in increments of $\Delta\psi = \frac{\pi}{18}$ [rad]. Then the true MIFTP is computed according to (4.19). To approximate the MIFTP, $\mathcal{D}$ is computed for each trial. If $\mathcal{D} \neq \emptyset$, the MIFTP estimate is set to -174 dBm (which is the thermal noise floor at 1 Hz bandwidth at room temperature), otherwise, the estimated MIFTP is computed using (4.25). Note that computation of the true MIFTP requires the solution of $N_T = 1 + \frac{2\pi}{\Delta\psi}$ one-dimensional optimization problems in (4.19), whereas for the proposed approximation approach given in (4.25) requires only one.

In Fig. 4.3, we plot the true and estimated MIFTP as a function of the distance d_{bp}. As expected, the estimated MIFTP increases with distance, but is always smaller than the

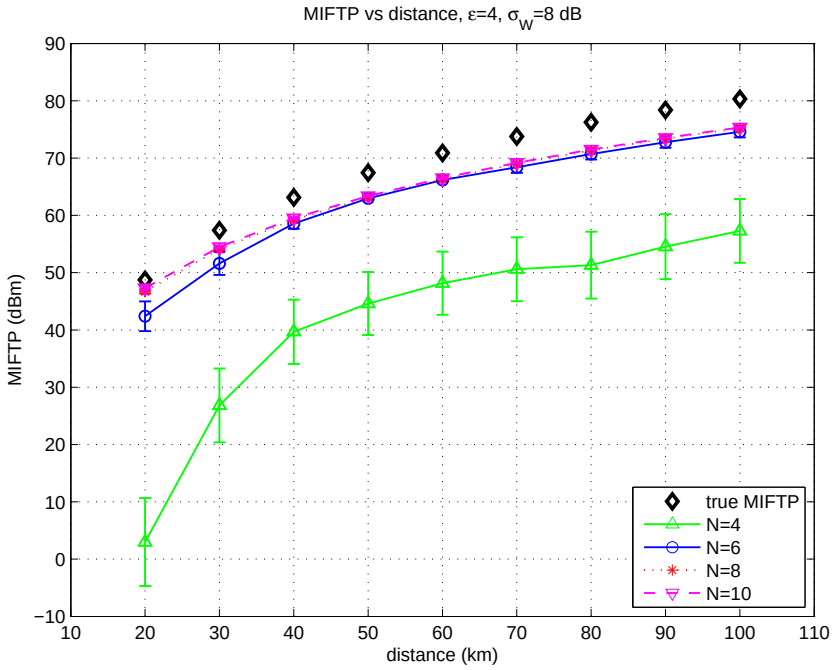

Figure 4.3: MIFTP vs. d_{bp}, for single primary transmitter p.

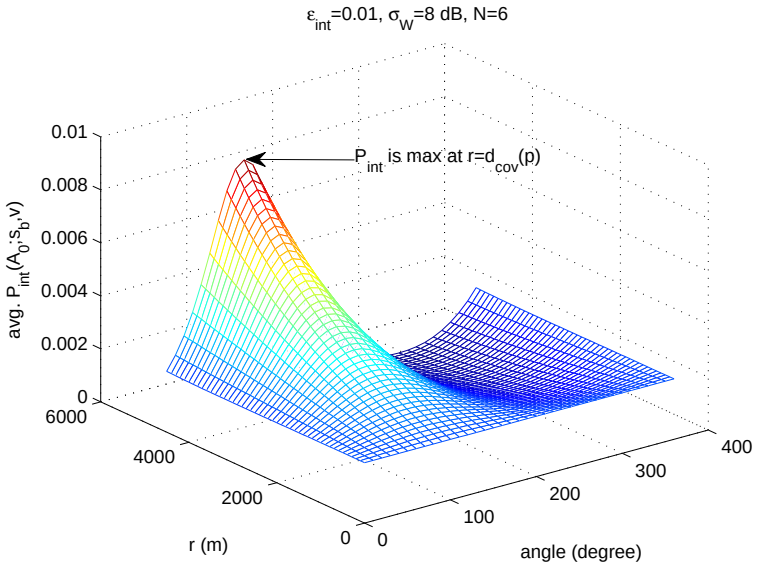

Figure 4.4: Average interference probability surface due to $\hat{s}_b^*(p)$ in the coverage region $\overline{B}_{\mathrm{cov}}(p)$.

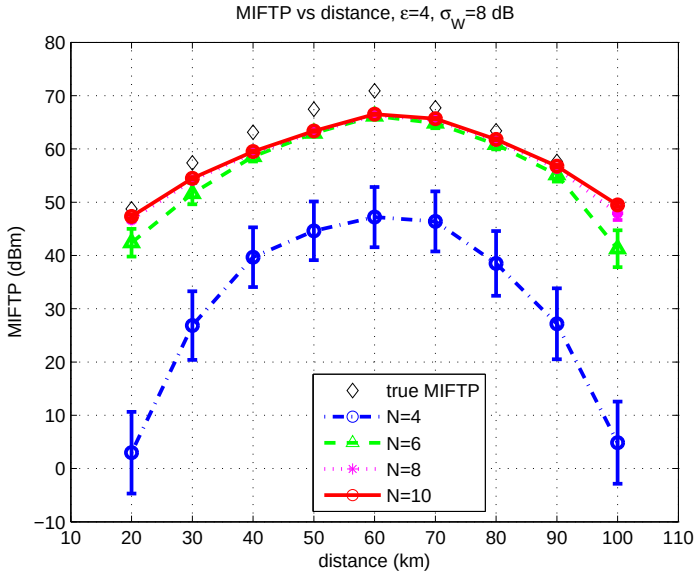

Figure 4.5: MIFTP vs. d_{bp}, for two primary transmitters, p and p'.

true MIFTP. Although for $N = 4$ the estimation is extremely conservative, a considerable improvement is seen when $N = 6$. Using more measurements is only useful for distances smaller than 50 km. On average, the estimated values are smaller than the true value by 5.35 dB, when $N = 6$ for all distances. We also plot the average interference probability (cf. (4.14)) perceived by victim nodes in $\overline{B}_{\text{cov}}(p)$ when node b transmits at $\hat{s}_b^*(p)$ for $d_{bp} = 20$ km and $N = 6$. As shown in Fig. 4.4, the interference probability surface is always less than the specified upper bound $\varepsilon_{\text{int}} = 0.01$. The same has been observed for the values of d_{bp} as well. Thus, the proposed MIFTP approximation can safely be used for opportunistic spatial spectrum access.

To study the effect of multiple primary transmitters, we consider the existence of another primary transmitter, p', in addition to p on the same channel and time, with $\boldsymbol{\theta}_{p'} = (0, 120, 80)$. Since the two transmitters are very far apart (120 km), we can ignore the effect of cochannel interference on localization. The true and approximate MIFTPs are calculated as $s_b^* = \min\{s_b^*(p), s_b^*(p')\}$ and $\hat{s}_b^* = \min\{\hat{s}_b^*(p), \hat{s}_b^*(p')\}$, respectively. Fig. 4.5 shows the variation of MIFTP as a function of distance. As node b moves away from transmitter p its MIFTP increases up to a certain level, then it decreases as it approaches p'.

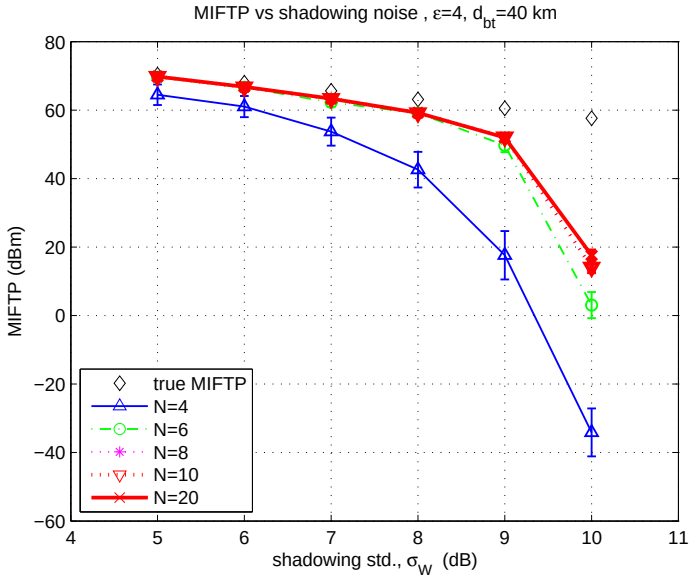

Figure 4.6: MIFTP vs. shadowing noise, σ_W.

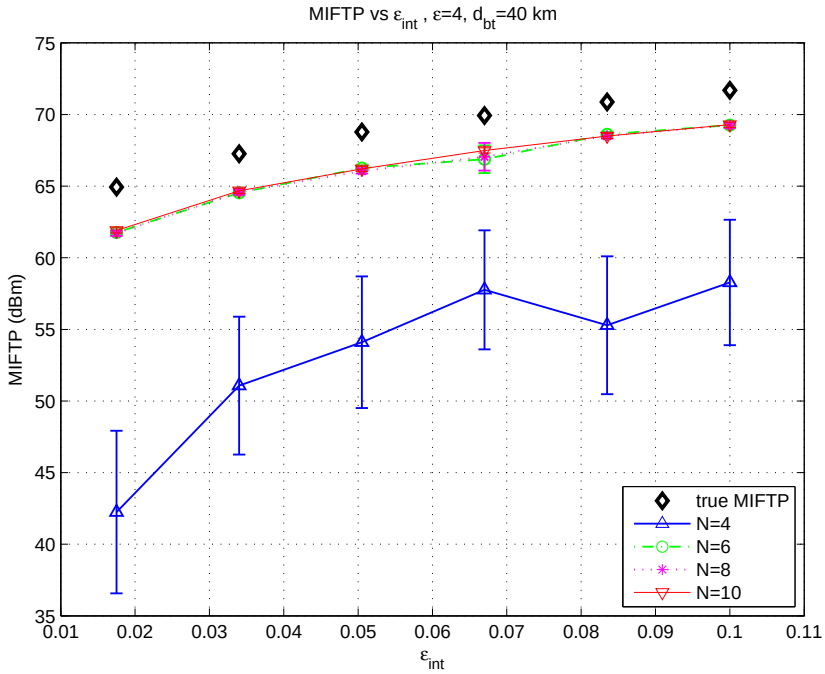

Figure 4.7: MIFTP vs. maximum interference probability threshold, ε_{int}.

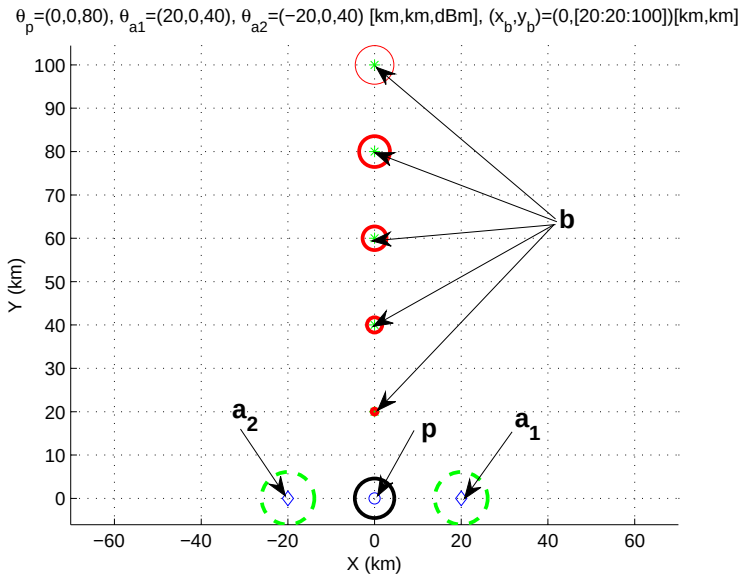

Figure 4.8: Pictorial illustration of a T-map and spectrum hole harvesting in space.

4.5.3 MIFTP vs. shadowing noise and interference probability threshold

We set $d_{bp} = 40$ km and in Fig. 4.6 plot the estimated MIFTP as a function of the shadowing noise standard deviation, σ_W. As anticipated, the MIFTP decreases with increasing noise. This is because as the noise power increases, the localization error and the associated CRB increases, which in turn makes the MIFTP more conservative. For $N = 4$ the estimated values are very loose, but it can be made reasonably tight using $N = 6$ for any $\sigma_W \leq 9$ dB. Note that the decrease in true MIFTP is linear for all σ_W, but for the estimated MIFTP it is approximately linear only for $\sigma_W \leq 9$ dB. For the extreme case of $\sigma_W > 9$ dB, the estimated MIFTP is very loose and increasing N helps very little. In Fig. 4.7, we set $\sigma_W = 8$ dB and vary ε_{int}. We notice that as expected, the MIFTP becomes more conservative as the imposed interference constraint becomes tighter (lower ε_{int}). For $N \geq 6$, on average the estimated MIFTP is within 2.7 dB of the true value.

4.5.4 T-map and spectrum hole harvesting

Consider the node configuration of Fig. 4.3. For this case Fig. 4.8 shows a pictorial illustration of the T-map for a particular channel. In this example, the estimated parameters

$\hat{\boldsymbol{\theta}}_p$ of primary transmitter p are available, while the true parameters $\boldsymbol{\theta}_{a_1}$ and $\boldsymbol{\theta}_{a_2}$ of existing secondary transmitters a_1 and a_2 are also known. All these parameters along with the appropriate CRB estimates are contained in the T-map and are propagated throughout the secondary network via a collaborative network protocol.

The circles around p, a_1 and a_2 represent their respective (estimated or true) coverage regions. The circle centered at p represents $\partial B_{\text{cov}}(p)$, inside which potential victim nodes reside. Given the information contained in the T-map, by computing $\mathcal{D}$ (see Section 4.4.2) node b can detect whether it is located inside a spectrum hole. If $\mathcal{D} = \emptyset$, node b can compute its MIFTP using the approximation presented in Section 4.4.3. The circle centered at node b represents its coverage area when it transmits at its MIFTP estimate $\hat{s}_b^*(p)$. As node b moves away from p the size of its perceived spectrum hole increases, which it can fill up by transmitting at higher transmit powers specified by its MIFTP. Hence, the information contained in the T-map characterizes the location and size of the available spectrum holes in the spatial domain.

4.6 Discussion

In this chapter, we presented a collaborative OSA scheme whereby multiple cochannel primary and secondary transmitters can co-exist in an interference-free condition. Based on a set of clustered measurements, secondary nodes estimate the power and location of primary transmitters that are located in their vicinity. Secondary nodes maintain a distributed database, called the *T-map*, containing location, power, and error estimates of cochannel nodes. The effect of cochannel interference is taken into account when global information about other cochannel transmitters becomes available via the T-map.

We developed a method for estimating the MIFTP available to a given secondary node in the presence of multiple cochannel primary transmitters. The proposed MIFTP estimation technique provides an approximate upper bound on the transmit power of a secondary

transmitter. The construction, sharing, and updating of the T-map is performed collaboratively by secondary nodes throughout the network, making the scheme adaptive and robust. Our numerical results validate the accuracy of the proposed scheme when a sufficient number of signal strength measurements is available. The approximation for MIFTP is conservative, ensuring that secondary nodes do not cause harmful interference to the primary system.

Chapter 5: Measurement clustering

5.1 Introduction

When multiple cochannel transmitters are present, accurate localization depends on using an appropriate set of SS measurements. For localizing a particular transmitter, the most useful measurements are received by nodes residing in its vicinity. This is because the effect of cochannel interference on these measurements is expected to be small. On the other hand, the worst measurements are the ones which have equal contributions of received power from multiple transmitters. Since it is difficult to resolve the power contribution from each transmitter, a large error in localization can be incurred in this case. Therefore, it is important to collect measurements that have the strongest contribution from a particular transmitter. This is equivalent to assigning each measurement to the transmitter closest to it. Therefore, to minimize the effect of cochannel interference, all the measurements should be *clustered* appropriately, where each measurement cluster represents the subset of measurements to be used in the localization of a particular transmitter. For this reason, the k-means clustering algorithm is used in [47,48], which requires that the total number of cochannel transmitters in the network, say M, be known *a priori*. This clustering technique, which is based on a distance metric, uses only the position information of the secondary nodes, but the measured SS information is not taken into account.

In this chapter[1], we assume that M is unknown and must be estimated, preferably by a central processor having access to the complete measurement set, before measurement clustering and localization can be performed. In essence this is a model identification problem and we need to select/estimate the number of cochannel transmitters, $\hat{M}$, that is most likely to generate the given measurement set. We propose two criteria to determine

[1]The contents of this chapter appeared in [86].

$\hat{M}$: (1) *net minimum mean square error* (MMSE), and (2) the *minimum description length* (MDL). The net MMSE criterion is based on the Cramér-Rao lower bound (CRB) on localization accuracy, whereas the MDL is an information-theoretic criterion that selects the most likely model generating the given observations taking into account the model complexity. Both criteria lead to a measurement clustering algorithm in a natural way. Although we consider only signal strength measurements, the approach can be generalized to include other types of observations (e.g., time and angle information) with independent measurements in additive noise.

We assume the same SS observation model of Chapter 3 and 4. The remainder of the chapter is organized as follows. The two measurement clustering criteria are presented in Section 5.2. Numerical results demonstrating the effectiveness of our approach are presented in Section 5.3. The chapter is concluded in Section 5.4.

5.2 Measurement clustering criteria

The set of independent SS observations is denoted by $\mathcal{O} \triangleq \{(R_a, \boldsymbol{L}_a) : a \in \mathcal{A}\}$, where R_a is the net SS received due to all cochannel transmitters at the secondary node a, located at $\boldsymbol{L}_a \triangleq (x_a \ y_a)$. Suppose that the SS measurements are generated due to concurrent transmissions of $M = |\mathcal{P}|$ primary transmitters. Clustering of the measurements is performed in two steps by a central processor: (1) find $\hat{M}$, and (2) cluster the set of observations $\mathcal{O}$ into $\hat{M}$ distinct subsets.

The set of unknown parameters is denoted by $\boldsymbol{\Theta}_M \triangleq \{\boldsymbol{\theta}_i\}_{i=1}^{M}$, where $\boldsymbol{\theta}_i \triangleq (x_{p_i}, y_{p_i}, s_{p_i})$ denotes the transmit power s_{p_i} of primary transmitter p_i located at (x_{p_i}, y_{p_i}). In the range of practical interest, $R_{ij} \in [-150, 100]$ dBm, the scaled observation conditioned on all the parameters can be modeled as:

$$\widetilde{R}_a | \{\boldsymbol{\theta}_i\}_{i=1}^{M} \sim \mathcal{N}\left(\ln\left(\sum_{i=1}^{M} e^{\kappa u_{ap_i}}\right), \kappa^2\sigma_W^2\right), \ \forall a \in \mathcal{A}, \tag{5.1}$$

where $\widetilde{R}_a \triangleq \kappa R_a$, $\kappa \triangleq \frac{\ln 10}{10}$ and $u_{ij} \triangleq s_j - g(d_{ij})$, (see Chapter 4). If $M = j$ and $N \triangleq |\mathcal{A}|$, the log-likelihood function is given by

$$L_j \equiv L(\{\boldsymbol{\theta}_i\}_{i=1}^{j}) \triangleq \sum_{a=1}^{N} \ln f_{\widetilde{R}_a|\{\boldsymbol{\theta}_i\}_{i=1}^{j}}(\widetilde{R}_a). \tag{5.2}$$

5.2.1 Net MMSE Criterion

We denote the CRB of $\boldsymbol{\Theta}_j$ by $\boldsymbol{J}_j^{-1}$, which is a matrix of dimension $3j \times 3j$. The components of the Fisher information matrix (FIM), $\boldsymbol{J}_j$, are given in Appendix C.1. Similar to the single and multiple transmitter cases discussed in Chapters 3 and 4, from (5.1) we conclude that $\boldsymbol{J}_j^{-1}$ will be achievable asymptotically as $\sigma_W \to 0$. For $j \geq 1$, define the following sets:

$$\mathcal{T}_1^{(j)} = \{1, 2, 4, 5, \cdots, 3j-2, 3j-1\}, \tag{5.3}$$

$$\mathcal{T}_2^{(j)} = \{3, 6, \cdots, 3j\}. \tag{5.4}$$

The net MMSE criterion for determining $\hat{M}$ is given by

$$\hat{M} = \arg \min_{j \in \mathcal{J}} \ \{\mathcal{E}_j\}, \tag{5.5}$$

$$\mathcal{E}_j \triangleq \frac{\sum_{\alpha \in \mathcal{T}_1^{(j)}} \left[\boldsymbol{J}_j^{-1}\right]_{(\alpha,\alpha)}}{2j} + \frac{\sum_{\beta \in \mathcal{T}_2^{(j)}} \left[\boldsymbol{J}_j^{-1}\right]_{(\beta,\beta)}}{j}, \tag{5.6}$$

where $\mathcal{J} = \{1, 2, \cdots, M_{\max}\}$ and $M_{\max}$ is an appropriately chosen integer that represents the maximum possible number of cochannel transmitters in the network.

The two terms in (5.6) represent the normalized (per transmitter) MMSE for location and transmit power estimation, respectively. The intuition behind this criterion is that, since the CRB is asymptotically achievable, the estimation error will be minimum when $\hat{M} = M$. In essence, the FIM represents the amount of information contained in the observations

about the unknown parameters. Note that the true CRBs, $\{\boldsymbol{J}_j^{-1}\}$ are functions of the true unknown parameters $\{\boldsymbol{\Theta}_j\}$, and hence the net MMSEs, $\{\mathcal{E}_j\}$, cannot be computed. Thus, we replace $\{\mathcal{E}_j\}$ by its maximum likelihood estimate (MLE), $\{\hat{\mathcal{E}}_j\}$. This is justified by the invariance principle, which states that the MLE of a function $q(\cdot)$ of $\boldsymbol{\Psi}$ is given by $q(\hat{\boldsymbol{\Psi}})$, where $\hat{\boldsymbol{\Psi}}$ denotes the MLE of $\boldsymbol{\Psi}$, (cf. [78, p. 217]).

5.2.2 MDL Criterion

The MDL criterion has been used successfully for identifying the number of sources impinging on an antenna array and is asymptotically efficient (cf. [87]). We propose to use the information theoretic criterion *minimum description length* (MDL) for estimating $\hat{M}$ [85,88]. For signal-strength-based localization, the MDL criterion is given by

$$\hat{M} = \arg \min_{j \in \mathcal{J}} \ \{\mathrm{MDL}(j)\}, \tag{5.7}$$

$$\mathrm{MDL}(j) \triangleq \ -\sum_{a \in \mathcal{A}} \ln f_{\widetilde{R}_a | \{\hat{\boldsymbol{\theta}}_i\}_{i=1}^{j}} + \frac{3j}{2} \ln N. \tag{5.8}$$

The first term in (5.7) represents the negative log-likelihood function of the independent and scaled signal strength observations, $\{\widetilde{R}_a\}$, evaluated at $\{\hat{\boldsymbol{\theta}}_i\}_{i=1}^{j}$, which represents the parameter set of ML location and transmit power estimates given that j cochannel transmitters are present. The second term is a penalty function that accounts for the model complexity.

5.2.3 Measurement clustering

Both the net MMSE and MDL criteria lead naturally to a measurement clustering scheme. Since, the above criteria require the computation of the MLE of the unknown parameters, $\hat{M}$ clusters can be obtained by simply assigning each SS measurement to the transmitter

located closest to it. The clusters obtained in this way are denoted as follows:

$$\mathcal{O}_j = \{R_a, \forall a \in \mathcal{A} : \min_{j \in \{1,\cdots,\hat{M}\}} \{\hat{D}_{aj}\}\},$$

where

$$\hat{D}_{aj} = \sqrt{(x_a - \hat{X}_{p_j})^2 + (y_a - \hat{Y}_{p_j})^2}, \tag{5.9}$$

denotes the MLE of d_{ap_j}.

The process of estimating M and measurement clustering can be summarized symbolically as follows:

$$\mathcal{O} \underset{j=1:M_{\max}}{\overset{\text{MLE}}{\longrightarrow}} \{\hat{\boldsymbol{\theta}}_j\} \underset{\{\hat{\text{MDL}}(j)\}}{\overset{\{\hat{\mathcal{E}}_j\}\text{or}}{\longrightarrow}} \hat{M} \overset{\text{clustering}}{\longrightarrow} \{\mathcal{O}_j\}_{j=1}^{\hat{M}}. \tag{5.10}$$

In the first step indicated in (5.10), computation of the MLE of the parameters involves solving $M_{\max}$ nonlinear optimization problems with the following nonlinear constraints:

$$d_{\text{cov}}(p_k) + d_{\text{cov}}(p_l) \leq \sqrt{(x_{p_k} - x_{p_l})^2 + (y_{p_k} - y_{p_l})^2}, \tag{5.11}$$

$\forall k \neq l$. Although in real networks, the coverage regions of multiple transmitters may overlap slightly, such constraints can help improve clustering accuracy by limiting the search space.

5.3 Numerical results

To study the effectiveness of the proposed net MMSE and MDL criteria we set $M = 3$, $M_{\max} = 8$, $\sigma_W = 6$ dB, $r_{\min} = -75$ dBm, $\varepsilon_{\text{cov}} = 0.01$, $\epsilon = 3$, $g(d) = 10\epsilon \log_{10}(d)$. Three cochannel primary transmitters are located at $(0, 0)$, $(4, 0)$, $(2.5, 4)$ [km], with randomly selected transmit powers in the range $[20, 40]$ dBm. We place N secondary nodes uniformly

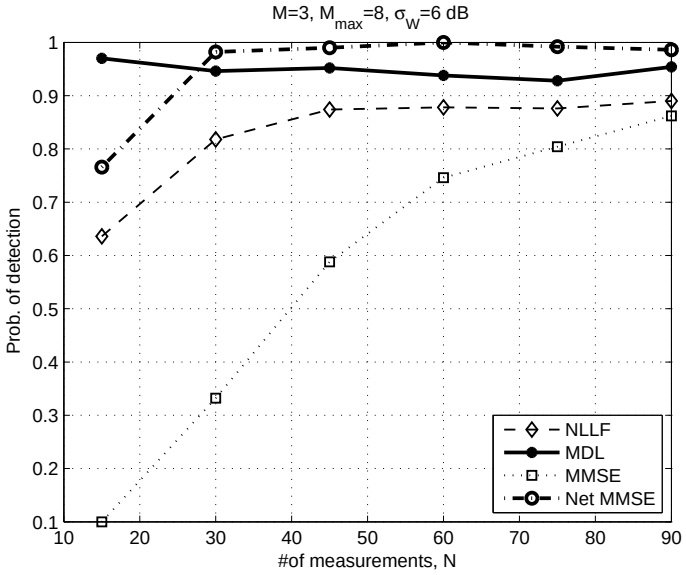

Figure 5.1: Average detection probability, $\widehat{\Pr}(\hat{M} = M)$ vs. N.

within the three coverage regions and perform model selection using the two criteria, as given by (5.5) and (5.7). In Fig. 5.1, we plot the estimated detection probability $\widehat{\Pr}(\hat{M} = M)$ as a function of the number of measurements, N, averaged over 500 trial runs. To show the necessity of the normalization of the net MMSE criterion, we plot the MMSE term, which represents the sum total of the estimation errors. Similarly, to illustrate the necessity of the penalty term in the MDL criterion, we also plot the negative log-likelihood function (NLLF).

We see that for the chosen parameter range, both the criteria are able to identify M with a high degree of accuracy. The MDL criterion is successful at least 92% of the time for all values of N, whereas for $N \geq 30$ the net MMSE criterion achieves an accuracy of at least 98%. The general trend of increase in detection accuracy with N can be explained by noting that as N becomes large: (1) the estimation error decreases, and (2) the density of the secondary nodes within each coverage region increases, which makes the true pattern of the clusters more evident.

In Fig. 5.2, we plot $\widehat{\Pr}(\hat{M} = M)$ as a function of shadowing noise, σ_W^2. For $\sigma_W \geq 6$ dB, both criteria perform very well with at least 96% accuracy. But for $\sigma_W < 6$ dB, the detection

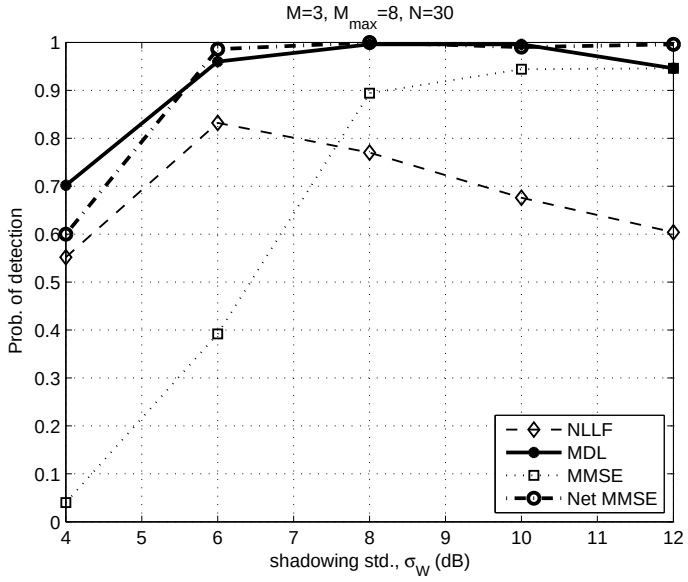

Figure 5.2: Average detection probability, $\hat{\Pr}(\hat{M} = M)$ vs. σ_W.

accuracy decreases considerably. This is because as the shadowing noise decreases, the coverage radius increases (cf. (3.5)), which in turn increases the overlap between different cochannel transmitters, making the true pattern of the clusters more difficult to identify.

An example of the effect of incorrect clustering is presented in Figs. 5.3–5.5. Fig. 5.3 shows the true locations of the primary transmitters indicated by stars, as well as the associated coverage regions enclosed by the large circles. The locations of the secondary nodes taking signal strength measurements are indicated by small circles. In Fig. 5.4 illustrates an example of correct cluster identification, i.e., $\hat{M} = M$. Here, the ML estimated locations of the primary transmitters are shown as diamonds and the associated coverage regions are shown enclosed by the large circles. Fig. 5.5 shows incorrect clustering resulting from an incorrect estimation of M, i.e., $\hat{M} = 4$. Clearly, the clustering of Fig. 5.5 will result in incorrect characterization of the primary system and hence may lead to harmful interference to the primary system due to secondary transmissions.

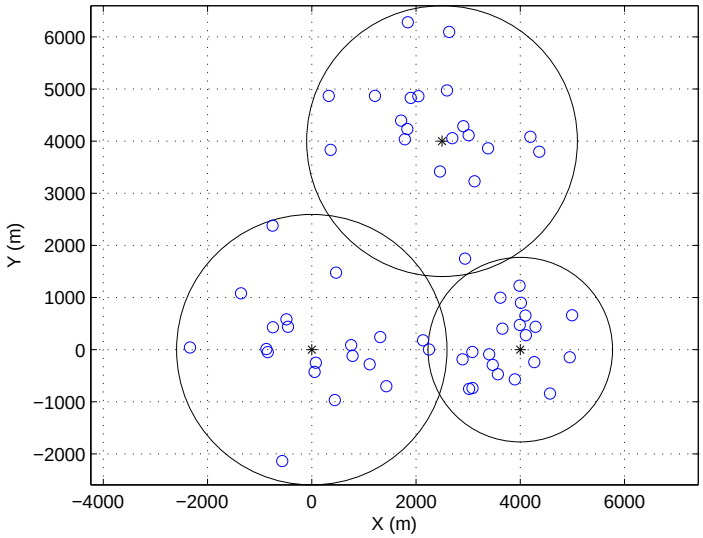

Figure 5.3: True locations and coverage radii of the primary transmitters.

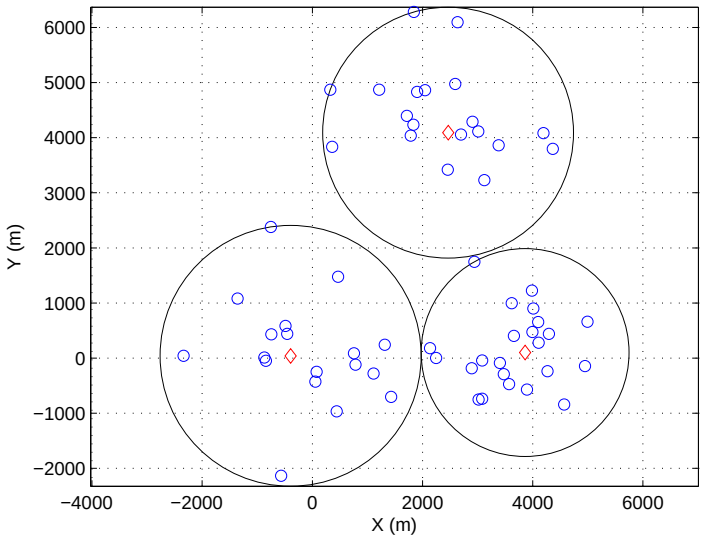

Figure 5.4: Clustering due to correct identification of M.

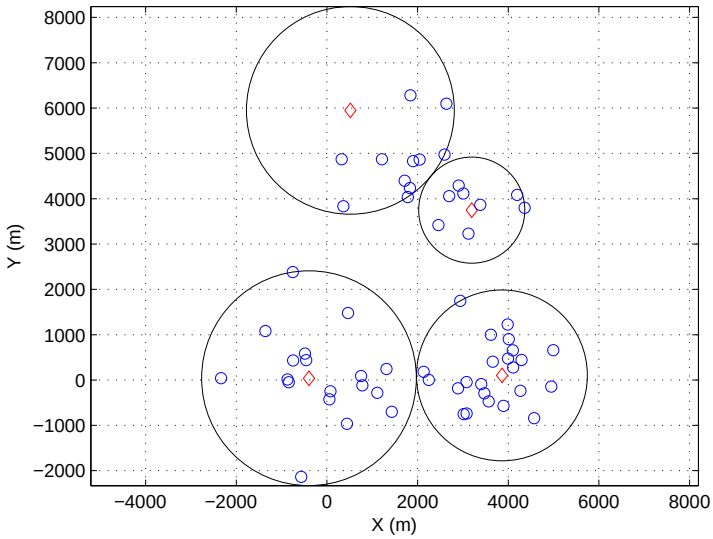

Figure 5.5: Clustering due to incorrect identification of M.

5.4 Discussion

We considered the model identification and measurement clustering problem for SS-based localization in the presence of multiple cochannel transmitters. The results presented can be utilized to perform localization-based spatial sensing suitable for opportunistic spectrum access. Our approach is to collect all the measurements at a central processor and apply one of two proposed selection criterion: net MMSE or MDL. For the particular simulation scenarios considered, the net MMSE criterion exhibited superior performance most of the time, although at the expense of more computation, compared to the MDL criterion.

Once the total number of transmitters is identified, the transmitter location estimates can be used as a basis for measurement clustering. Our numerical studies showed that the two criteria may result in incorrect clustering when there are very few measurements or the coverage regions have a high degree of overlap. Although only SS measurements were considered in this work, our approach can be generalized to other types of measurements (e.g., time delay or angle-of-arrival) observed in additive noise.

Chapter 6: Spectrum Sensing with SS-AOA Measurements and Directional Transmissions

6.1 Introduction

For successful opportunistic spectrum access according to our approach, a crucial first step is to accurately estimate the locations of the primary transmitters, along with any other relevant unknown parameters (e.g., transmit power). Certain military applications may also require this type of noncooperative geolocation scheme. In this chapter, we focus on a noncooperative localization scheme for which the location and transmit power of the primary transmitter is not known to the secondary nodes. The localization scheme proposed in this chapter is a hybrid approach making use of signal strength (SS) and angle-of-arrival (AOA) measurements.

Conventional localization schemes use the location information embedded in the received waveform, namely, time-of-arrival (TOA), time-difference-of-arrival (TDOA), angle-of-arrival (AOA) or signal strength (SS). In the presence of measurement noise, statistical location estimation methods can be used and have the potential to achieve optimality with respect to some error criterion (typically, the mean-squared-error). Hybrid *cooperative* positioning schemes that use more than one type of measurement have also been proposed (cf. [71, 89–91]).

In [71], an unified accuracy analysis of optimal wireless geolocation is presented. The accuracy of the localization schemes based on time-delay information (TOA or TDOA) fundamentally depend on the signal-to-noise-ratio (SNR) and signal bandwidth. Typically, knowledge of the transmitted waveform is required to extract TOA information from the received signal. In the TDOA approach, it is possible to extract the TDOA information

without the knowledge of the transmitted waveform, by cross-correlating the received signal at multiple secondary receivers [72]. In this approach, to extract each TDOA information, the two received signals must be sent to a single processor to perform the cross-correlation operation, which may incur considerable overhead on the control channel. On the other hand, SS-based schemes are cost-effective and easily implementable in practice. Nevertheless, SS-based schemes can suffer from poor accuracy because they are highly dependent on the parameters of the radio propagation environment, namely, the path loss exponent and shadowing noise, over which the receiver has no control. In AOA-based schemes, high accuracy can be achieved by using antenna arrays at line-of-sight (LOS) conditions with a sufficient number of elements at high SNR. But deployment of antenna arrays is relatively expensive, and degraded performance is expected when propagation is highly non-line-of-sight (NLOS) and large distances are involved.

In this chapter, we propose an optimal noncooperative hybrid SS-AOA localization scheme. To the best of our knowledge, optimal hybrid SS-AOA localization has not been studied in the research literature. Our simulation studies demonstrate that when only a handful of SS measurements are available, a considerable accuracy improvement can be achieved by using only one or two accurate AOA measurements. The second contribution of this chapter is a scheme, based on the Cramér-Rao bound (CRB), for selecting the optimal subset, with respect to localization accuracy, from among an available set of measurements. The scheme is useful for improving localization accuracy, and detecting faulty measurements.

Finally, we explore the possibility of spectrum hole harvesting by the secondary transmitters using directional antennas. In the previous chapters, we assumed that all secondary transmissions are omnidirectional, and used the MIFTP to characterize their maximum permissible transmit power. But if a secondary transmitter is equipped with an antenna array, via beamforming it could potentially transmit at higher power than its calculated MIFTP, depending on its location and orientation with respect to the primary transmitters. In particular, we specify the transmission direction and beamwidth of a secondary transmitter

in the presence of sensing error. The capability of the secondary nodes to perform spatial sensing using AOA measurements and to attain transmission directivity using beamforming, can increase the overall system capacity and reduce interference. Moreover, such a scheme is well-suited to the popular multiple input multiple output (MIMO) architecture, which has its own advantages to offer for communication over a wireless channel.

The remainder of the chapter is organized as follows. In Section 6.2, we present our proposed hybrid localization scheme based on SS and AOA measurements. In Section 6.3, we discuss the measurement selection rule. We discuss the angular specification for secondary directional transmissions in Section 6.4. Numerical results are presented in Section 6.5 and the chapter is concluded in Section 6.6.

6.2 Optimal Hybrid SS-AOA localization

We consider a scenario where a group of localizing nodes collaboratively try to estimate the location of a target transmitter in two-dimensional space transmitting on a particular frequency channel. The optimal location estimates can be found in two steps [92]:

1. Extract optimal intermediate estimates (namely, SS and AOA) from the received signal.

2. Find optimal location estimates based on these intermediate estimates.

In this section, we present models that represent the outcome of the first step and then focus on how the second step should be carried out.

We assume that there are N_1 nodes capable of taking only SS measurements, indexed as $i = 1, 2, \cdots, N_1$. Also, there are N_2 nodes capable of taking both SS and AOA measurements, indexed as $i = N_1 + 1, N_1 + 2, \cdots, N_1 + N_2$. The assumption is that these measurements have been collected after performing appropriate model identification and measurement clustering, as prescribed in Chapter 5. As a result, the effect of cochannel interference on these measurements becomes negligible, and we concentrate on the localization of a single primary transmitter.

The signal measurements can be collected by a mobile localizing node along its own trajectory and/or via measurement sharing among the collaborating localizing nodes within the network. The localizing nodes share the measurements, as well as their own locations, with each other. It is assumed that the localizing nodes know their own positions via GPS (Global Positioning System) or some other type of self-localization scheme (cf. [63, 65]). The transmitter is assumed to be stationary and to transmit at constant power during the window of measurement collection.

6.2.1 SS measurement model

We assume that all primary transmissions are omnidirectional and adopt the canonical signal strength measurement model given in (3.18)-(3.20) of Chapter 3. We briefly mention an approach to account for directional primary transmissions in Section 6.2.2. For the model presented in (3.18), in the absence of any a priori information about the transmitter's location, the optimal (in the mean-squared-error sense) location estimator is the ML estimator (MLE) (cf., Chapter 3). Given that a particular localizing node or a central processor collects N_1 uncorrelated SS measurements, the ML solution is found by solving the following optimization problem:

$$\hat{\boldsymbol{\Theta}}_{\mathrm{ML}}(\mathrm{SS}) = \arg\max_{\boldsymbol{\Theta}} \left[\prod_{i=1}^{N_1} \frac{1}{\sqrt{2\pi\sigma_W^2}} \exp\left\{ -\frac{(S_i - s_p + 10\epsilon \log_{10} d_i)^2}{2\sigma_W^2} \right\} \right],$$

where S_i is the i^{th} SS measurement taken by the secondary node located at (x_i, y_i), s_p is the transmit power of the primary transmitter located at (x_p, y_p), and $10\epsilon \log_{10} d_i$ represents the path loss function, with ϵ being the path loss factor and $d_i = \sqrt{(x_p - x_i)^2 + (y_p - y_i)^2}$. Equivalently, we can solve the minimization problem:

$$\hat{\boldsymbol{\Theta}}_{\mathrm{ML}}(\mathrm{SS}) = \arg\min_{\boldsymbol{\Theta}} \left\{ \sum_{i=1}^{N_1} \frac{(S_i - s_p + 10\epsilon \log_{10} d_i)^2}{\sigma_W^2} \right\}. \tag{6.1}$$

6.2.2 Directional primary transmissions

If the radiation pattern of the primary transmitter is not omnidirectional, this would lead to inaccuracies in our approach. As a first step to see how the estimation problem changes for directional radiation pattern of the primary transmitter, we assume that the side lobe leakage is negligible and all signal strength measurements are taken by nodes located within the main lobe of the primary's radiation pattern. In such a scenario, we need to estimate the primary antenna's beam pattern function, f, that characterizes the variation of the antenna's power pattern in the main lobe as a function of angle. To incorporate directional transmission in our framework, assuming that the form of $f(\cdot)$ is known, we estimate the parameters that define it, along with the previous parameters (namely, location and s_p). To generalize our approach we can model the i^{th} received power (in dB scale) as

$$S_i = s_p + 10\log_{10} f_i^2(\boldsymbol{p}) - g(d_i) + W_i \text{ [dBm]}, \tag{6.2}$$

where $\boldsymbol{p}$ denotes the vector of parameters that characterize f. If the form of $f(\cdot)$ is unknown, we approximate the function $f(\cdot)$ by a window-like function with an appropriate roll-off. In such a scenario, it may be necessary to employ array processing at the FAR nodes, at least in some of them. From the point of view of accuracy, the estimation of $f(\boldsymbol{p})$ will increase the error variance of the other parameters due to the nuisance parameter effect. As a result, roughly speaking, more measurements would be needed to offset the increase in error due to the estimation of $f(\boldsymbol{p})$. More details, and a simulation result related to directional attennas are provided in Appendix D.1.

6.2.3 AOA measurement model

We assume that a subset of the localizing nodes are equipped with narrowband antenna arrays. These nodes are capable of measuring both AOA and SS information. As an illustrative and introductory example, in this chapter, we consider nodes with uniform linear arrays (ULAs) and assume that the receivers can estimate AOA corresponding to

the line-of-sight (LOS) component of the received signal [93]. We note that in order to use NLOS AOA data for location estimation, we need to estimate the NLOS induced angle errors along with $\boldsymbol{L}_p$, which increases the model complexity and compromises the estimation accuracy significantly [71].

As a first approximation, we assume that there is negligible correlation between the two errors. In this case, the i^{th} AOA measurement is given by [71]:

$$U_i = 2\pi\Delta\cos\phi_i + \delta_i, \quad i = N_1+1, \cdots, N_1+N_2,$$

where $\phi_i = \tan^{-1}\left(\frac{y_p - y_i}{x_p - x_i}\right)$ represents the LOS angle between $\boldsymbol{L}_i$ and $\boldsymbol{L}_p$ and Δ is the distance between two adjacent antenna elements (normalized by the minimum carrier wavelength). The AOA estimation error, δ_i, is modeled as $\delta_i \sim \mathcal{N}(0, \sigma_i^2)$, with

$$\sigma_i^2 = \frac{3}{K(K+1)(2K+1)R_i},$$

where K is the number of antenna elements and R_i is the known received SNR [71]. We model R_i as $\frac{R_0}{d_i^{\epsilon}}$, where R_0 denotes the reference SNR measured at the reference distance, d_0. Note that, unlike the SS-case, where the receiver can do little to combat the shadowing noise, in the AOA-case accurate AOA estimates can be found by using a large number of antenna elements and high receiver sensitivity. The MLE is given by

$$\hat{\boldsymbol{\Theta}}_{\text{ML}}(\text{AOA}) = \arg\min_{\boldsymbol{\Theta}} \left\{ \sum_{i=N_1+1}^{N_1+N_2} \frac{(U_i - 2\pi\Delta\cos\phi_i)^2}{\sigma_i^2} + \sum_{i=N_1+1}^{N_1+N_2} \frac{(S_i - s_p + 10\epsilon\log_{10} d_i)^2}{\sigma_W^2} \right\}. \tag{6.3}$$

6.2.4 Hybrid SS-AOA localization

Under the assumption that the SS and AOA measurements are uncorrelated, the joint likelihood function of the hybrid SS-AOA model can be written as the product of the likelihood functions for the SS-only and AOA-only models. As a result, the optimal hybrid SS-AOA location estimate is given by

$$\hat{\boldsymbol{\Theta}}_{\mathrm{ML}}(\mathrm{SS}+\mathrm{AOA}) = \arg\min_{\boldsymbol{\Theta}} \left\{ \sum_{i=1}^{N_1+N_2} \frac{(S_i - s_p + 10\epsilon \log_{10} d_i)^2}{\sigma_W^2} + \sum_{i=N_1+1}^{N_1+N_2} \frac{(U_i - 2\pi\Delta\cos\phi_i)^2}{\sigma_i^2} \right\}. \tag{6.4}$$

6.3 Measurement Selection Scheme

For the observation models presented in Section 6.2, we develop a selection rule for measurements, based on the Cramér-Rao bound (CRB), such that localization error is minimized. Besides accuracy improvement, our rule can be used to determine whether or not a particular measurement can significantly degrade the estimation accuracy. This is similar to the Receiver Autonomous Integrity Monitoring (RAIM) problem in GPS localization [94]. An efficient measurement selection scheme is also useful when there is an upper bound on the number of measurements allowed for the estimation task. For example, if the localization algorithm can only use M measurements, this rule can be used to choose the best M measurements from an available set of N measurements, where $M < N$. Before presenting our proposed selection scheme, we consider the CRB for the measurement models given in Section 6.2.

6.3.1 CRB on localization error

For the SS measurements, $\{S_i\}_{i=1}^{N_1+N_2}$, we denote the FIM as $\boldsymbol{J}_{\boldsymbol{\Theta}}(\mathrm{SS})$, (see Chapter 3 for a closed-form expression). The FIM can be singular if $N_1 + N_2 < 3$, or the localizing nodes are collinear. Note that the accuracy of the SS-based localization depends on the shadowing noise, path loss factor, number of measurements and the geometry of the target

and localizing nodes.

For the AOA measurements, $\{U_i\}_{i=1}^{N_2}$, the FIM is given by [71]

$$\boldsymbol{J}_{\boldsymbol{\Theta}}(\text{AOA}) \;=\; \begin{bmatrix} \boldsymbol{J}_{\boldsymbol{L}_p} & 0 \\ 0 & 0 \end{bmatrix}, \tag{6.5}$$

where

$$\boldsymbol{J}_{\boldsymbol{L}_p} \;\triangleq\; 4\pi^2\Delta^2\boldsymbol{H}\boldsymbol{D}^2\boldsymbol{\Lambda}^2\boldsymbol{H}^T,$$

$$\boldsymbol{H} \triangleq \begin{bmatrix} \sin^2\phi_1 & \cdots & \sin^2\phi_{N_2} \\ -\sin\phi_1\cos\phi_1 & \cdots & -\sin\phi_{N_2}\cos\phi_{N_2} \end{bmatrix} \tag{6.6}$$

and

$$\boldsymbol{\Lambda} \;\triangleq\; \text{diag}\left[\sigma_1^{-1},\cdots,\sigma_{N_2}^{-1}\right].$$

Here, the accuracy of the AOA-based localization depends on the observation noise, ULA structure, number of measurements and the geometry of the target and localizing nodes. If all the observations are considered independent, then the CRB on the hybrid SS-AOA localization scheme is given by

$$\boldsymbol{J}_{\boldsymbol{\Theta}}^{-1}(\text{SS}+\text{AOA}) = \left(\boldsymbol{J}_{\boldsymbol{\Theta}}(\text{SS}) + \boldsymbol{J}_{\boldsymbol{\Theta}}(\text{AOA})\right)^{-1}. \tag{6.7}$$

6.3.2 Selection rule

The CRB is a useful measure of the *goodness* of a set of measurements for the following reasons:

1. The FIM is a measure of the amount of the "information" present in the observed data about $\boldsymbol{\Theta}$, [95, p. 330].

2. From [71], we know that the CRB can be achieved by the MLE asymptotically, as the noise power of the measurement model becomes vanishingly small. In other words, the MLE becomes an *efficient* estimator for the SS model as $\sigma_W^2 \rightarrow 0$ and for the AOA model as $\sigma^2 \rightarrow 0$, respectively. So, in this regime, the CRB is expected to *optimally* rank the "goodness" of the measurements.

Since the CRB, $\boldsymbol{J}_{\boldsymbol{\Theta}}^{-1}$, corresponding to (3.33), (6.5) or (6.7), is given in terms of the true values of the unknown parameters, $\boldsymbol{\Theta}$, we cannot calculate it directly. Instead, we evaluate the CRB at the maximum likelihood estimator (MLE), $\hat{\boldsymbol{\Theta}}_{\mathrm{ML}}$, i.e.,

$$\boldsymbol{J}_{\boldsymbol{\Theta}}^{-1} \mid_{\boldsymbol{\Theta}=\hat{\boldsymbol{\Theta}}_{\mathrm{ML}}} \triangleq \hat{\boldsymbol{J}}_{\boldsymbol{\Theta}}^{-1}, \tag{6.8}$$

where $\hat{\boldsymbol{J}}_{\boldsymbol{\Theta}}^{-1}$ denotes the MLE of $\boldsymbol{J}_{\boldsymbol{\Theta}}^{-1}$. Equation (6.8) is due to the invariance principle (cf. [78, p. 217]), which states that the MLE of a function $h(\cdot)$ of $\boldsymbol{x}$ is given by $h(\hat{\boldsymbol{X}}_{\mathrm{ML}})$, where $\hat{\boldsymbol{X}}_{\mathrm{ML}}$ denotes the MLE of $\boldsymbol{x}$.

Suppose we are given a set of N observations, $\boldsymbol{\mathcal{R}} = \{R_1, \cdots, R_N\}$ and we need to choose M observations from this set, when $M < N$, such that the MLE-based localization error is minimized. First, from $\boldsymbol{\mathcal{R}}$ we construct a set consisting of all possible subsets of cardinality M. We call this new set $\boldsymbol{\mathcal{T}}_M$, where $\boldsymbol{\mathcal{T}}_M = \{T_1, \cdots, T_C\}$, where $C = \begin{pmatrix} N \\ M \end{pmatrix}$. For every set $T_i \in \boldsymbol{\mathcal{T}}_M$, we compute $\hat{\boldsymbol{\Theta}}_{\mathrm{ML}}(i)$ and the corresponding $\hat{\boldsymbol{J}}_{\boldsymbol{\Theta}}^{-1}(i)$, where $i = 1, \cdots, C$. Then the index of the best measurement subset is given by

$$I \;=\; \arg\min_i \left\{ \hat{\boldsymbol{J}}_{\boldsymbol{\Theta}}^{-1}(i) \right\}. \tag{6.9}$$

Subject to the available computational resources, this rule can be further generalized by varying the value of M. In this case, we should consider all the sets $\boldsymbol{\mathcal{T}}_3, \cdots, \boldsymbol{\mathcal{T}}_N$ together. We require $M \geq 3$ to avoid a possible singularity in CRB calculation. A useful value of M in practice is $M = N - 1$, in which case $C = N$.

6.4 Angular thresholds for directional transmissions

In this section, we present the angular specification by which a secondary node can transmit directionally, and potentially at higher transmit power than its MIFTP. We assume that there is a single primary transmitter, and a group of collaborating secondary nodes estimate its location and transmit power using received SS measurements. We point out that, our approach can be readily generalized to include multiple cochannel primary transmitters using the scheme discussed in Chapters 4 and 5. As in Section 6.2, hybrid localization using both SS and AOA observations can also be performed to estimate the parameters of the primary transmitter(s) with increasing accuracy.

Suppose, a particular secondary node, a, is equipped with an antenna array and can dynamically perform beamforming to direct its transmissions toward a particular range of angles. Also, assume that it has access to the MLEs of the primary transmitter's location and transmit power, including the associated CRB estimates. Such information can be made available via the T-map construct mentioned in Chapter 4. It is also possible that node a only has a set of SS measurements taken at the vicinity of the primary transmitter and uses them to perform localization on its own. In such a circumstance, node a needs to decide its transmission direction, i.e., the heading of its mainlobe and its width, subject to a constraint on the amount of sidelobe leakage.

Such angular specification can occur with two different scenarios: (1) if the transmission mainlobe of node a contains the primary's coverage region, then its MIFTP, $\hat{s}_a$, characterizes its transmit power upper bound. (2) if node a chooses to transmit in a direction that does not contain the coverage region of any primary transmitter, then it can potentially transmit at more than its MIFTP (say at a maximum power level, $s_a^{\max}$ determined by its hardware specification and its intended receiver), provided that the sidelobe leakage towards any primary transmitter is upper bounded by $\hat{s}_a$. In other words, the sidelobe beam pattern function, f_{side}, must satisfy the condition (in dBm):

$$s_a^{\max} + 10\log_{10} f_{\text{side}}^2(\psi) \leq \hat{s}_a, \ \forall \psi \in \Psi_{pa}, \tag{6.10}$$

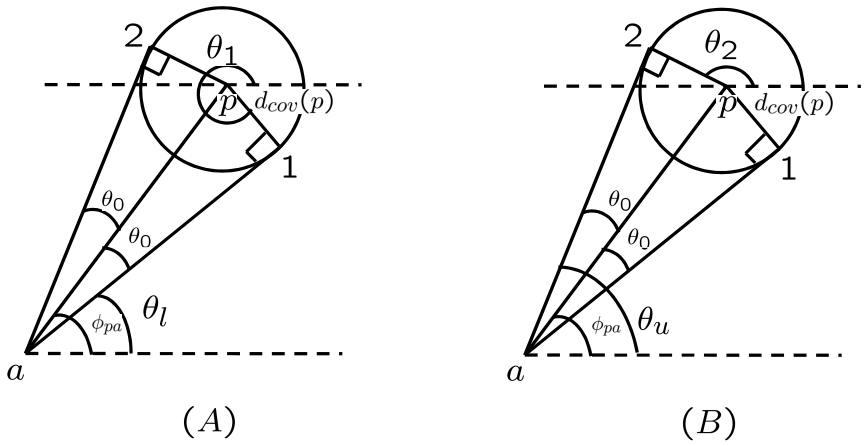

Figure 6.1: Determining θ_l and θ_u.

where Ψ_{pa} denotes the range of angles of the sidelobe of node a with respect to primary transmitter p. The second case is of interest to us, since if Ψ_{pa} does not contain the primary's coverage area, then there is the potential to transmit at higher power than $\hat{s}_a$ by node a. So it is clear that for the directional transmission case, the MIFTP varies as a function of its transmission direction (heading), mainlobe width, and sidelobe leakage. To realize such a directional transmission scheme, we first need to specify Ψ_{pa} such that it accounts for the observation noise and estimation error, and then employ an actual beamforming technique that satisfies the specified sidelobe constraint. In this section, we only focus on the angular specification aspect of the problem, and assume that an appropriate beamforming technique is can be applied subsequently.

Consider the scenario depicted in Figure 6.1. Here, the angles θ_l and θ_u define the true beamwidth of the sidelobe of a, where by definition $0 \leq \theta_l < \theta_u \leq 2\pi$. It is clear that

$\Psi_{pa} \in [\theta_l, \theta_u]$. It is easy to verify that these angles are given as follows:

$$(\theta_l, \theta_u) \triangleq \left(\tan^{-1}\left(\frac{y_1 - y_a}{x_1 - x_a}\right), \tan^{-1}\left(\frac{y_2 - y_a}{x_2 - x_a}\right)\right), \tag{6.11}$$

$$(x_1, y_1) \triangleq (x_p + d_{\text{cov}}(p)\cos\theta_1, y_p + d_{\text{cov}}(p)\sin\theta_1), \tag{6.12}$$

$$(x_2, y_2) \triangleq (x_p + d_{\text{cov}}(p)\cos\theta_2, y_p + d_{\text{cov}}(p)\sin\theta_2), \tag{6.13}$$

$$\theta_1 \triangleq \begin{cases} \frac{3\pi}{2} + \phi_{pa} - \theta_0, \text{ if } 0 \leq \phi_{pa} < \frac{\pi}{2}, \\ -\frac{\pi}{2} + \phi_{pa} - \theta_0, \text{ otherwise.} \end{cases} \tag{6.14}$$

$$\theta_2 \triangleq \begin{cases} \frac{\pi}{2} + \phi_{pa} + \theta_0, \text{ if } 0 \leq \phi_{pa} < \frac{3\pi}{2}, \\ -\frac{3\pi}{2} + \phi_{pa} + \theta_0, \text{ otherwise.} \end{cases} \tag{6.15}$$

$$\theta_0 \triangleq \sin^{-1}\left(\frac{d_{\text{cov}}(p)}{d_{pa}}\right), \ \phi_{pa} \triangleq \tan^{-1}\left(\frac{y_p - y_a}{x_p - x_a}\right). \tag{6.16}$$

Note that (θ_l, θ_u) are functions of (x_p, y_p, s_p). Therefore, the invariance principle allows us to compute their CRBs, which we denote by J_l^{-1} and J_u^{-1}, respectively. Similarly as in the previous chapters, these CRBs are achievable asymptotically as the measurement noise becomes vanishingly small. In this regime, $\hat{\theta}_l$ and $\hat{\theta}_u$ follow a truncated Gaussian distribution, namely, $\hat{\theta}_l \sim \frac{1}{A_l}\mathcal{N}(\theta_l, J_l^{-1})$ and $\hat{\theta}_u \sim \frac{1}{A_u}\mathcal{N}(\theta_u, J_u^{-1})$, where

$$A_l \triangleq Q\left(\frac{-\theta_l}{\sqrt{J_l^{-1}}}\right) - Q\left(\frac{2\pi - \theta_l}{\sqrt{J_l^{-1}}}\right), \tag{6.17}$$

$$A_u \triangleq Q\left(\frac{-\theta_u}{\sqrt{J_u^{-1}}}\right) - Q\left(\frac{2\pi - \theta_u}{\sqrt{J_u^{-1}}}\right), \tag{6.18}$$

represent normalization constants.

Instead of the true values, (θ_l, θ_u), node a can only estimate their MLEs, $(\hat{\theta}_l, \hat{\theta}_u)$. If

we use these MLEs to specify the width of the sidelobe, then, interference may be caused whenever for a particular realization $\hat{\theta}_l > \theta_l$ or $\hat{\theta}_u < \theta_u$. Since we do not have access to the true values, we can only ensure that these events happen with only vanishingly small probability, say ε_{th}. Thus, we propose the following two thresholds for specifying Ψ_{pa}:

$$\theta_l^{\text{th}} \triangleq \max\left\{\theta : \Pr(\hat{\theta}_l < \theta) \leq \varepsilon_{\text{th}}\right\} \tag{6.19}$$

$$= \theta_l + \sqrt{J_l^{-1}} \cdot Q^{-1}\left[Q\left(\frac{-\theta_l}{\sqrt{J_l^{-1}}}\right) - A_l\varepsilon_{\text{th}}\right] \tag{6.20}$$

$$\theta_u^{\text{th}} \triangleq \min\left\{\theta : \Pr(\hat{\theta}_u > \theta) \leq \varepsilon_{\text{th}}\right\} \tag{6.21}$$

$$= \theta_u + \sqrt{J_u^{-1}} \cdot Q^{-1}\left[Q\left(\frac{2\pi - \theta_u}{\sqrt{J_u^{-1}}}\right) + A_u\varepsilon_{\text{th}}\right]. \tag{6.22}$$

See Appendix D.3 for a derivation of θ_l^{th} and θ_u^{th}. Since these thresholds contain true parameters, we approximate them by their MLEs. For a particular realization $(\hat{\theta}_l, \hat{\theta}_u, \hat{J}_l^{-1}, \hat{J}_u^{-1}) = (a_l, a_u, b_l^2, b_u^2)$ we have

$$\hat{\theta}_l^{\text{th}} = a_l + b_l \cdot Q^{-1}\left[Q\left(\frac{-a_l}{b_l}\right) - \hat{A}_l\varepsilon_{\text{th}}\right], \tag{6.23}$$

$$\hat{\theta}_u^{\text{th}} = a_u + b_u \cdot Q^{-1}\left[Q\left(\frac{2\pi - a_u}{b_u}\right) + \hat{A}_u\varepsilon_{\text{th}}\right]. \tag{6.24}$$

We numerically study the effectiveness of these two thresholds in Section 6.5.

6.5 Numerical Results

6.5.1 Optimal hybrid SS-AOA localization

Antenna arrays are expensive to employ and are inherently inaccurate for localization when large distances or high NLOS environments are involved. Thus, we are particularly interested in the contribution of only one or two LOS AOA measurements, when there are not enough SS measurements available to attain satisfactory localization accuracy. We focus on the shadowing noise power for the SS model. For the AOA model, we study the effect of input SNR and the number of antenna elements of the ULA.

The coverage area is a square with length equal to 5 km. The target node is placed at $\boldsymbol{L}_p = [200, 200]^T$[m]. We assume that its transmit power $s_p = 50$ dBm, is unknown to the localizing nodes and needs to be estimated along with $\boldsymbol{L}_p$. For each trial, we randomly place N_{SS} localizing nodes capable of measuring only SS. We choose the path loss exponent, $\epsilon = 3$, which represents a typical value for urban outdoor environments. For the reasons mentioned earlier, we assume that N_{AOA} (typically only one or two) LOS AOA data are collected by localizing nodes equipped with ULAs. These nodes collect SS measurements as well. To make the LOS measurement condition realistic, we place these nodes randomly in a 2 km-by-2 km square region, instead of the entire coverage region. Since the localization accuracy depends on the measurement locations with respect to the target node (cf. (3.33) and (6.6)), we simulate 1000 independent trials to account for the effect of node geometry.

For the first set of results, shown in Fig. 6.2, we set the shadowing noise standard deviation, $\sigma_W = 6$ dB. We fix the number of antenna elements, $K = 10$ and vary the reference SNR, R_0, from 0 to 40 dB. The ML location estimates are found by solving the optimization problems (6.1), (6.3), and (6.4). For the location estimation performance we compute the root-mean-squared error according to the formula

$$\text{RMSE} = \sqrt{\frac{1}{N}\sum_{i=1}^{N}(\hat{X}_p(i) - x_p)^2 + (\hat{Y}_p(i) - y_p)^2},$$

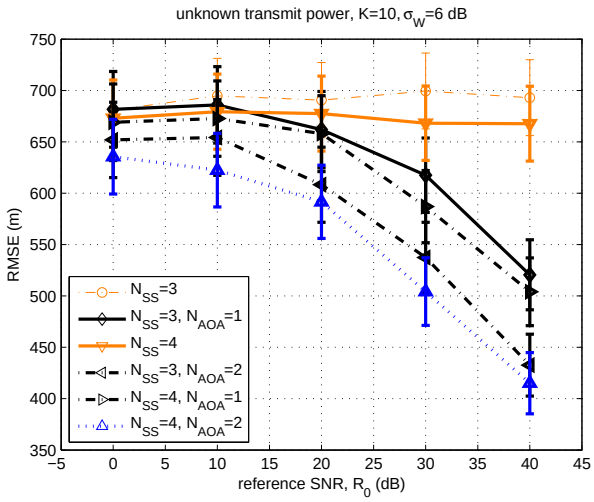

Figure 6.2: Localization error vs. reference SNR.

where $N = 1000$ and $\hat{\boldsymbol{L}}_p(i) = [\hat{X}_p(i), \hat{Y}_p(i)]^T$ denote the MLE of $\boldsymbol{L}_p = [x_p, y_p]^T$ during the i^{th} trial. The randomness in the simulation trials is due to the shadowing noise and the randomized placements of the secondary nodes.

In Fig. 6.2, the localization error is plotted for different measurement combinations, when $N_{\text{SS}} = 3$ or 4 and $N_{\text{AOA}} = 1$ or 2. As expected, the SS-only case does not depend on R_0. We observe that for $R_0 \geq 15$ dB, the combination of measurements $(N_{\text{SS}}, N_{\text{AOA}}) = (3, 1)$ performs better than $(N_{\text{SS}}, N_{\text{AOA}}) = (4, 0)$. This improvement continues as R_0 increases. The combination $(N_{\text{SS}}, N_{\text{AOA}}) = (3, 2)$ outperforms $(N_{\text{SS}}, N_{\text{AOA}}) = (4, 1)$ for all values of R_0. In particular, we observe that for $R_0 = 20$ dB and $N_{\text{SS}} = 3$, accuracy improvements of about 29 m and 80 m are achieved for $N_{\text{AOA}} = 1$ and 2, respectively.

For the results shown in Fig. 6.3, we set $R_0 = 20$ dB, $\sigma_W = 6$ dB and vary the value of K from 3 to 15. We notice that increasing the value of K helps improve accuracy, although the improvement is not dramatic. This suggests a trade-off between N_{AOA} and K. For example, the same accuracy, of approximately 625 m, can be achieved when $(N_{\text{SS}}, N_{\text{AOA}}) = (4, 1)$ with $K = 15$ and $(N_{\text{SS}}, N_{\text{AOA}}) = (3, 2)$ with $K = 10$.

Next, we fix $R_0 = 20$ dB, $K = 10$ and vary σ_W in the range $[4, 12]$ dB. In Fig. 6.4, we see that as expected the estimation accuracy decreases as σ_W is increased. The optimal hybrid

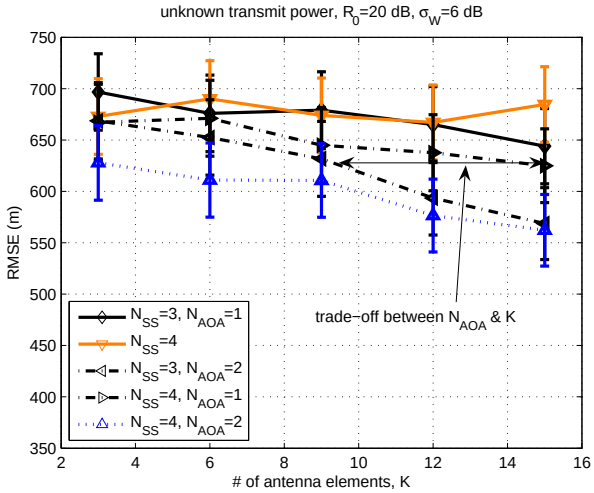

Figure 6.3: Localization error vs. number of antenna elements.

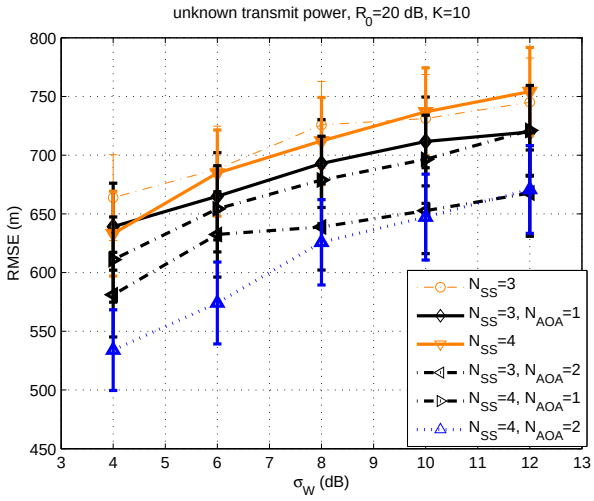

Figure 6.4: Localization error vs. shadowing noise.

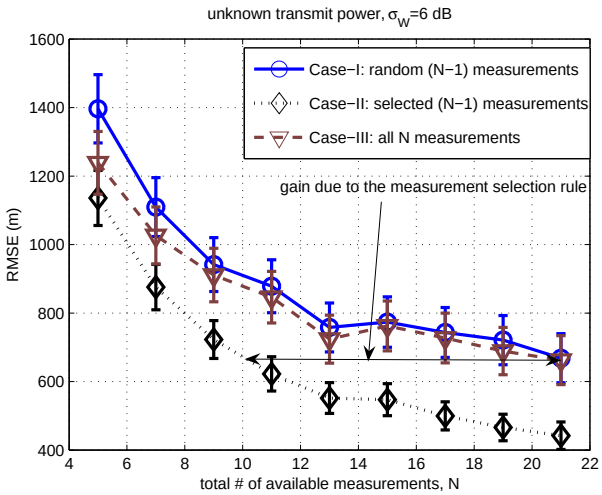

Figure 6.5: Impact of measurement selection in the case of unknown transmit power.

SS-AOA scheme outperforms the SS-only scheme for all $\sigma_W \geq 5$ dB. From the confidence intervals in Figs. 6.2, 6.3, and 6.4, we observe a deviation (due to random noise samples and the effect of localizing nodes' geometry) of about ± 35 m about the RMSE.

6.5.2 Measurement selection scheme

Next, we study the effectiveness of the proposed measurement selection rule. Due to the possible scarcity of available LOS AOA measurements in practice, we limit our measurement selection rule to the case of only SS measurements. As before, we randomly place the localizing nodes in the 25 km^2 coverage area and perform 1000 trial runs.

We set $s_p = 50$ dBm, $\epsilon = 3$ and $\sigma_W = 6$ dB. Before performing the ML location estimation, we use the rule given in (6.9) to choose the best $M = N - 1$ measurements, when a total of N measurements are available. We vary the value of N from 5 to 21. Fig. 6.5 plots the localization RMSE for the following three cases:

- Case-I: Randomly chosen $M = N - 1$ out of N measurements are used.
- Case-II: Using the rule given in (6.9), the best set of $M = N-1$ selected measurements out of N available measurements is used.
- Case-III: All available N measurements are used.

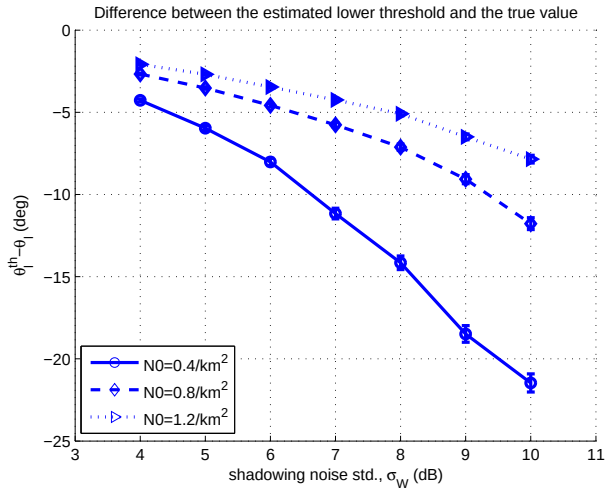

Figure 6.6: Difference between the estimated lower threshold, $\hat{\theta}_l^{\text{th}}$ and θ_l.

When the transmit power is unknown, the measurement selection scheme is especially effective. From Fig. 6.5, we see that the proposed measurement selection scheme (Case-II) is superior to both Case-I and Case-III for all values of N. We observe that using Case-II, an accuracy improvement from 103 m to 227 m can be achieved, relative to Case-III. In particular, we note that the same accuracy for both Case-I and Case-III when $N = 21$, is achieved by Case-II when $N = 10$.

6.5.3 Angular specification for directional transmissions

To study the effectiveness of using the angular thresholds $(\hat{\theta}_l^{\text{th}}, \hat{\theta}_u^{\text{th}})$ given in Section 6.4, we use SS measurements to generate the ML parameter estimates of primary ttransmitter, p. The target secondary node, a, which calculates the angular thresholds, is located at $(x_a, y_a) = (0, 0)$, and p is located at $(x_a + d_{pa} \cos \frac{\pi}{4}, y_a + d_{pa} \sin \frac{\pi}{4})$, with transmit power $s_p = 40$ dBm and $d_{pa} = 25$ km. Other simulation parameters are set as: $\varepsilon_{\text{th}} = 0.01$ and $\varepsilon_{\text{cov}} = 0.05$. In each trial, we uniformly place the secondary nodes (with receiver sensitivity of -83 dBm) within the primary's coverage area, and the SS measurements taken by these nodes are used to estimate MLEs of the location and transmit power of p. The relevant CRB estimates are also computed (see Appendix D.2). We calculate the threshold angles

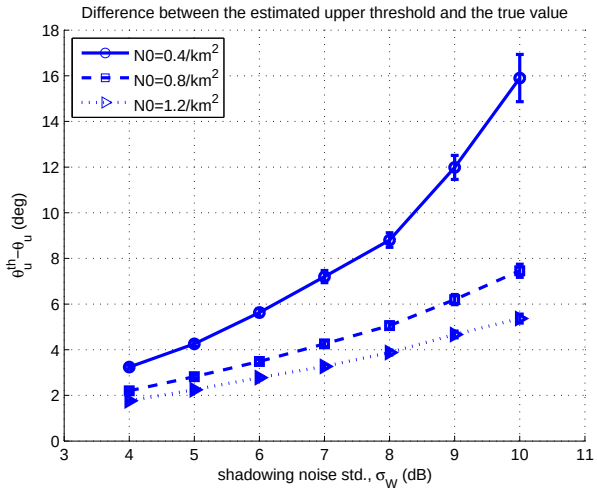

Figure 6.7: Difference between the estimated upper threshold, $\hat{\theta}_u^{\text{th}}$ and θ_u.

according to (6.23) and (6.24), and plot the result averaged over $K = 1000$ simulation trials with 95% confidence intervals. Three values are used for the secondary node density, $N_0 = 0.4, 0.8, 1.2$ per square km, and the shadowing noise standard deviation, σ_W is varied from 4 to 10 dB.

We study the difference of the threshold estimates $(\hat{\theta}_l^{\text{th}}, \hat{\theta}_u^{\text{th}})$ with respect to the true values (θ_l, θ_u), since this depicts how close (accurate) or far (inaccurate) the thresholds are from the true values. In Fig. 6.6 and Fig. 6.7, we plot $\frac{1}{K}\sum_{i=1}^{K} \hat{\theta}_l^{\text{th}}(i) - \theta_l$ and $\frac{1}{K}\sum_{i=1}^{K} \hat{\theta}_u^{\text{th}}(i) - \theta_u$ as a function of σ_W. We see that in both cases, as expected, the difference between the estimated threshold and the true value decreases with decreasing σ_W and increasing N_0. Also, we observe that, most of the time, $\hat{\theta}_l^{\text{th}} < \theta_l$ and $\hat{\theta}_u^{\text{th}} > \theta_u$, which ensures that these estimated thresholds serve as a valid specification for beamforming to achieve directional transmissions.

6.6 Discussion

In this chapter, we presented an optimal hybrid SS-AOA localization scheme suitable for localization in a noncooperative scenario, where the target transmitter's transmitted power and waveform are unknown to the localizing nodes. Our numerical results show that when

a limited number of SS measurements is available, considerable accuracy improvement can be achieved by using only one or two LOS AOA measurements. For cases where redundant measurements are available, we presented a measurement selection scheme to select the best subset of available measurements, such that localization error was minimized. For SS measurements, this rule yields considerable accuracy gain when the transmit power is unknown.

The proposed hybrid SS-AOA localization scheme has application to opportunistic spectrum access, where the objective is to locate primary transmitters to avoid causing harmful interference to primary receivers. In this application, a set of secondary nodes exchange SS and AOA measurement information to localize the primary transmitters collaboratively. In such a scenario, selection of a suitable subset of the available measurements is crucial to maximizing localization accuracy. We also proposed two threshold angle estimates which can be used by a secondary node to specify its beam pattern in order to achieve directional transmissions.

Chapter 7: Conclusions

In this dissertation, we considered opportunistic spectrum access (OSA) in the spatial domain for cognitive radios. We have presented algorithms where a group of frequency agile unlicensed (secondary) cognitive radios, can collaboratively detect spectrum holes in the spatial domain and opportunistically reuse it to improve spectrum utilization, while guaranteeing that the operation of the primary is not disrupted. The contributions of this dissertation include the characterization of the spectrum hole in terms of the maximum interference-free transmit power (MIFTP) using localization techniques, development of measurement clustering criteria involving multiple cochannel transmitters, a noncooperative hybrid SS-AOA localization scheme to improve spatial sensing accuracy, and angular specification to enable directional secondary transmissions.

- **Chapter 3:** In a single primary transmitter scenario, we used signal strength (SS) measurements, taken collaboratively by a group of secondary nodes, to find the maximum likelihood estimate (MLE) the unknown parameter of the primary, consisting of its location and transmit power. The estimation error is characterized by the Cramér-Rao bound (CRB), which is shown to be achievable asymptotically as the measurement noise becomes vanishingly small. The spectrum hole is characterized by approximating the MIFTP, which is an upper bound on the secondary's transmit power such that no harmful interference is incurred on primary receivers. The approximation takes into account the estimation error in terms of the CRB, and is seen to be quite accurate when a sufficient number of measurements is available. In the absence of sufficient measurements and/or under highly noisy environment the approximation tends to be conservative, which is a desirable property, since secondary transmissions

should not disrupt the operation of the primary system. The proposed MIFTP approximation can be used to develop traditional power control and allocation schemes to establish multiple secondary links.

- **Chapter 4:** To generalize our developments, a scenario of multiple cochannel primary transmitters is considered. A distributed and iterative localization scheme based on SS measurements is proposed, which is shown to improve location accuracy in the presence of significant cochannel interference. An approximation of the MIFTP that takes into account the presence of multiple cochannel transmitters is developed. To enable the iterative localization scheme and to approximate the MIFTP, a framework of collaboration among secondary nodes is proposed, which involves maintaining a database consisting of estimates of the primary's parameters, error estimates and other information.

- **Chapter 5:** Two model identification criteria, and a measurement clustering scheme is proposed to facilitate localization in the presence of unknown number of cochannel transmitters in the system. The two criteria, namely, the net minimum mean square error (net MMSE) and the minimum description length (MDL), are shown to be able to identify the number of cochannel transmitters in the system with high accuracy.

- **Chapter 6:** A noncooperative hybrid SS and angle-of-arrival (AOA) localization scheme is proposed. Localization accuracy is shown to improve in the presence of a few line-of-sight AOA measurements. To further improve the localization accuracy and to identify faulty measurements, a measurement selection rule based on the CRB is proposed. Finally, the prospect of directional secondary transmissions is considered by characterizing the orientation and width of the mainlobe/sidelobe of the secondary's beam pattern. Implementation of directional transmissions via an appropriate beamforming technique brings the possibility of further increasing capacity and reducing interference to primary users.

Some future directions of our work are discussed below.

- We employed SS measurements as the major source of information to perform localization, and assumed that the actual path loss function is known exactly a priori. But in real environments it may not be possible to capture the power decay properties of the RF signal by a single known path loss function. Through extensive field measurements it may be possible to characterize the path loss phenomenon as a group of functions, instead of having an unique one for all distances. In this approach, the basic localization scheme changes in that now it becomes necessary to infer which of the available path loss functions most closely represents the observed SS measurements. It may be possible to formulate in an iterative approach, where an initial path loss function is chosen, and based on collaboration among neighboring nodes and other inferred information a suitable path loss function is finally chosen.

- In Chapter 6, we have only considered LOS AOA measurements without any cochannel interference. Typically, in the wireless communications literature, the problem of NLOS propagation and cochannel interference, these two impairments are not addressed together [93, 96–99]. There is scope to address these two issues jointly. It is also of interest to explore the capability of multi-antenna systems to sense the primary system more accurately. For example, a straightforward extension of Chapter 5 is to incorporate AOA observation in the proposed model identification criteria.

- In this dissertation, we have limited our localization schemes to use only SS and AOA information. Although time-of-arrival (TOA) approach is not suitable for noncooperative localization, for some scenarios time-delay-of-arrival (TDOA) may be considered. This gives an alternative to perform localization suitable for OSA applications.

- Our model assumes that the primary and secondary systems are static during the period of observation, sensing and opportunistic access. In some scenarios, the primary and secondary systems may be mobile and/or their transmit powers may vary with time. To deal with such time-varying scenarios, the temporal aspects of spectrum sensing have to be considered in conjunction with the spatial spectrum sensing

techniques developed in this dissertation.

Appendix A:

A.1 Proof of Proposition 2

The score function $\frac{\partial}{\partial \boldsymbol{\Theta}} \ln f_{\boldsymbol{S}|\boldsymbol{\Theta}}(\boldsymbol{S})$ can be expressed as

$$\frac{\partial}{\partial \boldsymbol{\Theta}} \ln f_{\boldsymbol{S}|\boldsymbol{\Theta}}(\boldsymbol{S}) = \frac{1}{\sigma_W^2} \boldsymbol{BGDW}, \tag{A.1}$$

where $\boldsymbol{B}$ is given by (3.30) and $\boldsymbol{D}$ is given by (3.25). So the FIM is given by

$$\boldsymbol{J}_{\boldsymbol{\Theta}} = \frac{1}{\sigma_W^4} E_{\boldsymbol{\Theta}} \left[\boldsymbol{BGDW} (\boldsymbol{BGDW})^T \right] = \frac{1}{\sigma_W^4} \boldsymbol{BGD} \cdot E[\boldsymbol{W}\boldsymbol{W}^T] \cdot \boldsymbol{D}\boldsymbol{G}^T\boldsymbol{B} = \frac{1}{\sigma_W^2} \boldsymbol{BGD}^2\boldsymbol{G}^T\boldsymbol{B}. \tag{A.2}$$

A.2 Proof of Proposition 3

Differentiating z_i with respect to $\boldsymbol{\Theta} = [x_p, y_p, s_p]^T$, we obtain

$$\frac{\partial z_i}{\partial \boldsymbol{\Theta}} = \left[\frac{-10\epsilon \cos\phi_i}{d_i \ln 10}, \frac{-10\epsilon \sin\phi_i}{d_i \ln 10}, 1 \right]^T. \tag{A.3}$$

Hence,

$$\frac{\partial \boldsymbol{z}}{\partial \boldsymbol{\Theta}} = \boldsymbol{BGD}. \tag{A.4}$$

Let $\Delta\boldsymbol{\Theta} \triangleq \hat{\boldsymbol{\Theta}} - \boldsymbol{\Theta}$. Then for sufficiently small $|\Delta\boldsymbol{\Theta}|$, we can write

$$\Delta \boldsymbol{z} \approx (\boldsymbol{BDG})^T \Delta\boldsymbol{\Theta}, \tag{A.5}$$

where $\Delta\boldsymbol{z} = \hat{\boldsymbol{z}} - \boldsymbol{z}$, and $\hat{\boldsymbol{z}}$ is an estimate of $\boldsymbol{z}$. Under the assumption that the variance of W_i is sufficiently small, Δz_i can be interpreted as the error in the SS estimate S_i. Hence,

$\boldsymbol{S} = \hat{\boldsymbol{z}}$, which implies that for sufficiently small σ_W^2, $\Delta\boldsymbol{z} = \boldsymbol{S} - \boldsymbol{z} = \boldsymbol{W}$, and under this condition, (A.5) can be written as

$$\boldsymbol{S} - \boldsymbol{z} = \boldsymbol{W} = (\boldsymbol{BDG})^T(\hat{\boldsymbol{\Theta}} - \boldsymbol{\Theta}). \tag{A.6}$$

The conditional pdf $f_{\boldsymbol{S}|\boldsymbol{\Theta}}(\boldsymbol{S})$ has the form of a multivariate Gaussian distribution:

$$f_{\boldsymbol{S}|\boldsymbol{\Theta}}(\boldsymbol{S}) \propto \exp\left\{-\frac{1}{2}(\boldsymbol{S} - \boldsymbol{z})^T\boldsymbol{\Lambda}^{-1}(\boldsymbol{S} - \boldsymbol{z})\right\}, \tag{A.7}$$

where $\boldsymbol{\Lambda} = \sigma_W^2\boldsymbol{I}$ and $\boldsymbol{I}$ is the $N \times N$ identity matrix. Substituting (A.6) into (A.7), we obtain (3.37).

A.3 Derivation of (3.38)

Using (A.4) and (A.6), we have

$$\frac{\partial}{\partial\boldsymbol{\Theta}} \ln f_{\boldsymbol{S}|\boldsymbol{\Theta}}(\boldsymbol{S}) = \frac{\partial\boldsymbol{z}}{\partial\boldsymbol{\Theta}} \cdot \frac{\partial}{\partial\boldsymbol{z}} \ln f_{\boldsymbol{S}|\boldsymbol{\Theta}}(\boldsymbol{S}) = \boldsymbol{BGD} \cdot \boldsymbol{\Lambda}^{-1}(\boldsymbol{S} - \boldsymbol{z}) = \boldsymbol{J}_{\boldsymbol{\Theta}}(\hat{\boldsymbol{\Theta}} - \boldsymbol{\Theta}).$$

A.4 Proof of Proposition 4

Let $\theta \triangleq d_{p,a}$ denote the true distance between the primary transmitter and the FAR node. The observation equation for estimating θ is given by

$$\hat{\boldsymbol{L}} = \boldsymbol{u} + \boldsymbol{W}_{\boldsymbol{L}}, \tag{A.8}$$

where $\boldsymbol{u} = [u_1, u_2]^T$ with

$$u_1 = x_a + \theta\cos\phi_{p,a} \text{ and } u_2 = y_a + \theta\sin\phi_{p,a},$$

and $\boldsymbol{W_L} \sim \mathcal{N}(\mathbf{0}, \boldsymbol{J_L}^{-1})$. Differentiating $\boldsymbol{u}$ with respect to θ, we have

$$\frac{\partial \boldsymbol{u}}{\partial \theta} = [\cos\phi_{p,a},\ \ \sin\phi_{p,a}] = \boldsymbol{H}_{p,a}^T. \tag{A.9}$$

Let $\Delta\theta = \hat{\theta} - \theta$, where $\hat{\theta} \triangleq \hat{D}_{p,a}$. For sufficiently small $|\Delta\theta|$, we can write

$$\Delta\boldsymbol{u} \approx \boldsymbol{H}_{p,a}\Delta\theta. \tag{A.10}$$

Assuming that σ_W is small, $\Delta\boldsymbol{u}$ can be interpreted as the error in the location estimate $\hat{\boldsymbol{L}}$, in which case

$$\hat{\boldsymbol{L}} - \boldsymbol{u} = \boldsymbol{W_L} = \boldsymbol{H}_{p,a}(\hat{\theta} - \theta). \tag{A.11}$$

Hence,

$$f_{\hat{\boldsymbol{L}}|\theta}(\hat{\boldsymbol{L}}) \propto \exp\left\{-\frac{1}{2}(\hat{\boldsymbol{L}} - \boldsymbol{u})^T \boldsymbol{J_L}(\hat{\boldsymbol{L}} - \boldsymbol{u})\right\} = \exp\left\{-\frac{1}{2}(\hat{\theta} - \theta)^T \boldsymbol{H}_{p,a}^T \boldsymbol{J_L} \boldsymbol{H}_{p,a}(\hat{\theta} - \theta)\right\}, \tag{A.12}$$

which implies that $E[\hat{\theta}] = \theta$. Hence $\hat{\theta}$ is unbiased in the asymptotic regime $\sigma_W \to 0$. In the asymptotic regime, the score function is

$$\frac{\partial}{\partial\theta} \ln f_{\hat{\boldsymbol{L}}|\theta}(\hat{\boldsymbol{L}}) = \boldsymbol{H}_{p,a}^T \boldsymbol{J_L} \boldsymbol{H}_{p,a}(\hat{\theta} - \theta) = J_{p,a}(\hat{\theta} - \theta). \tag{A.13}$$

The last equality (see [78], p. 230) allows us to conclude that the CRB is achieved by the MLE $\hat{\theta} = \hat{D}_{p,a}$. Note that this achievability result implies that in the asymptotic regime, the estimation error can be modeled as $E_{p,a} \triangleq \hat{D}_{p,a} - d_{p,a} \sim \mathcal{N}(0, J_{p,a}^{-1})$.

A.5 Proof of Proposition 5

First, we prove the proposition for the case $r \geq 0$.

$$P_{\text{int}}(a, v|E_{p,a} = r) = \Pr\{I_v \geq i_{\max}|E_{p,a} = r\} \leq \Pr\{W \geq i_{\max} + g(d_a^*) - s_a|E_{p,a} = r\} \tag{A.14}$$

$$= Q\left(\frac{i_{\max} + 10\epsilon \log_{10} d_a^* - s_a}{\sigma_W}\right) = Q\left(\frac{i_{\max} + \frac{10\epsilon}{\ln 10}\ln(\beta - r) - s_a}{\sigma_W}\right). \tag{A.15}$$

We expand $\ln(\beta - r)$ in a Taylor series and lower bound it as follows:

$$\ln(\beta - r) = \ln\beta - \sum_{i=1}^{\infty} \frac{1}{i}\left(\frac{r}{\beta}\right)^i \geq \ln\beta - \frac{kr}{\beta},$$

for $0 \leq \frac{r}{\beta} \leq t_k < 1$, where t_k denotes the root of the function $f(t) = \ln(1-t) + kt$ near 1 with $t \in [0, 1)$ and $k > 0$. The value of t_k can be chosen arbitrarily close to one, for example, when $k = 5$, we have $t_k = 0.993$. Hence, we can write

$$P_{\text{int}}(a, v|E_{p,a} = r) \leq Q\left(\frac{i_{\max} + \frac{10\epsilon}{\ln 10}\left(\ln\beta - \frac{5r}{\beta}\right) - s_a}{\sigma_W}\right) = Q(b_1 + b_2 r).$$

Similarly, for $r < 0$ we can write

$$P_{\text{int}}(a, v|E_{p,a} = r) < Q\left(\frac{i_{\max} + \frac{10\epsilon}{\ln 10}\ln(\beta + r) - s_a}{\sigma_W}\right).$$

Again, using Taylor series expansion we can lower bound $\ln(\beta + r)$ as follows:

$$\ln(\beta + r) = \ln\beta + \sum_{i=1}^{\infty} \frac{(-1)^{i+1}}{i}\left(\frac{r}{\beta}\right)^i \geq \ln\beta + \frac{kr}{\beta},$$

for $-1 < t_k \leq \frac{r}{\beta} < 0$, where t_k denotes the root of the function $f(t) = \ln(1+t) - kt$ near -1 with $t \in (-1, 0)$ and $k > 0$. Like before, t_k can be chosen arbitrarily close to -1, for example, when $k = 5$, we have $t_k = -0.993$. Therefore, for $r < 0$, we can write

$$P_{\text{int}}\left(a, v \mid E_{p,a} = r\right) < Q\left(\frac{i_{\max} + \frac{10\epsilon}{\ln 10}\ln\left(\beta + \frac{5r}{\beta}\right) - s_a}{\sigma_W}\right) = Q(b_1 - b_2 r).$$

A.6 Derivation of (3.46)

Since $E_{p,a} \sim \mathcal{N}(0, J_{p,a}^{-1})$, we can evaluate $\Pr(|E_{p,a}| < \tilde{\beta})$ as follows.

$$\Pr(|E_{p,a}| < \tilde{\beta}) \quad = \quad \int_{-\tilde{\beta}}^{\tilde{\beta}} f_{E_{p,a}}(r)dr = 1 - 2Q\left(\frac{\tilde{\beta}}{\sqrt{J_{p,a}^{-1}}}\right). \tag{A.16}$$

We can find β^* by solving for the minimum value of $\tilde{\beta}$ such that $\Pr(|E_{p,a}| < \tilde{\beta}) \geq \varepsilon$ is satisfied. Using (A.16), this condition implies

$$\beta^* \quad = \quad \sqrt{J_{p,a}^{-1}} \cdot Q^{-1}\left(\frac{1-\varepsilon}{2}\right). \tag{A.17}$$

A.7 Proof of Proposition 6

Since we have two parameters $\boldsymbol{\Theta}$ and $\widetilde{\boldsymbol{\Theta}}$, where $\widetilde{\boldsymbol{\Theta}}$ is a function of $\boldsymbol{\Theta}$, then there exists a simple transformation (under some regularity conditions) relating their associated CRBs, $\boldsymbol{J}_{\boldsymbol{\Theta}}^{-1}$ and $\boldsymbol{J}_{\widetilde{\boldsymbol{\Theta}}}^{-1}$, [78] p. 229. Particularly,

$$\boldsymbol{J}_{\widetilde{\boldsymbol{\Theta}}}^{-1} \quad = \quad \boldsymbol{H}_1^T \boldsymbol{J}_{\boldsymbol{\Theta}}^{-1} \boldsymbol{H}_1 \tag{A.18}$$

where

$$\boldsymbol{H}_1 \triangleq \begin{bmatrix} \cos\phi_{p,a} & 0 \\ \sin\phi_{p,a} & 0 \\ 0 & \frac{\ln 10}{10\epsilon} d_{\text{cov}}(p) \end{bmatrix}. \tag{A.19}$$

Recall from Section 3.3.3 that the MLE, $\hat{\boldsymbol{\Theta}}_{\text{ML}}$, achieves the CRB asymptotically as $\sigma_W^2 \to 0$. Then, using similar arguments to Proposition 4, we can conclude that in the asymptotic regime, $\hat{\tilde{\boldsymbol{\Theta}}}_{\text{ML}}$ also achieves its corresponding CRB. This means that for vanishingly small noise, E_1 can be modeled as $E_1 \sim \mathcal{N}(0, J_1^{-1})$, where J_1^{-1} can be computed as follows.

$$\begin{aligned} J_1^{-1} &= E\left[E_{p,a} - E_{\text{cov}}\right]^2 && \text{(A.20)} \\ &= E\left[E_{p,a}^2 + E_{\text{cov}}^2 - 2E_{p,a}E_{\text{cov}}\right] && \text{(A.21)} \\ &= \text{Tr}\left(\boldsymbol{J}_{\tilde{\boldsymbol{\Theta}}}^{-1}\right) - 2\left[\boldsymbol{J}_{\tilde{\boldsymbol{\Theta}}}^{-1}\right]_{(1,2)}. && \text{(A.22)} \end{aligned}$$

Appendix B:

B.1 CRB of $\hat{\boldsymbol{\theta}}_{1B}$ and $\hat{\boldsymbol{\theta}}_{1C}$

Suppose there are M cochannel primary transmitters. The scaled observations conditioned on all the parameters can be modeled as (cf. Section 4.3.2)

$$\widetilde{R}_a | \{\boldsymbol{\theta}_i\}_{i=1}^M \sim \mathcal{N}\left(\ln\left(\sum_{i=1}^M e^{c\bar{R}_{ap_i}}\right), c^2\sigma_W^2\right). \tag{B.1}$$

Given the set of independent observations $\widetilde{\mathcal{O}}_1 \triangleq \left\{(\widetilde{R}_a, \boldsymbol{L}_a) : a \in \mathcal{A}_1\right\}$ and known parameters $\{\boldsymbol{\theta}_i\}_{i=2}^M$, we are interested in calculating the CRB, $\boldsymbol{J}_{\boldsymbol{\theta}_{1B}}^{-1}$, corresponding to estimator $\hat{\boldsymbol{\theta}}_{1B}$. The Fisher Information matrix (FIM) is given by

$$\boldsymbol{J}_{\boldsymbol{\theta}_{1B}} \equiv \boldsymbol{J}_{\boldsymbol{\theta}_1|\{\boldsymbol{\theta}_i\}_{i=2}^M} = E_{\{\boldsymbol{\theta}_i\}_{i=1}^M}\left[\left(\frac{\partial l(\boldsymbol{\theta}_1)}{\partial \boldsymbol{\theta}_1}\right)\left(\frac{\partial l(\boldsymbol{\theta}_1)}{\partial \boldsymbol{\theta}_1}\right)^T\right], \tag{B.2}$$

where $E_{\{\boldsymbol{\theta}_i\}_{i=1}^M}[\cdot]$ denotes conditional expectation with respect to $\{\boldsymbol{\theta}_i\}_{i=1}^M$. $l(\boldsymbol{\theta}_1)$ represents the log-likelihood function, which can be written as

$$l(\boldsymbol{\theta}_1) = \sum_{a\in\mathcal{A}_1} \ln f_{\widetilde{R}_a|\{\boldsymbol{\theta}_i\}_{i=1}^M}(\widetilde{R}_a), \tag{B.3}$$

where $f_{\widetilde{R}_a|\{\boldsymbol{\theta}_i\}_{i=1}^M}(\cdot)$ denotes the probability density function of $\widetilde{R}_a | \{\boldsymbol{\theta}_i\}_{i=1}^M$. Using (B.1)-(B.3), it is simple to verify that $\boldsymbol{J}_{\boldsymbol{\theta}_{1B}} = \frac{1}{\sigma_W^2}\sum_{a\in\mathcal{A}_1} k_a \boldsymbol{G}_a \boldsymbol{G}_a^T$, where

$$\boldsymbol{G}_a \triangleq \begin{bmatrix} \dot{g}(d_{ap_1})\cos\phi_{ap_1} & \dot{g}(d_{ap_1})\sin\phi_{ap_1} & -1 \end{bmatrix}^T, \quad k_a \triangleq \frac{e^{c\bar{R}_{ap_1}}}{\sum_{i=1}^M e^{c\bar{R}_{ap_i}}} \leq 1. \tag{B.4}$$

For the case of $\hat{\boldsymbol{\theta}}_{1C}$, the scaled observations can be modeled as (cf. Section 4.3.3)

$$\widetilde{R}_a|\boldsymbol{\theta}_1, \{\hat{\boldsymbol{\theta}}_i\}_{i=2}^M \sim \mathcal{N}\left(\ln\left(\sum_{i=1}^{M} e^{c\bar{R}_{ap_i}+\frac{c^2\hat{\sigma}_{ia}^2}{2}}\right), c^2\sigma_W^2\right), \tag{B.5}$$

where $\hat{\sigma}_{ia}^2 \triangleq \hat{\boldsymbol{G}}_a\hat{\boldsymbol{J}}_{\boldsymbol{\theta}_i}^{-1}\hat{\boldsymbol{G}}_a^T$ with $\hat{\sigma}_{1a}^2 \triangleq 0$. Recall that in our notation $\hat{\boldsymbol{A}}$ denotes the MLE of $\boldsymbol{A}$. As before, we have $\boldsymbol{J}_{\boldsymbol{\theta}_{1C}} = \frac{1}{\sigma_W^2}\sum_{a\in\mathcal{A}_1} m_a\boldsymbol{G}_a\boldsymbol{G}_a^T$, where

$$m_a \triangleq \frac{e^{c\bar{R}_{ap_1}}}{\sum_{i=1}^{M} e^{c\bar{R}_{ap_i}+\frac{c^2\hat{\sigma}_{ia}^2}{2}}} \leq k_a \leq 1. \tag{B.6}$$

If no information is available about the multiple cochannel transmitters (cf. Section 4.3.1), then the net SS can be assumed to result from a single *virtual transmitter*. Interestingly, the FIM corresponding to the virtual transmitter $V \equiv p_1$ is given by $\boldsymbol{J}_{\boldsymbol{\theta}_V} = \frac{1}{\sigma_W^2}\sum_{a\in\mathcal{A}_1}\boldsymbol{G}_a\boldsymbol{G}_a^T$. It is easy to show that $\boldsymbol{J}_{\boldsymbol{\theta}_{1C}}^{-1} \geq \boldsymbol{J}_{\boldsymbol{\theta}_{1B}}^{-1} \geq \boldsymbol{J}_{\boldsymbol{\theta}_V}^{-1}$, where $\boldsymbol{Y} \geq \boldsymbol{Z}$ should be interpreted to mean that $\boldsymbol{Y}-\boldsymbol{Z}$ is non-negative definite. Similar to the single transmitter case, from (B.1) and (B.5) we conclude that the above CRBs will be achievable asymptotically as $\sigma_W \to 0$.

B.2 Proof of Proposition 8

The interference caused to v located at $(x_v, y_v) \in \overline{B}_{\text{cov}}(p)$ due to all secondary transmissions is given by $I_v = 10\log_{10}\left(\sum_{a\in\mathcal{A}_0} 10^{\frac{I_{va}}{10}}\right)$, where $I_{va} = s_a - g(d_{va}) + W_{va}$ and $W_{va} \sim \mathcal{N}(0, \sigma_W^2)$, $\forall a \in \mathcal{A}_0$. Similar to Section 4.3, given $\boldsymbol{\Theta}$, I_v can be modeled as $I_v \sim \mathcal{N}(\frac{\mu}{\kappa}, \frac{\sigma^2}{\kappa^2})$. So the interference probability $P_{\text{int}}(\mathcal{A}_0; s_b, v)$ is given by

$$P_{\text{int}}(\mathcal{A}_0; s_b, v) \triangleq \Pr(I_v \geq i_{\max}) = Q\left(\frac{i_{\max}-\frac{\mu}{\kappa}}{\frac{\sigma}{\kappa}}\right) \overset{(4.15)}{=} Q\left(\frac{\kappa i_{\max} - \frac{\kappa^2\sigma_W^2}{2} + \frac{\sigma^2}{2} - h}{\sigma}\right).$$

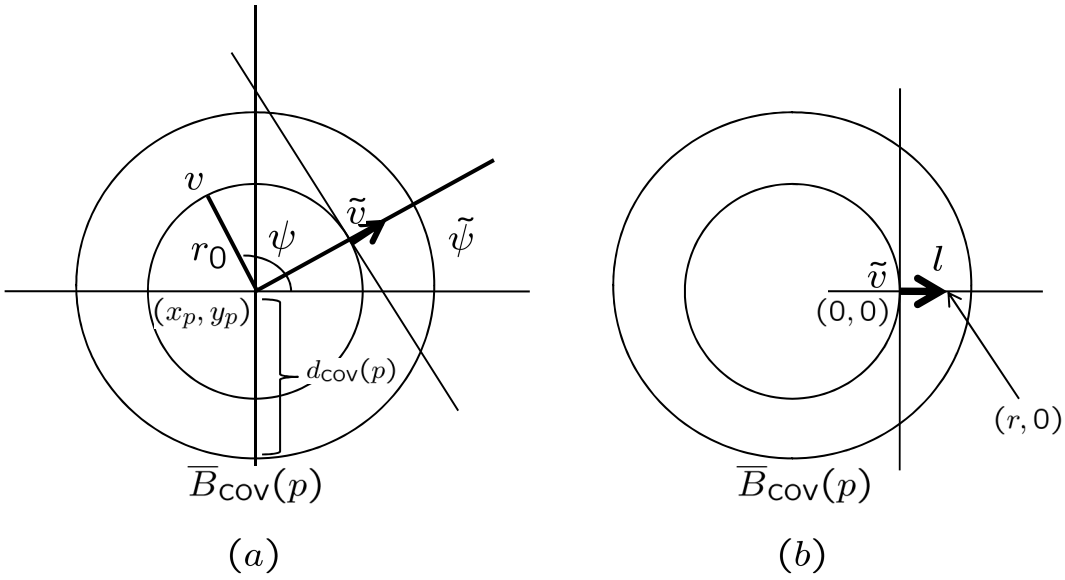

Figure B.1: Diagram for the proof of Proposition 9. In (a), node v located at $(x_p + r_0\cos\psi, y_p + r_0\sin\psi) \in \overline{B}_{\mathrm{cov}}(p)$ represents an arbitrary victim. There exists a node $\tilde{v}$ at angle $\tilde{\psi}$ located at $(x_p + r_0\cos\tilde{\psi}, y_p + r_0\sin\tilde{\psi})$, such that $I_v \leq I_{\tilde{v}}$. In (b), the location of $\tilde{v}$ is chosen as the new origin. Because of the way the angle $\tilde{\psi}$ is chosen, the interference on the line l is monotonically increasing in r.

B.3 Proof of Proposition 9

Suppose $g(d) = 10\epsilon\log_{10}(d)$. Let I_v be the interference power at an arbitrary victim node v located at $(x_p + r_0\cos\psi, y_p + r_0\sin\psi)$ where $r_0 < d_{\mathrm{cov}}(p)$, (see Fig. B.1a). There exists a particular victim node $\tilde{v}$ located at $(x_p + r_0\cos\tilde{\psi}, y_p + r_0\sin\tilde{\psi})$, such that $I_v \leq I_{\tilde{v}}$. Choose $(x_p + r_0\cos\tilde{\psi}, y_p + r_0\sin\tilde{\psi})$ as the new origin (see Fig. B.1b), and denote the shortest straight line connecting this origin to $\partial B_{\mathrm{cov}}(p)$ as l. Then the aggregate interference power (in absolute scale) at any point $(r, 0)$ on l is given by

$$I_l = \sum_{a\in\mathcal{A}_T} \frac{10^{\frac{s_a}{10}}}{[(\tilde{x}_a - r)^2 + \tilde{y}_a^2]^{\frac{\epsilon}{2}}}, \tag{B.7}$$

where $(\tilde{x}_a, \tilde{y}_a)$ is the location of secondary transmitter a with respect to the new origin. The value of I_l will monotonically increase with increasing r, since it points to the direction of the stronger interferers. This is because, staying on l as we move towards the edge, we move towards the stronger interferers and move away from the weaker ones, and as a result, the increase in interference due to the stronger interferers will offset the decrease in interference due to the weaker interferers. Therefore, we can always start at an arbitrary interior point of $\overline{B}_{\text{cov}}(p)$ and reach a point on its boundary $\partial B_{\text{cov}}(p)$ where the interference is greater. The conclusion continues to hold for different path loss functions $g(d)$ that are monotonically increasing.

B.4 Proof of Lemma 1

Suppose there exists only one victim node located at $(x, y) \in \overline{B}_{\text{cov}}(p)$. Note that $(x, y) = (x_p + r\cos\psi, y_p + r\sin\psi)$, where $(r, \psi) \in (0, d_{\text{cov}}(p)] \times [0, 2\pi)$. Then, the true MIFTP of node b with respect to this particular victim node is defined as:

$$s_b^*(p; x, y) \triangleq \max\{s_b : P_{\text{int}}(\mathcal{A}_0; s_b, x, y) \leq \varepsilon_{\text{int}}\}. \tag{B.8}$$

Since the interference constraint must be satisfied $\forall (x, y) \in \overline{B}_{\text{cov}}(p)$, the true MIFTP is given by $s_b^*(p) = \min_{(x,y)\in\overline{B}_{\text{cov}}(p)} s_b^*(p; x, y)$.

B.5 Proof of Corollary 1

Consider an arbitrary victim node v located at $(x_p + r\cos\psi, y_p + r\sin\psi) \in \overline{B}_{\text{cov}}(p)$, where $(r, \psi) \in (0, d_{\text{cov}}(p)] \times [0, 2\pi) \triangleq \mathcal{F}_1 \times \mathcal{F}_2$. Let $i_v(r, \psi, s_b)$, parameterized in the 3-tuple (r, ψ, s_b), denote the aggregate interference power at v (in absolute scale) without any

shadowing noise, W. We can upper bound the interference probability as follows.

$$\begin{aligned}
\mathrm{P}_{\mathrm{int}}(\mathcal{A}_0; s_b, v) &\triangleq \Pr(I_v \geq i_{\max}) \\
&= \Pr\left(i_v(r,\psi,s_b)\cdot 10^{\frac{W}{10}} \geq 10^{\frac{i_{\max}}{10}}\right) \\
&\leq \Pr\left(10^{\frac{W}{10}} \geq \frac{10^{\frac{i_{\max}}{10}}}{\max\limits_{(r,\psi)\in\mathcal{F}_1\times\mathcal{F}_2} i_v(r,\psi,s_b)}\right) \\
&\overset{\text{Prop.9}}{=} \Pr\left(10^{\frac{W}{10}} \geq \frac{10^{\frac{i_{\max}}{10}}}{i_v(d_{\mathrm{cov}}(p),\psi^*,s_b)}\right), \qquad \text{(B.9)}
\end{aligned}$$

for a particular ψ^*. Since (B.9) is an upper bound on $\mathrm{P}_{\mathrm{int}}(\mathcal{A}_0; s_b, v)$, for MIFTP computation, we can fix $r = d_{\mathrm{cov}}(p)$ and it is sufficient to restrict the search to $\psi \in [0, 2\pi)$.

B.6 Proof of Proposition 10

From the definition of h in (4.15) we have

$$\begin{aligned}
e^{2h} &= L_b^2(v) + \left(\sum_{a\in\mathcal{A}_T} L_a(v)\right)^2 + 2L_b(v)\left(\sum_{a\in\mathcal{A}_T} L_a(v)\right) > L_b^2(v) + \sum_{a\in\mathcal{A}_T} L_a^2(v) \\
\Leftrightarrow e^{\kappa^2\sigma_W^2} - 1 &> e^{-2h}\left(e^{\kappa^2\sigma_W^2} - 1\right)\left(L_b^2(v) + \sum_{a\in\mathcal{A}_T} L_a^2(v)\right) \overset{(4.16)}{=} \frac{k_6^2}{k_5^2} \\
\Leftrightarrow \kappa^2\sigma_W^2 &> \ln\left(1 + \frac{k_6^2}{k_5^2}\right) \overset{(4.15)}{=} \sigma^2. \qquad \text{(B.10)}
\end{aligned}$$

Consider the interference probability:

$$P_{\mathrm{int}}(\mathcal{A}_0; s_b, v) \underset{(4.15)}{\overset{(4.14)}{=}} Q\left(\frac{\kappa i_{\max} - \frac{\kappa^2\sigma_W^2}{2} + \frac{\sigma^2}{2} - h}{\sigma}\right) \overset{(B.10)}{\leq} Q\left(\frac{\kappa i_{\max} - \frac{\kappa^2\sigma_W^2}{2} + \frac{\sigma^2}{2} - h}{\kappa\sigma_W}\right) = Q(\gamma).$$

B.7 Value of $\boldsymbol{H}_0$

Define the following terms:

$$c_1 \triangleq \left(\kappa\sigma_W(k_5^2+k_6^2)\right)^{-1},\ c_2 \triangleq e^{\kappa^2\sigma_W^2}\left(e^{\kappa^2\sigma_W^2}-1\right),\ c_3 \triangleq \left(k_5^2+2k_6^2\right)e^{-h}. \tag{B.11}$$

It can be verified that $\boldsymbol{H}_0 = -\kappa c_1\left((c_2L_b(v)-c_3)\,\boldsymbol{H}_b + \sum_{a\in\mathcal{A}_T}(c_2L_a(v)-c_3)\,\boldsymbol{H}_a\right)$, where

$$\boldsymbol{H}_b \triangleq L_b(v)\dot{g}(d_{vb})\begin{bmatrix}\cos\phi_{vb}\\ \sin\phi_{vb}\\ -\dot{d}_{\text{cov}}(p)\end{bmatrix},\ \boldsymbol{H}_a \triangleq L_a(v)\dot{g}(d_{va})\begin{bmatrix}\cos\phi_{va}-\frac{d_{\text{cov}}(p)\sin\phi_{bp}\sin(\phi_{bp}-\phi_{va})}{d_{bp}}\\ \sin\phi_{va}+\frac{d_{\text{cov}}(p)\cos\phi_{bp}\sin(\phi_{bp}-\phi_{va})}{d_{bp}}\\ \dot{d}_{\text{cov}}(p)\cos(\phi_{bp}-\phi_{va})\end{bmatrix},$$

with $\phi_{ij} \triangleq \tan^{-1}\left(\frac{y_i-y_j}{x_i-x_j}\right)$, $\dot{g}(d) \triangleq \frac{\partial g(d)}{\partial d}$ and $\dot{d}_{\text{cov}}(p) \triangleq \frac{\partial d_{\text{cov}}(p)}{\partial s_p}$.

Appendix C:

C.1 The components of the FIM, $\boldsymbol{J}_j$

The components of the FIM, $\boldsymbol{J}_j$, are given as follows [79].

$$J_{x_{p_k},x_{p_l}} = \frac{1}{\sigma_W^2}\sum_{a=1}^{N}\frac{e^{\kappa(u_{ak}+u_{al})}\dot{g}(d_{ak})\dot{g}(d_{al})\cos(\phi_{ak})\cos(\phi_{al})}{\left(\sum_{i=1}^{j}e^{\kappa u_{ai}}\right)^2},$$

$$J_{y_{p_k},y_{p_l}} = \frac{1}{\sigma_W^2}\sum_{a=1}^{N}\frac{e^{\kappa(u_{ak}+u_{al})}\dot{g}(d_{ak})\dot{g}(d_{al})\sin(\phi_{ak})\sin(\phi_{al})}{\left(\sum_{i=1}^{j}e^{\kappa u_{ai}}\right)^2},$$

$$J_{s_{p_k},s_{p_l}} = \frac{1}{\sigma_W^2}\sum_{a=1}^{N}\frac{e^{\kappa(u_{ak}+u_{al})}}{\left(\sum_{i=1}^{j}e^{\kappa u_{ai}}\right)^2},$$

$$J_{x_{p_k},y_{p_l}} = \frac{1}{\sigma_W^2}\sum_{a=1}^{N}\frac{e^{\kappa(u_{ak}+u_{al})}\dot{g}(d_{ak})\dot{g}(d_{al})\cos(\phi_{ak})\sin(\phi_{al})}{\left(\sum_{i=1}^{j}e^{\kappa u_{ai}}\right)^2},$$

$$J_{s_{p_k},x_{p_l}} = \frac{1}{\sigma_W^2}\sum_{a=1}^{N}\frac{e^{\kappa(u_{ak}+u_{al})}\dot{g}(d_{al})\cos(\phi_{al})}{\left(\sum_{i=1}^{j}e^{\kappa u_{ai}}\right)^2},$$

$$J_{s_{p_k},y_{p_l}} = \frac{1}{\sigma_W^2}\sum_{a=1}^{N}\frac{e^{\kappa(u_{ak}+u_{al})}\dot{g}(d_{al})\sin(\phi_{al})}{\left(\sum_{i=1}^{j}e^{\kappa u_{ai}}\right)^2},$$

where $\phi_{ab} \triangleq \tan^{-1}\frac{y_a - y_{p_b}}{x_a - x_{p_1 b}}$ and $k, l \in \{1, 2, \cdots, j\}$.

Appendix D:

D.1 A Simulation example with directional primary transmissions

In general, $f(\cdot)$ depends on the wavelength and the details of the geometric structure of the transmit antenna. For our purposes, we characterize the main lobe by two parameters: (1) antenna heading (orientation of its main response axis with respect to the horizontal axis), θ_h, and (2) null-to-null beamwidth, Δ. As an example, we consider the beam pattern of a standard uniformly weighted linear array. In such a case, the beam pattern for the i^{th} observation is given by

$$f_i(\theta_h, \Delta) = \frac{\Delta}{4} \cdot \frac{\sin\left[\frac{2\pi}{\Delta}\cos\left(\theta_h - \tan^{-1}\left(\frac{y_i}{x_i}\right) - \frac{\pi}{2}\right)\right]}{\sin\left[\frac{\pi}{2}\cos\left(\theta_h - \tan^{-1}\left(\frac{y_i}{x_i}\right) - \frac{\pi}{2}\right)\right]}, \tag{D.1}$$

where (x_i, y_i) is the position of the i^{th} FAR node, (cf. (2.95) and (2.105) of [100]). The power pattern f^2 for $\theta_h = 45^\circ$ and for different Δ values is shown in Fig. D.1.

To simulate the effect of directional transmission on estimation accuracy, we use the modified observation model of (6.2), where $f(\boldsymbol{p})$ is known and is given by (D.1). We assume that Δ is known a priori, so now we estimate θ_h along with location and s_p. In principle, we could also estimate Δ, but as an initial consideration we focus on θ_h. Other parameters of the simulation are kept the same as the paper. Error in location estimation is measured in terms of *average missed distance*,

$$E_{\text{md}} \triangleq \frac{1}{K}\sum_{i=1}^{K}\sqrt{(\hat{x}_p(i) - x_p)^2 + (\hat{y}_p(i) - y_p)^2},$$

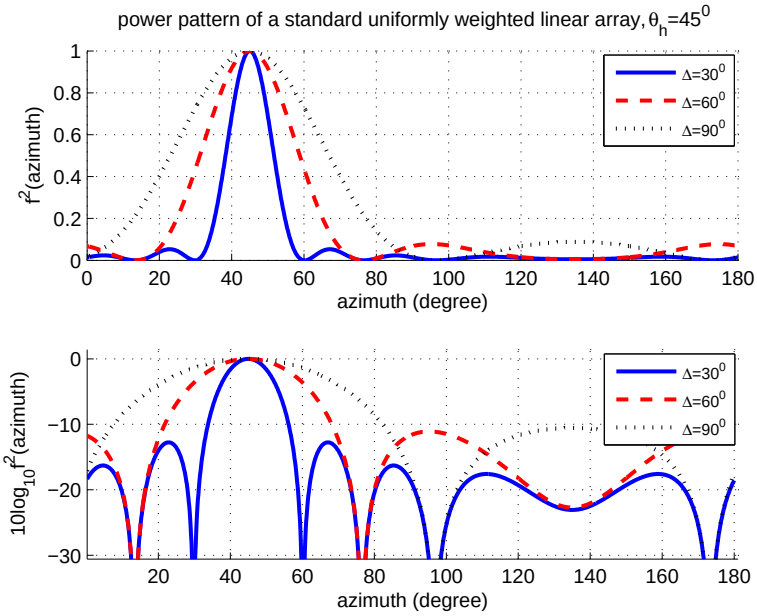

Figure D.1: Power pattern of a directional antenna.

and error in transmit power estimation is measured in terms of *average error magnitude*,

$$E_{s_p} \triangleq \frac{1}{K}\sum_{i=1}^{K} |\hat{s}_p(i) - s_p|,$$

where $(\hat{x}_p(i), \hat{y}_p(i)\hat{s}_p(i))$ denote the estimated values on the i^{th} iteration.

We consider three cases: (i) θ_h is estimated in addition to (x_p, y_p, s_p) to take into account directional transmission, (ii) the effect of directional transmission is ignored (i.e., only (x_p, y_p, s_p) is estimated and as a result the observations become more noisy leading to reduced accuracy), and (iii) equivalent omnidirectional transmission (i.e. $f = 1$ in (6.2) for all directions) to compare as a baseline. For location accuracy, the first subplot of Fig. D.2 shows the average missed distance error ratios

$$\frac{E_{\text{md}}(\text{case i})}{E_{\text{md}}(\text{case iii})} \text{ and } \frac{E_{\text{md}}(\text{case ii})}{E_{\text{md}}(\text{case iii})},$$

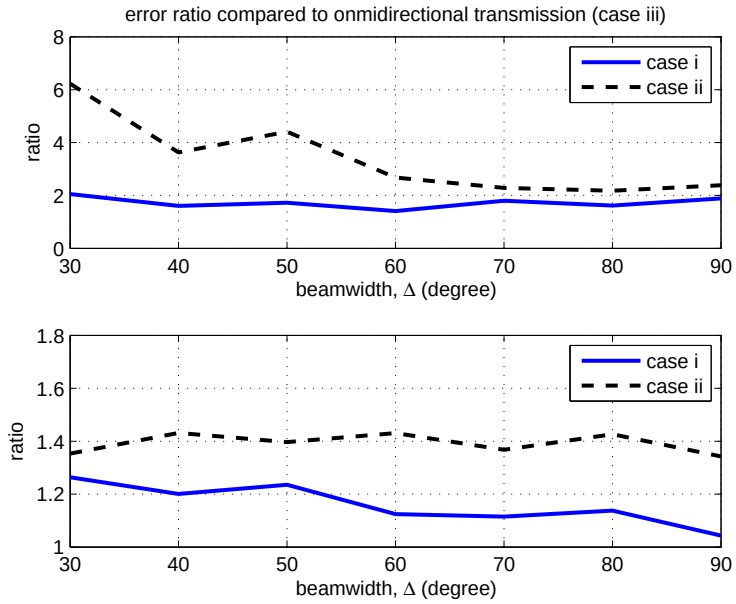

Figure D.2: Estimation accuracy due to directional transmission.

as functions of Δ. When averaged over the range of Δ, location estimation error increases (with respect to the omnidirectional case) about 1.7 times for case (i) and about 3.4 times for case (ii). We observe that case (i) is relatively insensitive to the variation of Δ. A significant improvement over case (ii), especially for smaller values of Δ, is possible by estimating θ_h. This is because a narrower beam (smaller Δ) can induce more error in case (ii), (cf. Fig. D.1). In the second subplot of Fig. D.2, we plot the transmit power error ratios

$$\frac{E_{S_p}(\text{case i})}{E_{S_p}(\text{case iii})} \text{ and } \frac{E_{S_p}(\text{case ii})}{E_{S_p}(\text{case iii})},$$

observe that the transmit power error increases by about 20% (averaged over all Δ), whereas the corresponding number for case (ii) is about 40%. For case (i), as the main lobe widens, the accuracy approaches the omnidirectional case.

Hence, this initial simulation result shows that our model can be modified to relax the omnidirectional transmission assumption made in the paper, although at the cost of reduced accuracy.

D.2 CRB on the estimation error of θ_l and θ_u

Let $\boldsymbol{J}_p^{-1}$ denote the CRB of the parameter vector $\boldsymbol{\theta}_p \triangleq [x_p, y_p, s_p]^T$, which is a 3×3 matrix. The CRBs on the estimation error of J_l^{-1} and J_u^{-1} can be computed as follows [78]:

$$
\begin{aligned}
J_l^{-1} &= \boldsymbol{H}_l^T \boldsymbol{J}_p^{-1} \boldsymbol{H}_l, \quad J_u^{-1} = \boldsymbol{H}_u^T \boldsymbol{J}_p^{-1} \boldsymbol{H}_u, \\
\boldsymbol{H}_l^T &\triangleq \left[\frac{\partial \theta_l}{\partial x_p} \ \frac{\partial \theta_l}{\partial y_p} \ \frac{\partial \theta_l}{\partial s_p} \right]^T = \begin{bmatrix} \frac{1}{d_{1a}} \left\{ \cos\phi_{1a} \frac{\partial y_1}{\partial x_p} - \sin\phi_{1a} \frac{\partial x_1}{\partial x_p} \right\} \\ \frac{1}{d_{1a}} \left\{ \cos\phi_{1a} \frac{\partial y_1}{\partial y_p} - \sin\phi_{1a} \frac{\partial x_1}{\partial y_p} \right\} \\ \frac{1}{d_{1a}} \left\{ \cos\phi_{1a} \frac{\partial y_1}{\partial s_p} - \sin\phi_{1a} \frac{\partial x_1}{\partial s_p} \right\} \end{bmatrix}, \\
\boldsymbol{H}_u^T &\triangleq \left[\frac{\partial \theta_u}{\partial x_p} \ \frac{\partial \theta_u}{\partial y_p} \ \frac{\partial \theta_u}{\partial s_p} \right]^T = \begin{bmatrix} \frac{1}{d_{2a}} \left\{ \cos\phi_{2a} \frac{\partial y_2}{\partial x_p} - \sin\phi_{2a} \frac{\partial x_2}{\partial x_p} \right\} \\ \frac{1}{d_{2a}} \left\{ \cos\phi_{2a} \frac{\partial y_2}{\partial y_p} - \sin\phi_{2a} \frac{\partial x_2}{\partial y_p} \right\} \\ \frac{1}{d_{2a}} \left\{ \cos\phi_{2a} \frac{\partial y_2}{\partial s_p} - \sin\phi_{2a} \frac{\partial x_2}{\partial s_p} \right\} \end{bmatrix}, \\
\frac{\partial y_1}{\partial x_p} &= \frac{d_{\mathrm{cov}}(p)\cos\theta_1}{d_{pa}} \left(-\sin\phi_{pa} + \frac{d_{\mathrm{cov}}(p)}{d_{1a}} \cos\phi_{pa} \right), \\
\frac{\partial y_2}{\partial x_p} &= -\frac{d_{\mathrm{cov}}(p)\cos\theta_2}{d_{pa}} \left(\sin\phi_{pa} + \frac{d_{\mathrm{cov}}(p)}{d_{1a}} \cos\phi_{pa} \right), \\
\frac{\partial y_1}{\partial y_p} &= 1 + \frac{d_{\mathrm{cov}}(p)\cos\theta_1}{d_{pa}} \left(\cos\phi_{pa} + \frac{d_{\mathrm{cov}}(p)}{d_{1a}} \sin\phi_{pa} \right), \\
\frac{\partial y_2}{\partial y_p} &= 1 + \frac{d_{\mathrm{cov}}(p)\cos\theta_2}{d_{pa}} \left(\cos\phi_{pa} - \frac{d_{\mathrm{cov}}(p)}{d_{1a}} \sin\phi_{pa} \right), \\
\frac{\partial y_1}{\partial s_p} &= -\frac{d_{\mathrm{cov}}(p)\cos\theta_1 \dot{d}_{\mathrm{cov}}(p)}{d_{1a}} + \dot{d}_{\mathrm{cov}}(p)\sin\theta_1, \\
\frac{\partial y_2}{\partial s_p} &= \frac{d_{\mathrm{cov}}(p)\cos\theta_2 \dot{d}_{\mathrm{cov}}(p)}{d_{1a}} + \dot{d}_{\mathrm{cov}}(p)\sin\theta_2, \\
\frac{\partial x_1}{\partial x_p} &= 1 + \frac{d_{\mathrm{cov}}(p)\sin\theta_1}{d_{pa}} \left(\sin\phi_{pa} - \frac{d_{\mathrm{cov}}(p)}{d_{1a}} \cos\phi_{pa} \right), \\
\frac{\partial x_2}{\partial x_p} &= 1 + \frac{d_{\mathrm{cov}}(p)\sin\theta_2}{d_{pa}} \left(\sin\phi_{pa} + \frac{d_{\mathrm{cov}}(p)}{d_{1a}} \cos\phi_{pa} \right),
\end{aligned}
$$

$$
\begin{aligned}
\frac{\partial x_1}{\partial y_p} &= -\frac{d_{\rm cov}(p)\sin\theta_1}{d_{pa}}\left(\cos\phi_{pa}+\frac{d_{\rm cov}(p)}{d_{1a}}\sin\phi_{pa}\right),\\
\frac{\partial x_2}{\partial y_p} &= -\frac{d_{\rm cov}(p)\sin\theta_2}{d_{pa}}\left(\cos\phi_{pa}-\frac{d_{\rm cov}(p)}{d_{1a}}\sin\phi_{pa}\right),\\
\frac{\partial x_1}{\partial s_p} &= \frac{d_{\rm cov}(p)\sin\theta_1\dot{d}_{\rm cov}(p)}{d_{1a}}+\dot{d}_{\rm cov}(p)\cos\theta_1,\\
\frac{\partial x_2}{\partial s_p} &= -\frac{d_{\rm cov}(p)\sin\theta_2\dot{d}_{\rm cov}(p)}{d_{1a}}+\dot{d}_{\rm cov}(p)\cos\theta_2,\\
d_{1a} &= \sqrt{(x_1-x_a)^2+(y_1-y_a)^2},\ \dot{d}_{\rm cov}(p)\triangleq\frac{\partial d_{\rm cov}(p)}{\partial s_p}.
\end{aligned}
$$

D.3 Derivation of thresholds $\theta_l^{\rm th}$ and $\theta_u^{\rm th}$

Since $\hat{\theta}_l \sim \frac{1}{A_l}\mathcal{N}(\theta_l, J_l^{-1})$ and $\hat{\theta}_u \sim \frac{1}{A_u}\mathcal{N}(\theta_u, J_u^{-1})$, we can evaluate $\Pr(\hat{\theta}_l < \theta)$ and $\Pr(\hat{\theta}_u > \theta)$ as follows.

$$
\Pr(\hat{\theta}_l<\theta) = \frac{1}{A_l}\int_0^{\theta}\mathcal{N}(\theta_l,J_l^{-1})dx = \frac{1}{A_l}\left[Q\left(\frac{-\theta_l}{\sqrt{J_l^{-1}}}\right)-Q\left(\frac{\theta-\theta_l}{\sqrt{J_l^{-1}}}\right)\right], \quad \text{(D.2)}
$$

$$
\Pr(\hat{\theta}_u>\theta) = \frac{1}{A_u}\int_{\theta}^{2\pi}\mathcal{N}(\theta_u,J_u^{-1})dx = \frac{1}{A_u}\left[Q\left(\frac{\theta-\theta_u}{\sqrt{J_u^{-1}}}\right)-Q\left(\frac{2\pi-\theta_u}{\sqrt{J_u^{-1}}}\right)\right]. \quad \text{(D.3)}
$$

We can find $\theta_l^{\rm th}$ by solving for the maximum value of θ such that $\Pr(\hat{\theta}_l < \theta) \le \varepsilon_{\rm th}$ is satisfied. Using (D.2), this condition implies

$$
\theta_l^{\rm th} = \theta_l + \sqrt{J_l^{-1}}\cdot Q^{-1}\left[Q\left(\frac{-\theta_l}{\sqrt{J_l^{-1}}}\right)-A_l\varepsilon_{\rm th}\right]. \quad \text{(D.4)}
$$

Similarly, for θ_u^{th} we find the minimum value of θ such that $\Pr(\hat{\theta}_u > \theta) \leq \varepsilon_{\text{th}}$ is satisfied. Using (D.3), this condition implies

$$\theta_u^{\text{th}} = \theta_u + \sqrt{J_u^{-1}} \cdot Q^{-1}\left[Q\left(\frac{-\theta_u}{\sqrt{J_u^{-1}}}\right) - A_u \varepsilon_{\text{th}}\right]. \tag{D.5}$$

Bibliography

Bibliography

[1] M. McHenry, "Frequency agile spectrum access technologies," in *Proc. FCC Workshop on Cognitive Radio*, May 2003.

[2] G. Staple and K. Werbach, "The end of spectrum scarcity," *IEEE Spectrum*, vol. 41, no. 3, pp. 48–52, March 2004.

[3] DARPA XG Working Group, "The XG Vision, request for comments," July 2003.

[4] National Science Foundation, "Networking Technology and Systems (NeTS) program solicitation," [Online], 2003, Available at: http://www.nsf.gov/pubs/2005/nsf05505/nsf05505.htm.

[5] S. Haykin, "Cognitive radio: Brain-empowered wireless communications," *IEEE J. Selected Areas in Comm.*, vol. 23, no. 2, pp. 201–220, Feb. 2005.

[6] Q. Zhao and B. M. Sadler, "A survey of dynamic spectrum access," *IEEE Signal Processing Magazine*, vol. 24, no. 3, pp. 79–89, May 2007.

[7] C. Cordeiro, K. Challapali, and D. Birru, "IEEE 802.22: an introduction to the first wireless standard based on cognitive radios," *IEEE J. of Communications*, vol. 1, no. 1, pp. 38–47, Apr. 2006.

[8] D. Hatfield and P. Weiser, "Property rights in spectrum: Taking the next step," in *Proc. IEEE Int. Symp. on New Frontiers in Dynamic Spectrum Access Networks (DySPAN)*, Nov. 2005, pp. 43–55.

[9] L. Xu, R. Tonjes, T. Paila, W. Hansmann, M. Frank, and M. Albrecht, "DRiVE-ing to the internet: Dynamic radio for IP services in vehicular environments," in *Proc. 25th Annual IEEE conf. Local Computer Networks*, Nov. 2000, pp. 281–289.

[10] C. Raman, R. Yates, and N. Mandayam, "Scheduling variable rate links via a spectrum server," in *Proc. IEEE Int. Symp. on New Frontiers in Dynamic Spectrum Access Networks (DySPAN)*, Nov. 2005, pp. 110–118.

[11] O. Ileri, D. Samardzija, and N. Mandayam, "Demand Responsive Pricing and Competetive Spectrum Allocation via a spectrum server," in *Proc. IEEE Int. Symp. on New Frontiers in Dynamic Spectrum Access Networks (DySPAN)*, Nov. 2005, pp. 194–202.

[12] S. Chung, S. Kim, J. Lee, and J. Cioffi, "A game-theoretic approach to power allocation in frequency-selective Gaussian interfrence channels," in *Proc. IEEE Int. Symp. Information Theory*, June 2003, pp. 316–316.

[13] R. Etkin, A. Parekh, and D. Tse, "Spectrum sharing for unlicensed bands," in *Proc. IEEE Int. Symp. on New Frontiers in Dynamic Spectrum Access Networks (DySPAN)*, Nov. 2005, pp. 251–258.

[14] J. Huang, R. Berry, and M. Honig, "Spectrum sharing with distributed interference compensation," in *Proc. IEEE Int. Symp. on New Frontiers in Dynamic Spectrum Access Networks (DySPAN)*, Nov. 2005, pp. 88–93.

[15] V. D. Chakravarthy, Z. Wu, A. Shaw, M. A. Temple, R. Kannen, and F. Garber, "A general overlay/underlay analytic expression representing cognitive radio waveform," in *Proc. IEEE Int. Waveform Diversity and Design Conf.*, June 2007, pp. 69–73.

[16] J. Mitola, "Cognitive Radio: An Integrated Agent Architecture for Software Defined Radio," Ph.D. dissertation, Royal Institute of Technology (KTH), Stockholm, Sweden, May 2000.

[17] FCC, "FCC 05-57," [Online], Mar. 2005, Available at: http://hraunfoss.fcc.gov/edocs_public/attachmatch/FCC-05-57A1.pdf.

[18] GNU Radio, [Online], 2005, Available at: http://www.gnu.org/software/gnuradio/.

[19] J. Mitola and G. Q. Maguire, "Cognitive radio: Making software radios more personal," *IEEE Pers. Commun.*, vol. 6, no. 4, pp. 13–18, Aug. 1999.

[20] FCC, "FCC 03-322," [Online], Dec. 2003, Available at: http://hraunfoss.fcc.gov/edocs_public/attachmatch/FCC-03-322A1.pdf.

[21] P. Kolodzy *et al.*, "Next generation communications: Kickoff meeting," in *Proc. DARPA*, Oct. 17 2001.

[22] B. Wild and K. Ramchandran, "Detecting primary receivers for cognitive radio applications," in *Proc. IEEE DySPAN*, Nov. 2005, pp. 124–130.

[23] M. McHenry, "The probe spectrum access method," in *Proc. IEEE Int. Symp. on New Frontiers in Dynamic Spectrum Access Networks (DySPAN)*, Nov. 2005, pp. 346–351.

[24] S. Geirhofer, L. Tong, and B. M. Sadler, "Dynamic spectrum access in the time domain: Modeling and exploiting white space," *IEEE Communications Magazine*, vol. 45, pp. 66–72, May 2007.

[25] ——, "A measurement-based model for dynamic spectrum access in WLAN channels," in *Proc. IEEE MILCOM*, Washington DC, Oct. 2006, pp. 1–7.

[26] Q. Zhao, S. Geirhofer, L. Tong, and B. M. Sadler, "Optimal dynamic spectrum access via periodic channel sensing," in *Proc. IEEE Wireless Communications and Networking Confernece (WCNC'07)*, Hong Kong, Mar. 2007, pp. 33–37.

[27] Y. Chen, Q. Zhao, and A. Swami, "Joint Design and Separation Principle for Opportunistic Spectrum Access in the Presence of Sensing Errors," *IEEE Trans. on Information Theory*, vol. 54, no. 5, pp. 2053–2071, May 2008.

[28] A. N. Mody *et al.*, "Machine learning based cognitive communications in white as well as the gray space," in *Proc. IEEE MILCOM*, FL, U.S.A., Oct. 2007, pp. 1–7.

[29] D. Cabric and S. M. Mishra and R. W. Brodersen, "Implementation issues in spectrum sensing for cognitive radios," in *Proc. Thirty-Eighth Asilomar Conf. on Signals, Systems and Computers*, Nov. 2004, pp. 772–776.

[30] H. Zheng and C. Peng, "Collaboration and fairness in opportunistic spectrum access," in *Proc. IEEE ICC'05*, Korea, May 2005, pp. 3132–3136.

[31] W. Wang and X. Liu, "List-coloring based channel allocation for open-spectrum wireless networks," in *Proc. IEEE VTC*, Sept. 2005, pp. 690–694.

[32] D. Wilkins, G. Denker, M.-O. Stehr, D. Elenius, R. Senanayake, and C. Talcott, "Policy-Based Cognitive Radios," *IEEE Wireless Communications Magazine*, vol. 14, pp. 41–46, Aug. 2007.

[33] A. Sahai, N. Hoven, S. M. Mishra, and R. Tandra, "Fundamental tradeoffs in robust spectrum sensing for opportunistic frequency reuse," University of California, Berkeley, Tech. Rep., March 2006.

[34] A. Ghasemi and E. Sousa, "Collaborative spectrum sensing for opportunistic access in fading environments," in *Proc. IEEE Int. Symp. on New Frontiers in Dynamic Spectrum Access Networks (DySPAN)*, Nov. 2005, pp. 131–136.

[35] A. Ghasemi and E. S. Sousa, "Optimization of Spectrum Sensing for Opportunistic Spectrum Access in Cognitive Radio Networks," in *proc. 4th IEEE Consumer Communications and Networking Conference, CCNC'07*, Las Vegas, NV, U.S.A., Jan. 2007, pp. 1022–1026.

[36] G. Ganesan and L. Ye, "Cooperative Spectrum Sensing in Cognitive Radio, Part I: Two User Networks," *IEEE Trans. on Wireless Communications*, vol. 6, no. 6, pp. 2204–2213, June 2007.

[37] ——, "Cooperative Spectrum Sensing in Cognitive Radio, Part II: Multiuser Networks," *IEEE Trans. on Wireless Communications*, vol. 6, no. 6, pp. 2214–2222, June 2007.

[38] S.-C. Hong and M. H. Vu and V. Tarokh, "Cognitive sensing based on side information," in *Proc. IEEE Sarnoff Symposium*, Apr. 2008, pp. 1–6.

[39] M. Gastpar, "On capacity under receive and spatial spectrum-sharing constraints," *IEEE Trans. on Information Theory*, vol. 53, no. 2, pp. 471–487, Feb. 2007.

[40] A. Ghasemi and E. S. Sousa, "Fundamental limits of spectrum-sharing in fading environments," *IEEE Trans. on Wireless Comm.*, vol. 6, no. 2, pp. 649–658, Feb. 2007.

[41] S. Srinivasa and S. A. Jafar, "Soft sensing and optimal power control for cognitive radio," in *Proc. IEEE Globecom'07*, Nov. 2007, pp. 1380–1384.

[42] F. F. Digham, "Joint Power and Channel Allocation for Cognitive Radios," in *Proc. IEEE WCNC'08*, Mar.-Apr. 2008, pp. 882–887.

[43] N. Gatsis, A. G. Marques, and G. B. Giannakis, "Utility-based power control for peer-to-peer cognitive radio networks with heterogeneous QoS constraints," in *Proc. IEEE ICASSP'08*, Mar.-Apr. 2008, pp. 2805–2808.

[44] N. Clemens and C. Rose, "Intelligent power allocation strategies in an unlicensed spectrum," in *Proc. IEEE DySPAN'05*, Nov. 2005, pp. 37–42.

[45] X. Li, J. Chen, and F. Ng, "Secure transmission power of cognitive radios for dynamic spectrum access applications," in *Proc. 42nd Annual Conf. on Information Sciences and Systems, CISS'08*, Mar. 2008, pp. 213–218.

[46] S. Kim, H. Jeon, and J. Ma, "Robust localization with unknown transmission power for cognitive radio," in *Proc. IEEE Int. Conf. on Military Communications*, Oct. 2007.

[47] J. K. Nelson, M. U. Hazen, and M. R. Gupta, "Global Optimization for Multiple Transmitter Localization," in *IEEE MILCOM'06*, Oct. 2006, pp. 1–7.

[48] J. K. Nelson and M. R. Gupta, "An EM technique for multiple transmitter localization," in *Annual Conf. on Information sciences and systems (CISS'07)*, Mar. 2007, pp. 610–615.

[49] H. Celebi and H. Arslan, "Cognitive Positioning Systems," *IEEE Trans. on Wireless Communications*, vol. 6, no. 12, pp. 4475–4483, Dec. 2007.

[50] ——, "Utilization of location information in cognitive wireless networks," *IEEE Wireless Communications Magazine*, vol. 14, no. 4, pp. 6–13, Aug. 2007.

[51] L.-C. Wang and A. Chen, "Effects of Location Awareness on Concurrent Transmissions for Cognitive Ad Hoc Networks Overlaying Infrastructure-based Systems," *IEEE Trans. on Mobile Computing*, 2008 (accepted).

[52] J. Riihijärvi and P. Mähönen, "Exploiting spatial statistics of primary and secondary users towards improved cognitive radio networks," in *Proc. CrownCom'08*, May 2008, pp. 1–7, invited paper.

[53] D. Gong *et al.*, "High Order Geometric Range Free Localization in Opportunistic Cognitive Sensor Networks," in *Proc. IEEE Int. Conf. on Communications, ICC'08*, May 2008, pp. 139–143.

[54] B. L. Mark and A. O. Nasif, "Estimation of Interference-Free Transmit Power for Opportunistic Spectrum Access," in *Proc. IEEE Wireless Communications and Networking Confernece (WCNC'08)*, Apr. 2008.

[55] B. L. Mark and A. O. Nasif, "Estimation of maximum interference-free power level for opportunistic spectrum access," *IEEE Transactions on Wireless Communications*, Dec. 2008 (accepted).

[56] R. Menon, R. M. Buehrer, and J. H. Reed, "Outage probability based comparison of underlay and overlay spectrum sharing techniques," in *Proc. IEEE DySPAN*, Nov. 2005, pp. 101–109.

[57] N. Hoven and A. Sahai, "Power scaling for cognitive radio," in *Proc. IEEE Int. Conf. on Wireless Networks, Communications and Mobile Computing*, June 2005, pp. 250–255.

[58] L. Qian, X. Li, J. Attia, and Z. Gajic, "Power control for cognitive radio ad hoc networks," in *Proc. 15th IEEE Workshop on LANMAN*, NJ, U.S.A., June 2007, pp. 7–12.

[59] K. Hamdi, W. Zhang, and K. B. Letaief, "Power Control in Cognitive Radio Systems Based on Spectrum Sensing Side Information," in *Proc. IEEE Int. Conf. on Communications, ICC'07*, June 2007, pp. 5161–5165.

[60] A. E. Leu, M. McHenry, and B. L. Mark, "Modeling and analysis of interference in Listen-Before-Talk spectrum access schemes," *Int. J. Network Mgmt*, vol. 16, pp. 131–147, 2006.

[61] S. Tang and B. L. Mark, "Performance analysis of a wireless network with opportunistic spectrum sharing," in *Proc. IEEE Globecom*, Washington DC, Nov. 2007.

[62] Q. Zhao and A. Swami, "A decision-theoretic framework for opportunistic spectrum access," *IEEE Communications Magazine: Special Issue on Cognitive Wireless Networks*, vol. 14, no. 4, pp. 14–20, Aug. 2007.

[63] S. Capkun, M. Hamdi, and J.-P. Hubaux, "GPS-Free positioning in mobile ad-hoc networks," in *Proc. 34th Hawaii Int. Conf. System Sciences*, Jan. 2001.

[64] D. Moore, J. Leonard, D. Rus, and S. Teller, "Robust distributed network localization with noisy range measurements," in *Proc. 2nd ACM SenSys*, Nov. 2004.

[65] P. Biswas and Y. Ye, "Semidefinite programming for ad hoc wireless sensor network localization," in *3rd Int. Symp. on Information Processing in Sensor Networks, IPSN 2004*, April 2004, pp. 46–54.

[66] L. Doherty, K. S. J. Pister, and L. E. Ghaoui, "Convex position estimation in wireless sensor networks," in *Proc. IEEE INFOCOM'01*, vol. 3, April 2001, pp. 1655–1663.

[67] M. Gudmundson, "Correlation model for shadow fading in mobile radio systems," *Electronics Letters*, vol. 47, no. 23, pp. 2145–2146, Nov. 1991.

[68] M. N. Lustgarten and J. A. Madsen, "An empirical propagation model (EPM-73)," *IEEE Trans. on Electromagnetic Compatibility*, vol. 19, no. 3, August 1977.

[69] A. G. Longley and P. L. Rice, "Prediction of tropospheric transmission loss over irregular terrain, a computer method - 1968," U.S. Dept. of Commerce, Office of Telecommunications, Boulder, CO, ESSA 79-ITSS 67, July 1968.

[70] N. S. Adawi *et al.*, "Coverage prediction for mobile radio systems operating in the 800/900 MHz frequency range," *IEEE Trans. on Vehicular Technology*, vol. 37, pp. 3–44, 1988.

[71] Y. Qi, H. Kobayashi, and H. Suda, "Analysis of wireless geolocation in a non-line-of-sight environment," *IEEE Trans. on Wireless Comm.*, vol. 5, no. 3, pp. 672–681, March 2006.

[72] J. J. Caffery, *Wireless Location in CDMA Cellular Radio Systems.* Massachusetts: Kluwer Academic Publishers, 1999.

[73] Y. Qi, "Wireless geolocation in a non-line-of-sight environment," Ph.D. dissertation, Princeton University, Princeton, New Jersey, 2003.

[74] A. J. Weiss, "On the accuracy of a cellular location system based on RSS measurements," *IEEE Trans. on Vehicular Tech.*, vol. 52, no. 6, pp. 1508–1518, Nov. 2003.

[75] V. Erceg *et al.*, "An empirically based path loss model for wireless channels in suburban environment," *IEEE J. Selected Areas in Comm.*, vol. 17, no. 7, pp. 1205–1211, July 1999.

[76] C. Pérez-Vega and J. M. Zamanillo, "Path-loss model for broadcasting applications and outdoor communication systems in the VHF and UHF bands," *IEEE Trans. on Broadcasting*, vol. 48, no. 2, pp. 91–96, June 2002.

[77] C. R. Rao, *Linear Statistical Inference and Its Applications*, 2nd ed. New York: John Wiley & Sons, Inc., 1965.

[78] L. L. Scharf, *Statistical Signal Processing: Detection, Estimation, and Time Series Analysis.* New York: Addison-Wesley, 1991.

[79] H. L. Van Trees, *Detection, Estimation and Modulation Theory: Part I.* New York: John Wiley & Sons, Inc., 2001.

[80] S. Verdú, *Multiuser Detection.* New York: Cambridge University Press, 1998.

[81] "Longley-Rice Methodology for evaluating TV coverage and Interference." Office of Engineering and Technology (OET), Federal Communications Commission, Tech. Rep. OET Bulletin 69, Feb. 2004.

[82] A. O. Nasif and B. L. Mark, "Collaborative opportunistic spectrum access in the presence of multiple transmitters," in *Proc. IEEE Globecom'08*, New Orleans, LA, Nov. 30-Dec. 4 2008.

[83] B. L. Mark and A. E. Leu, "Local averaging for fast handoffs in cellular networks," *IEEE Transactions on Wireless Communications*, vol. 6, no. 3, pp. 866–874, March 2007.

[84] N. C. Beaulieu, A. A. Abu-Dayya, and P. J. McLane, "Estimating the distribution of a sum of independent lognormal random variables," *IEEE Trans. on Communications*, vol. 43, no. 12, pp. 2869–2873, Dec. 1995.

[85] J. Rissanen, "Modeling by shortest data description," *Automatica*, vol. 14, pp. 465–471, 1978.

[86] A. O. Nasif and B. L. Mark, "Measurements Clustering Criteria for Localization of Multiple Transmitters," in *Annual Conf. on Information sciences and systems (CISS'09)*, Mar. 2009.

[87] M. Wax and T. Kailath, "Detection of signals by information theoretic criteria," *IEEE Trans. on Acoustics, speech, and signal processing*, vol. 33, no. 2, pp. 387–392, Apr. 1985.

[88] J. Rissanen, "Universal coding, information, prediction, and estimation," *IEEE Trans. on Info. Theory*, vol. 30, no. 4, pp. 629–636, July 1984.

[89] P. Deng and P. Z. Fan, "An AOA assisted TOA positioning system," in *Proc. Int. Conf. on Communication Technology*, vol. 2, Aug. 2000, pp. 1501–1504.

[90] L. Cong and W. Zhuang, "Hybrid TDOA/AOA mobile user location for wideband CDMA cellular systems," *IEEE Trans. Wireless Commun.*, vol. 1, no. 3, pp. 439–447, July 2002.

[91] Z. Wang and S. A. Zekavat, "Manet localization via multi-node toa-doa optimal fusion," in *Proc. IEEE MILCOM*, Washington DC, Oct. 2006.

[92] Y. Qi and H. Kobayashi, "An unified analysis for Cramer-Rao Lower Bound for non-line-of-sight geolocation," in *Proc. 36th Conf. on Information Sciences and Systems (CISS)*, Mar. 2002.

[93] R. Klukas and M. Fattouche, "Line-of-Sight Angle of Arrival Estimation in the Outdoor Multipath Environment," *IEEE Trans. on Vehicular Tech.*, vol. 47, no. 1, pp. 342–351, Feb. 1998.

[94] J. Chaffe and J. Abel, "GDOP and the Cramer-Rao bound," in *Proc. IEEE Position Location and Navigation Symp. 1994*, Apr. 1994, pp. 663–668.

[95] T. M. Cover and J. A. Thomas, *Elements of Information Theory.* New York: John Wiley & Sons, Inc., 1991.

[96] L. Xiong, "A selective model to suppress NLOS signals in angle-of-arrival (AOA) location estimation," in *Proc. IEEE PIMRC'98*, 1998, pp. 461–465.

[97] S. Yoo, S. Kim, D. H. Youn, and C. Lee, "Multipath mitigation technique using null-streeing beanformer for positioning system," in *Proc. Vehicular Technology Conf. Spring*, 2003, pp. 602–605.

[98] S. Al-Jazzar, M. Ghogho, and D. McLernon, "A joint TOA/AOA constrained minimization method for locating wireless devices in non-line-of-sight environment," *IEEE Trans. on Vehicular Tech.*, vol. 58, no. 1, pp. 468–472, Jan. 2009.

[99] A. J. Weiss and A. Amar, "Direct position determination of multiple radio signals," *EURASIP J. on Applied Signal Processing*, vol. 2005, no. 1, pp. 37–49, 2005.

[100] H. L. Van Trees, *Optimum Array Processing (Detection, Estimation and Modulation Theory): Part IV*. New York: John Wiley & Sons, Inc., 2002.

Curriculum Vitae

Ahmed O. Nasif graduated from Government Laboratory High School and Notre Dame College, Dhaka, Bangladesh, in 1994 and 1996, respectively. He received the Bachelor of Science in Electrical and Electronic Engineering from Bangladesh University of Engineering and Technology, Dhaka, Bangladesh, in 2003. He came to U.S.A. to pursue his graduate studies in 2003 and received the Master of Science in Electrical Engineering from Wright State University, Dayton, Ohio, in 2005.